Mechanical Properties of the Temporal Muscle

Vera Luísa Allen Celestino da Silva Trindade

Thesis

FEUP Supervisor: Professor Doutor Renato Manuel Natal Jorge

Faculdade de Engenharia da Universidade do Porto

Mestrado Integrado em Engenharia Mecânica

Julho de 2010

Agradecimentos

Em primeiro lugar quero agradecer ao meu orientador, o Professor Doutor Renato Natal Jorge, que acredita em mim, que sabiamente me aconselha em todos os momentos, que me dá todas as condições para o meu sucesso e que se esforça todos os dias por me mostrar o caminho do que há de melhor no trabalho assim como na vida.

Ao Professor Doutor Augusto Fernandes, na qualidade do presidente do Instituto de Engenharia Mecânica, IDMEC, e á S^{ra} Júlia Meira do secretariado.

Ao Instituto Nacional de Medicina Legal na pessoa do Professor Doutor Agostinho Santos assim como a sua equipa, composta por pessoas como a Dr. Liliana Santos e o Dr. José Fernandes, sempre atenciosos e diligentes no cumprimento de todas as tarefas necessárias ao projecto.

Ao Professor Doutor Pedro Martins que teve a árdua tarefa de me iniciar ás práticas laboratoriais e que me apoiou sempre , facultando-me sabiamente guias que moldaram o meu trabalho.

Aos meus colegas na unidade de concepção e validação experimental do IDMEC; o Professor Doutor Marco Parente, paciente fonte dos recursos informáticos utilizados na realização do trabalho, o Engenheiro Helder Mata e a Engenheira Filipa Sousa companheiros imprescindíveis.

Ao meu "grilo falante", a Engenheira Sónia Santos, amiga e mentora.

Aos meus pais, família e amigos que me apoiam desde sempre, e que sem eles não seria possível ter chegado até aqui.

Resumo

Estudo das características biomecânicas do músculo temporal humano e suas estruturas; a fascia e o tendão temporais, com o intuito de melhor compreender o funcionamento dos músculos envolvidos no processo da mastigação. O músculo temporal é um dos principais músculos envolvidos no processo mastigatório e é responsável pela elevação e retracção da mandíbula. Estudar o temporal é um passo importante na compreensão de patologias relativas ao aparelho bucal, que segundo o "American Institute of Health" afectam a qualidade de vida de entre 14,4 e 43,2 milhões de americanos com sintomas que passam pela cefaleia, insónia e até dor ou maxilar doloroso. Estes sintomas são causados por distúrbios da articulação temporomandibular devido a uma actividade oral parafuncional, caracterizada pelo ranger dos dentes; o bruxismo. O bruxismo caracteriza-se pela activação involuntária dos músculos da mastigação principalmente durante o sono, causando assim o desgaste anormal dos dentes, podendo inclusivé estender-se até à gengiva.

Este estudo pretende caracterizar o comportamento do músculo escolhido bem como da fascia temporal e os tendões, através do uso de modelos constitutivos não-lineares. Um ponto de vista fundamental será caracterizar as diferenças entre estas estruturas considerando para isso factores como a idade, sexo e constituição da boca pela falta de dentes. Um outro ponto importante será definir o mecanismo de deformação da estrutura microscópica do tipo fascial, o endomísio, utilizando para isso uma abordagem dentro do regime não-linear e da teoria das grandes deformações.

Todos estes objectivos foram concretizados; as respectivas constantes de cada modelo constituivo utilizado foram recomendadas consoante determinados grupos divididos de acordo com idade e sexo. Foi estabelecida também a equação que caracteriza o comportamento do endomísio no regime não-linear.

O factor idade no tecido muscular esquelético mostra-se influente para o parâmetro rigidez, uma vez que os grupos de amostras mais jovens são mais rígidos do que os grupos mais velhos, enquanto para os tendões e fáscias ocorre o oposto; os tecidos pertencentes a grupos de idade superior geralmente mostram maior rigidez do que os pertencentes aos grupos jovens.

Quanto ao género, tanto para o exemplo das fáscias como dos tendões, os grupos mais velhos do sexo masculino são os que têm maiores valores de tensão relativamente aos dos grupos do sexo feminino. Para o caso do tecido muscular, este parâmetro comporta-se de tal maneira que os valores de tensão máxima apresentados pelo grupo masculino mais velho são sistematicamente superiores aos valores de tensão máxima apresentados pelos grupos femininos.

Todas estas conclusões, significam um passo importante no reconhecimento da importância do temporal sobre os músculos e transtornos da mastigação como bruxismo e patologias da articulação temporomandibular.

Abstract

This is a study of the biomechanical characteristics of the human temporal muscle and its associated structures the temporal fascia and tendon; in an attempt to be a further step on the comprehension of the mastication muscles. The temporal muscle is one of the main muscles involved in the process of mastication and it is responsible for the elevation and retraction of the mandible. Studying the mastication muscles such as the temporal, it is an important step on understanding a disease like bruxism, which is responsible for many unpleasant symptoms affecting the patient's life quality, such as chronic headache, insomnia and sore or painful jaw. It is an oral parafunctional activity, characterized by the grinding of the teeth and is typically accompanied by the clenching of the jaw occurring mostly during sleep ultimately leading to temporomandibular joint dysfunction [Jadidi, F., et al., 2007].

This biomechanical study of the temporalis pretends to characterize the chosen muscle's behavior by means of the constitutive non-linear equations and their constants as well as the associated structures like the temporalis fasciae and the tendons. This structures' differences between each other considering age, gender and mouth constitution and lacking of teeth are an imperative perspective. Another objective is to define the deformation mechanism for the microscopic structure, the endomysium, having a different approach in order to describe the muscle's behavior within the nonlinear regime and the large deformations' theory, as it has already been described by the linear sold mechanics theory.

All these objective were accomplished as muscles, fasciae and tendons were appointed constants. These recommended constants were divided in different groups according to age and gender but not according to the mouth constitution, this particular problem was not to able to be addressed.

An equation concerning the endomysium behavior within the nonlinear regime and the large deformations' theory has been also drawn.

Using the calculated constants some plotting work was done has done to help and determine what would the differences between muscles and the other studied tissues be. Age in muscles becomes an important factor as younger groups are stiffer than older ones, while for fasciae and tendons it is the opposite; higher age generally is shown to lead to stiffer tissues than younger ones. Concerning gender both fascia and tendons, for the older male groups stress values are consistently higher than the female groups. For muscles this parameter behaves quite the opposite way has both the male group's maximum stress value are consistently higher than the values of maximum stress for the female groups.

All of these conclusions will signify an important step on recognizing the temporalis importance on the mastication muscles and on oral health disorders such as bruxism and temporomandibular joint pathologies.

Contents

List of Figures

List of Tables

1. Introduction

The theme of this thesis is the study of biomechanical characteristics of the human temporal muscle and its associated structures on the grounds that biomechanics assumes a key role in understanding some human macroscopic and microscopic mechanical phenomena.

The temporal muscle is one of the main muscles involved in the process of mastication and it is responsible for the elevation and retraction of the mandible. It arises from the temporal fossa and the deep part of temporal fascia and passes medial to the zygomatic arch inserting itself onto the coronoid process of the mandible. The temporal muscle is covered by the temporal fascia, also known as the temporal aponeurosis. The muscle is accessible on the temples and can be seen and felt contracting during mandibular movement.

Studying the mastication muscles such as the temporal, it is an important step on understanding a disease like bruxism, which is responsible for anxiety, stress, and even depression symptoms, as well as chronic headache, insomnia and sore or painful jaw. It is an oral parafunctional activity, characterized by the grinding of the teeth and is typically accompanied by the clenching of the jaw occurring mostly during sleep. Eventually to extreme cases, bruxism causes teeth shortening, wearing down of teeth incisal edges, myofascial muscle pain and temporomandibular joint dysfunction [Jadidi, F., et al., 2007].

Of all the mastication muscles, the temporalis was chosen due to logistical matters. From the forensic point of view it is the easiest muscle to dissect during an autopsy, and because it was a project capital goal to work with experimental data.

A microscopic approach is pursued by studying the endomysium nonlinear performance via the large deformations' theory pretending to relate the deformation mechanism with the microscopic structure of the material.

Defining the appropriate material model and its constants for each type of tissue that compiles the temporalis is an important phase in order to understand its behavior and consequence. Some specific applications include employment on 3D models using the finite element method that pretend to simulate/study the chewing process and its associated diseases like bruxism, and chronic headache.

The conclusions taken from this work will contribute for the skeletal muscle's properties knowledge and to further understanding the temporalis interaction with the complex human masticatory system.

2. Anatomy, Histology and Physiology of muscles

This chapter presents the organization of the human muscles, its main structures and functions by exploring the already very well established literature on anatomy, histology and physiology of muscles. Anatomy is the study of the structure of the body and the physical relations between body parts. Physiology is the study of how the body parts work together, so anatomy and physiology are intimately connected. Histology is a relatively recent area as it's the study of the microscopic anatomy of cells and tissues and an important tool in cancer (and other diseases) diagnosis. Together these three branches of science have the task of explaining how muscle cells work to produce the forces responsible for the movement of limbs, heart and other body parts [Seeley, et al., 2003].

2.1. Muscular system

The human musculoskeletal system, also known as the locomotor system it's an organ system that provides support, stability, and movement to the body. It is structured of the skeleton, muscles, cartilage, tendons, ligaments, joints, and other connective tissue. There are approximately 640 skeletal muscles in the human body and almost every muscle constitutes one part of a pair of identical bilateral muscles.

Diseases of the musculoskeletal system mostly encompass functional disorders or motion discrepancies; the level of impairment depends specifically on the problem and its severity. Articular disorders, such as the temporomandibular joint dysfunction and muscular dystrophies are the most common. Muscular dystrophy it's a medical condition first acknowledged in the 1860s and refers to a group of hereditary muscle diseases that weaken the muscles that move the human body with manifestations in body systems including the heart, gastrointestinal and nervous systems, endocrine glands, skin, eyes and other organs, namely the brain. Nine diseases are classified as muscular dystrophy but there are more than 100 diseases in total with similarities to muscular dystrophy

Many other body systems, including the vascular, nervous, and integumentary systems, are interrelated; disorders of one of these systems may also affect the musculoskeletal system and complicate the diagnosis of the disorder's origin.

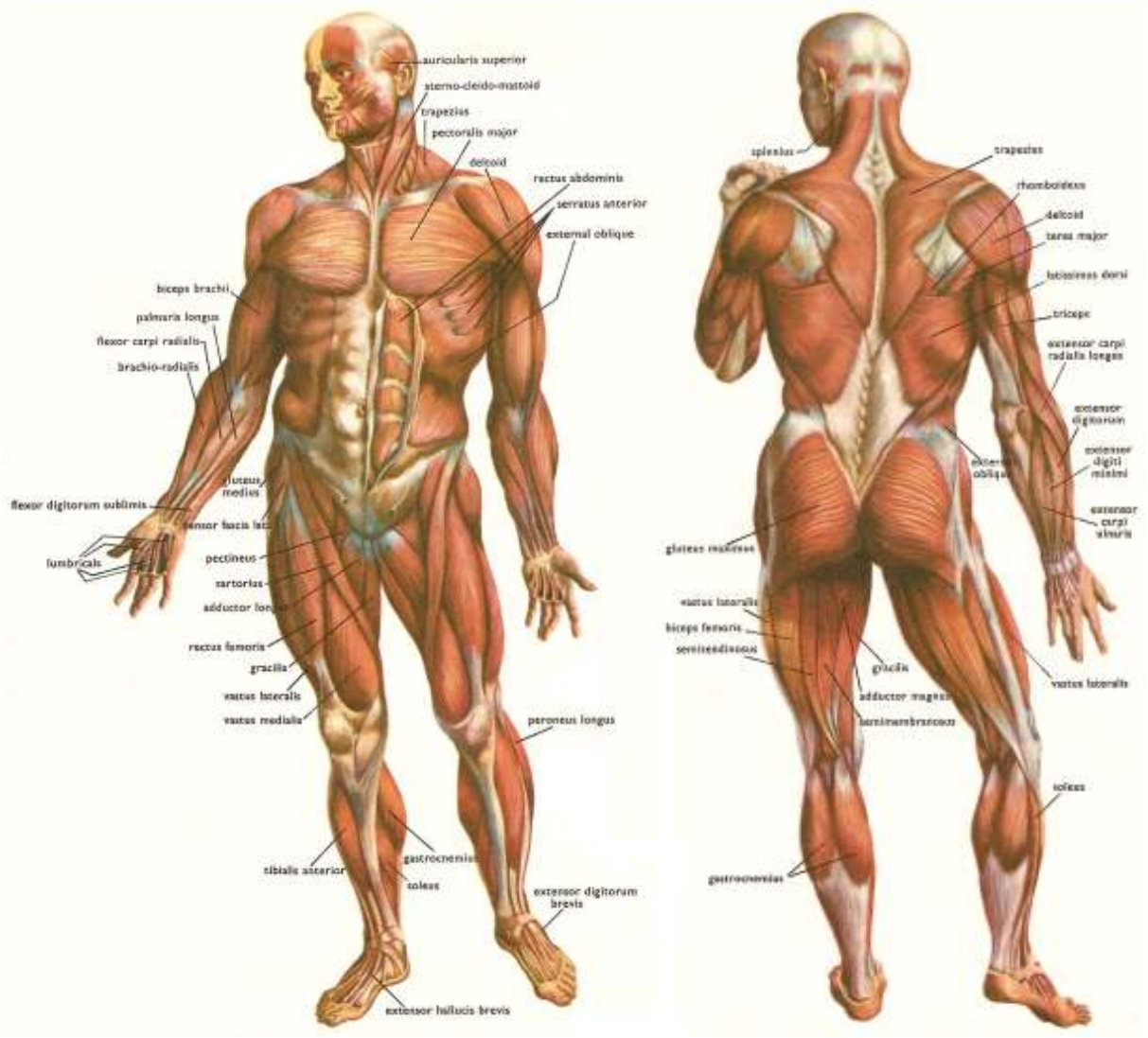

Figure 1 The muscular human system [D'Alessandro, M.P., 1995].

2.1.1. Muscle's Function

The muscle tissue is highly specialized [Seeley, et al., 2003]. It has four functional elements of movement: contractility, excitability, extensibility and elasticity. Contractility is the ability of producing a given muscle the twitch force. Excitability is the muscle's ability to respond to stimuli sent by the nervous system in case of skeletal muscles, or by the combination of hormones and nervous system in the case of smooth and cardiac muscle. Extensibility is the

muscle's ability to be stretched and lastly elasticity means that after being stretched to a certain point, muscles return to their resting length.

2.1.2. Muscle's Shapes

The muscles have a variety of shapes, depending on its function since the ability to generate contraction is in direct relation to its size and shape (see Figure 2 Muscle shapes above [Seeley, et al., 2003], the temporalis insertion below [Gray, H., et al. 1995].Figure 2.). Muscles can be grouped into four types according to their beams main orientation; as pennate where tendons run through the middle of the muscle and fascicles converge at it; parallel where fascicles are arranged parallel to each other, the epimysium surrounds it and the tendons extend out till each end; convergent where fascicles are arranged in such a way that one end converges at a point, like a fan and both tendons and fasciae converge at the same point (e.g. the pectoralis in the chest) and finally circular shaped (also called sphincters) where fascicles are arranged in a circle with no tendons. They control openings (e.g. orbicularis oris in the mouth).

The temporalis is a flapped fan shaped muscle with fascicles descending from the parietal bone downwards through the zygomatic arch and inserting into the coronoid process. This description is consistently covered by the convergent shape type of muscle (see Figure 2).

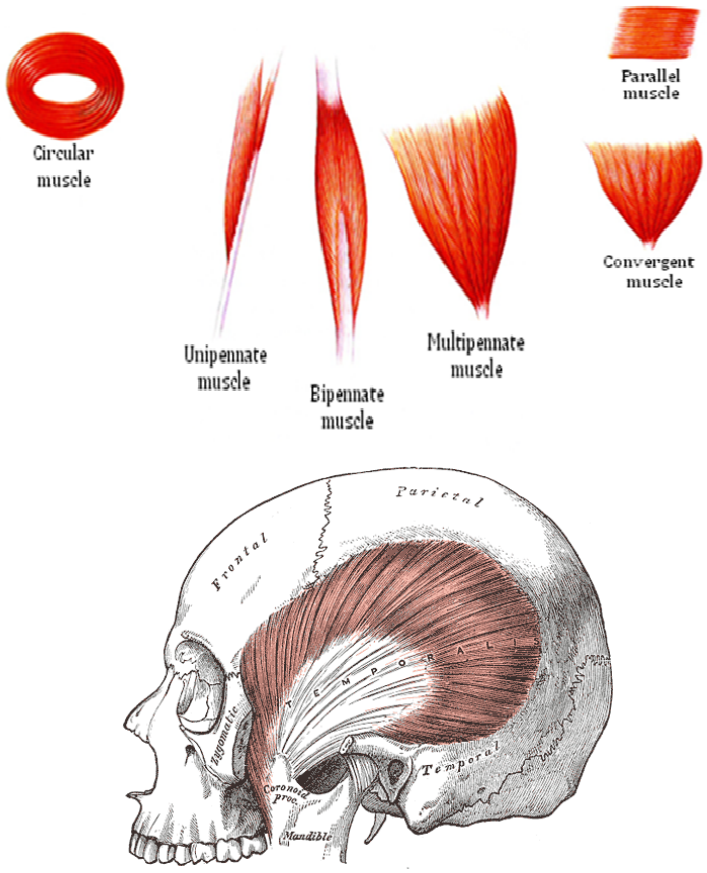

Figure 2 Muscle shapes above [Seeley, et al., 2003], the temporalis insertion below [Gray, H., et al. 1995].

Muscle tissue is comprised of three types according to their morphological and functional characteristics: the skeletal muscle is capable of rapid, vigorous contraction and subject to voluntary control, the cardiac muscle whose contraction is involuntary, vigorous and rhythmic and the smooth muscle which contraction is subjected to slow and involuntary control.

Muscles consist of elongated cells containing cytoplasmic filaments of contractile proteins that generate the necessary forces using the energy contained in ATP molecules (Adenosine Triphosphate) [Junqueira, L.C., et al., 2005] . ATP molecules' presence is mandatory in the shortening of actin and myosin therefore imperative to muscle contraction. Skeletal muscle cells are elongated, have multiple peripheral nuclei and visible striations (see Figure 3). Cardiac muscle cells are branching ones having single central nucleus and visible striations (see Figure 3) as opposed to smooth muscle cells that are spindle-shaped with a single central nucleus and no visible striations (see Figure 5).

Figure 3 Longitudinal and cross section of skeletal muscle tissue. Tissue composed of fibbers with large diameter, long and multi-nucleated [Junqueira, L.C., et al., 2005].

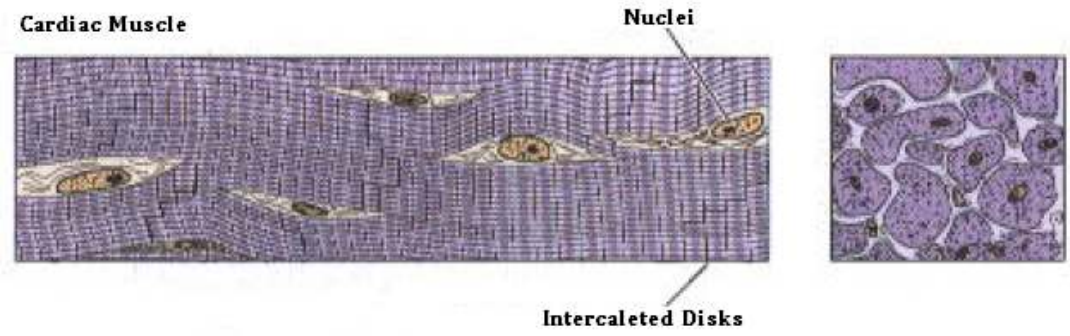

Figure 4 Longitudinal section and cross section of heart muscle. Tissue composed of cells branched and joined by intercalated disks. Each cell has only one or two cores located in the centre of the cell [Junqueira, L.C., et al., 2005].

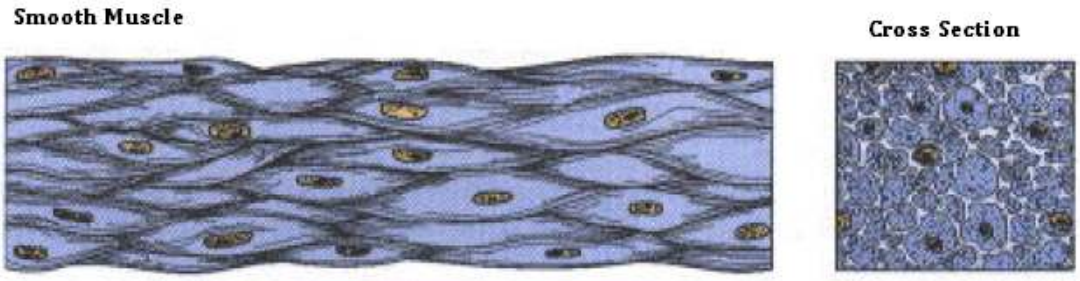

Figure 5 Longitudinal and cross section of the smooth muscle tissue. Tissue composed of an aggregate of spindle cells with one or two nuclei, located in the thickest part of the cell [Junqueira, L.C., et al., 2005].

Muscle cells have mesodermal origin which means they were originated by the mesoderm that is the middle layer of the three fundamental layers of embryonic tissues of the body.

Their differentiation occurs by filamentous protein synthesis, concomitant with the cells elongation [Junqueira, L.C., et al., 2005].

2.1.3. Skeletal Muscle

The skeletal muscle associated with the connective tissue comprises about 40% of body weight and is associated with locomotion, facial expression, chewing, posture and volunteer breathing movements'. It is formed by cylindrical cells up to 30 mm long, multi-nucleated containing the myofibrils. Each myofibril's diameter varies from 10 to 100 μm [Junqueira, L.C., et al., 2005].

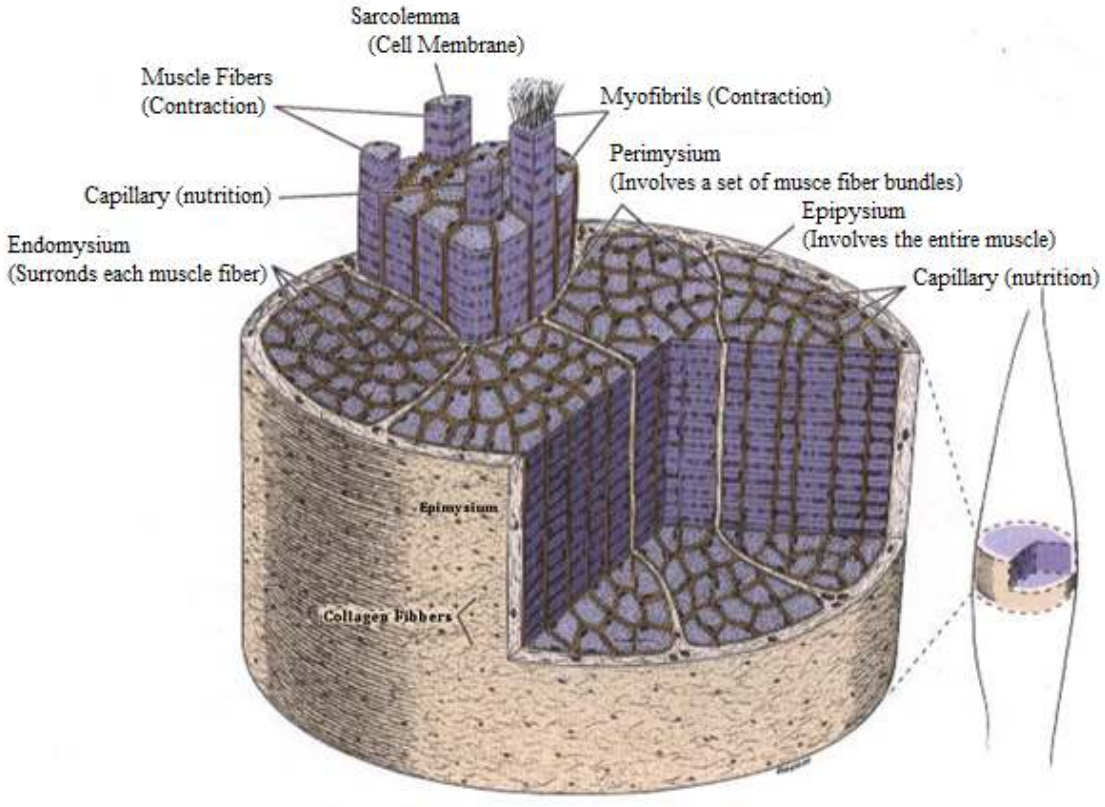

Figure 6 Schematic illustrating revealing the organization of the skeletal muscle [Junqueira, L.C., et al., 2005].

Skeletal muscle is composed of an orderly arrangement of connective tissue and contractile cells. It is surrounded by an external connective tissue wrapping called the epimysium and it

is organized in fascicles, which are bundles of individual muscle cells, each fascicle surrounded also by a tissue layer called the perimysium, as shown in the previous picture. Within the fascicle, the third connective layer, the endomysium separates and electrically insulates the muscle cells from each other [Junqueira, L.C., et al., 2005].
All three connective tissue layers are expressions of the same tissue type, known as the fascia and bind the muscle cells together providing strength to the entire muscle. They emerge at the end of the muscle and are continuous with tendons.

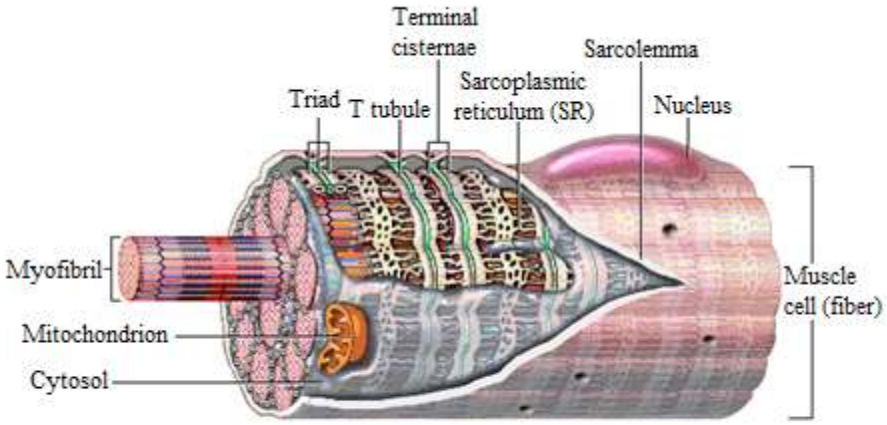

Figure 7 Internal structure of the skeletal muscle cell [D'Alessandro, M.P., 1995].

Because the skeletal muscle cells are elongated they are often referred to as muscles fibbers. Each of the organelles referred to on the previous picture are described in the glossary of terms.

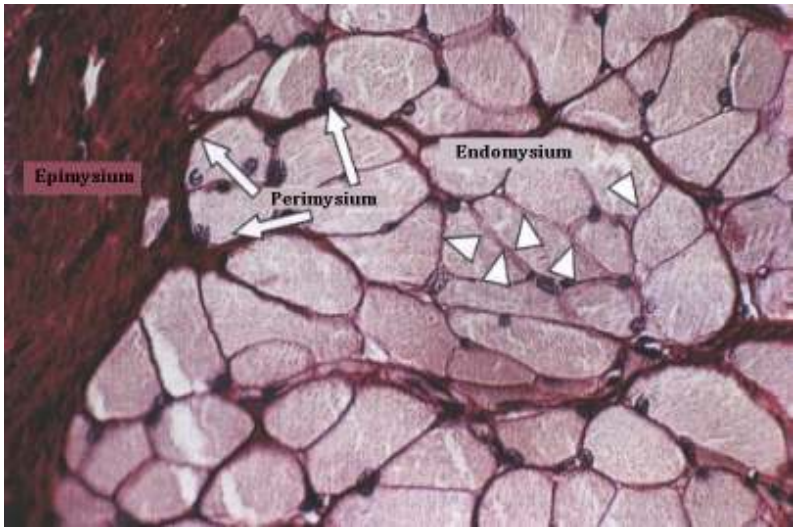

Figure 8 Skeletal muscle cross section. The epimysium, perimysium and the endomysium is shown. No information on magnifying [Junqueira, L.C., et al., 2005].

Each muscle fibber contains many cylindrical bundles of filaments, the myofibrils, which measure 1 to 2 μm in diameter [Junqueira, L.C., et al., 2005] , to contain four major proteins: myosin, actin, tropomyosin and troponin. On the electron microscope it's revealed the presence of thin filaments of actin and myosin thick filaments, arranged along the myofibrils. Myosin and actin together represent about 55% of the total protein of striated muscle.

The arrangement of thick and thin myofilaments forms light and dark alternating bands or striations along the myofibril.

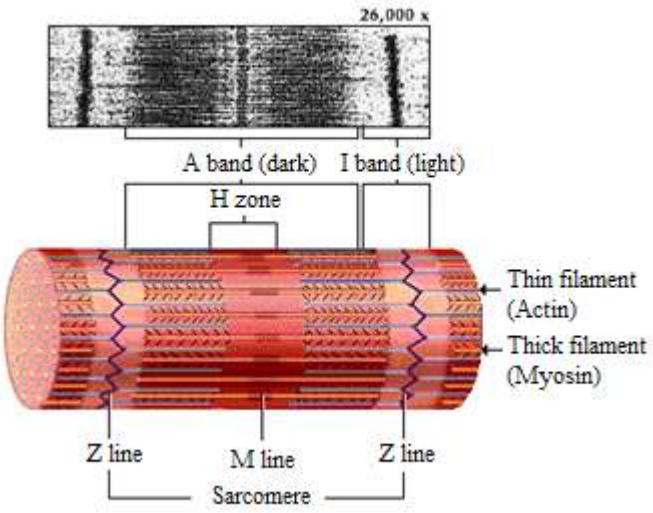

Figure 9 Arrangement of myofilaments on the myofibril [D'Alessandro, M.P., 1995].

The I band is the region of the myofibril's striation that alternates with dark A bands; containing the thin filaments. The I band's width is the distance between adjacent thick filaments therefore the I band gets narrower during muscle contraction. A lighter stripe in the center of the A band, is the H zone, corresponding to the region between thin filaments; the H zone is widest when the muscle is relaxed and stretched. A Z line bisects the I band on a zigzag; it's actually a protein disc that anchors the I bands and connects the myofibrils. Finally the M line in the center of the H zone consists of protein fibbers that connect neighbor myosin filaments.

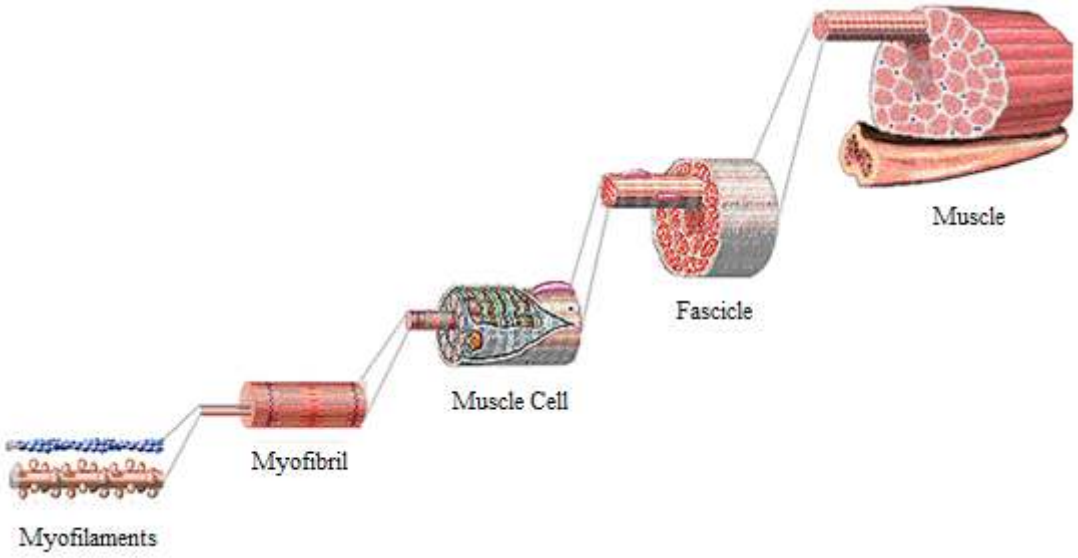

Figure 10 Organization levels of skeletal muscle [D'Alessandro, M.P., 1995].

2.1.4. Contraction Mechanism – the Sliding Theory

The current theory of how a muscle cell contracts is the sliding filament theory [Junqueira, L.C., et al., 2005] which states that the contraction occurs as the actin filaments slide past the myosin filaments. During contraction, the sarcomere shortens and the filaments overlap to a greater degree.

The sliding filament theory involves the activities' of five different molecules plus calcium ions; myosin, actin, tropomyosin, troponin, ATP (adenosine Triphosphate) and calcium ions (once again, all these terms are presented on the glossary of terms).

The myosin molecule is the shape of a golf club with two heads. The head (cross bridge) has the ability to move back and forth, such flexing movement provides muscle contraction. The hinge portion of the tail allows vertical movement so that the cross bridge can bind to actin as such this movements combined are necessary to perform muscle contraction.

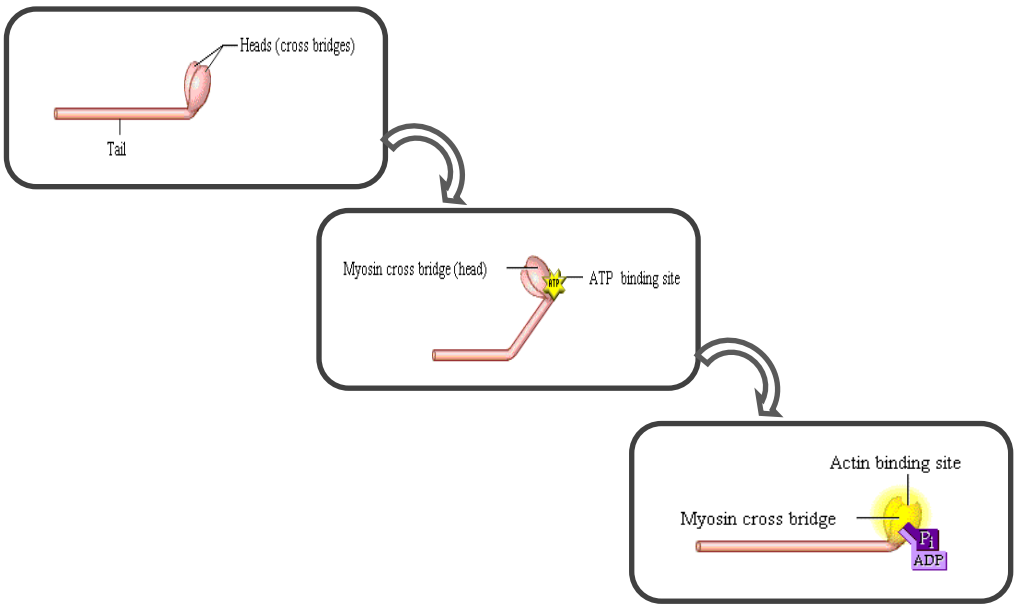

Figure 11 A Myosin molecule.

The cross bridge has two binding sites, one specifically binds ATP and by doing so ATP transfers energy to the myosin making the cross bridge in its high-energy conformation. The other site has a strong attraction for binding to actin.

Actin is a major component of the skeletal muscle's cells where the actin's subunits are arranged into a double helical chain, each one has a specific binding site which the myosin cross bride binds into.

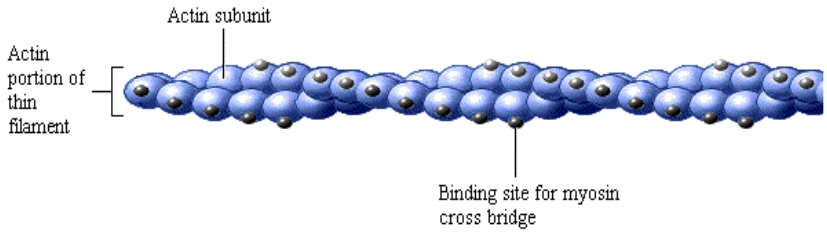

Figure 12 Actin's double helical chain [D'Alessandro, M.P., 1995].

The regulatory protein tropomyosin entwines the actin and in the unstimulated muscle, the position of the tropomyosin covers the binding sites on the actin subunits preventing myosin cross bridges to bind. To expose the binding sites for binding with myosin, the tropomyosin must be moved aside, this is done by a third molecular complex, the troponin, which is periodically spaced along the tropomyosin strand.

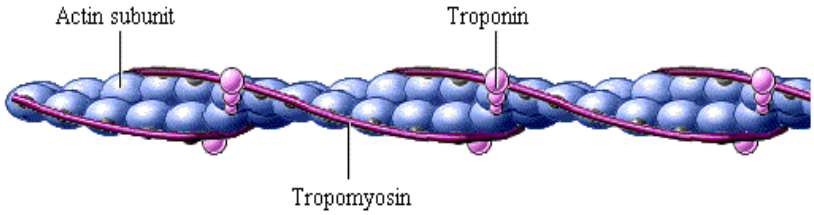

Figure 13 Tropomyosin entwining the actin double helical chain and troponin [D'Alessandro, M.P., 1995].

Troponin itself is not able to move the tropomyosin away from the binding sites, this process requires calcium ions. After an action potential, calcium ions are released from the terminal cisternae and bind to troponin. This causes a conformational change in the tropomyosin-troponin complex making the tropomyosin strands off the binding sites.

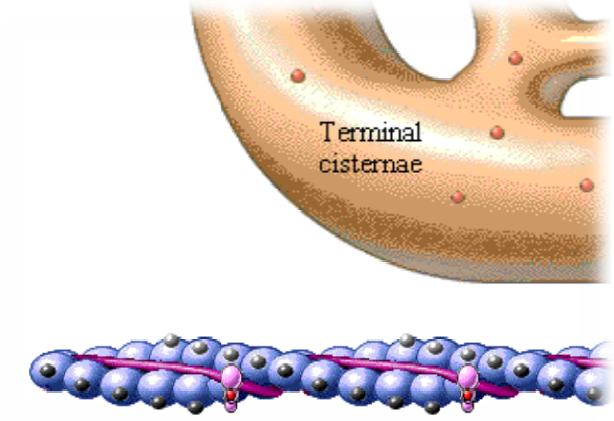

Figure 14 Calcium ions binding the tropomyosin-troponin complex [D'Alessandro, M.P., 1995].

Retracing this cycle it can be admitted as a continuous process that can be split into six steps for easier understanding;

1. The influx of calcium from the terminal cisternae, triggering the exposure of binding sites on actin. An action potential release the calcium ions form the terminal cisternae of the sarcoplasmic reticulum, by doing so the ions flood the cytosol and bond to troponin causing a conformational change on the troponin-tropomyosin complex thus exposing the biding sites of actin.

2. The binding of myosin to actin. When a binding site on actin is exposed, an energized cross bridge can bind to it.

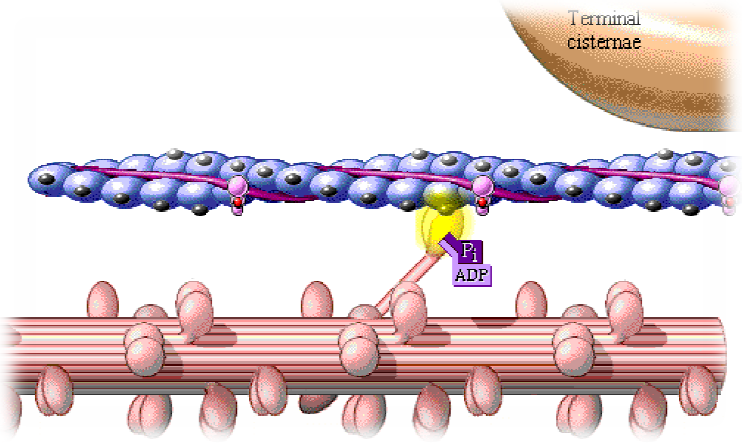

Figure 15 The binding of myosin to actin [D'Alessandro, M.P., 1995].

3. The power stroke of cross bridges that causes the binding of the actin filaments. The binding of the myosin to actin brings about a change in the conformation of the cross bridge, resulting in the release of ATP and inorganic phosphate. At the same time, the cross bridge flexes, pulling the actin filament inward toward the center of the sarcomere, the power stroke. As such the chemical energy of ATP is transformed into mechanical energy of a contraction.

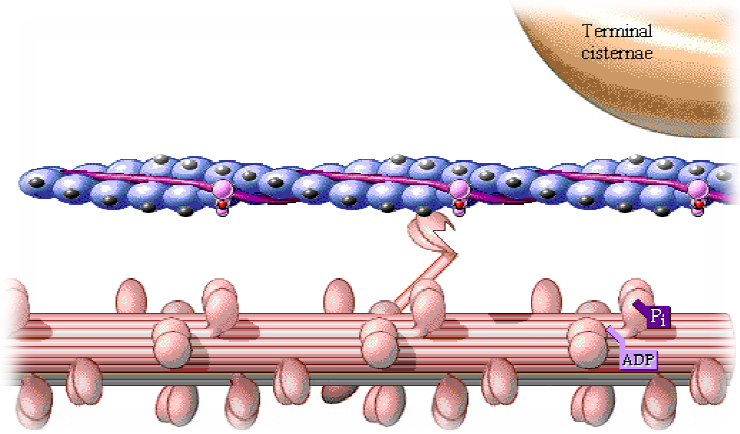

Figure 16 The binding of the myosin to actin brings about a change in the conformation of the cross bridge [D'Alessandro, M.P., 1995].

4. The binding of the ATP to the cross bridge, which results in the cross bridge disconnecting from actin.

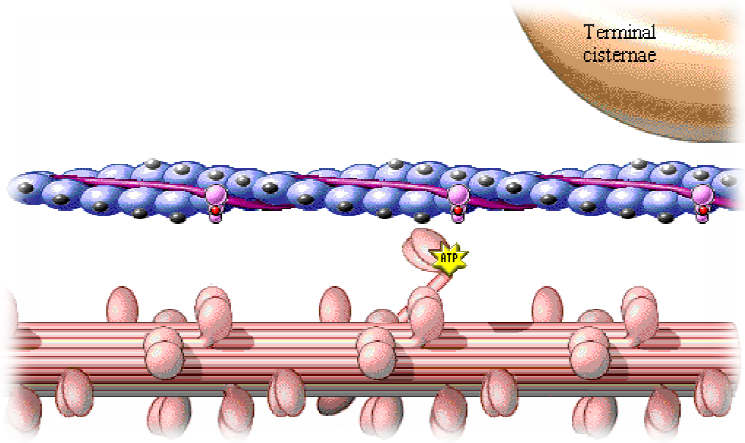

Figure 17 The binding of the ATP to the cross bridge [D'Alessandro, M.P., 1995].

5. The hydrolysis of ATP, which leads to the re-energizing and repositioning of the cross bridge. The ATP hydrolysis is triggered by the release of the myosin cross bridge form actin, into ADP and inorganic phosphate.

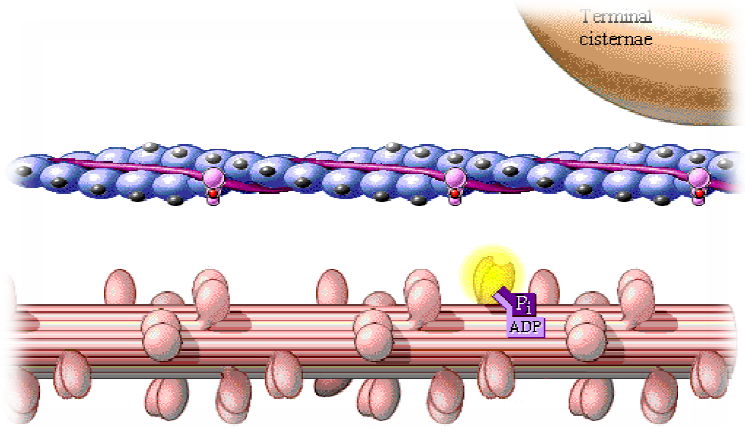

Figure 18 The hydrolysis of ATP [D'Alessandro, M.P., 1995].

6. The transport of calcium ions by ion pumps from the cytosol back into sarcoplasmic reticulum. As the calcium is removed, the troponin-tropomyosin complex recovers the binding sites on actin and because all the sarcomeres contract together, the entire muscle shortens at the same rate.

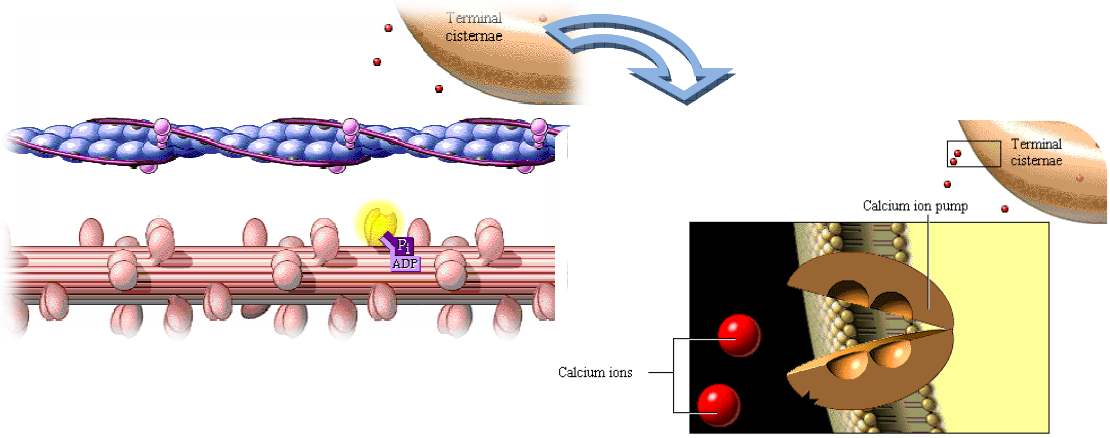

Figure 19 The transport of calcium ions by ion pumps.

In conclusion a muscle contraction can be explained by the cycle of molecular events that take place between actin and myosin filaments and for this sliding filament mechanism occur it is necessary to have sufficient calcium ions Ca^{2+} and ATP available.

2.1.5. Chewing Muscles

The act of chewing involves the use of mastication muscles, hiodeus muscles and although the tongue and buccinator are not directly connected with the act of grinding itself, they help to move the food in the mouth. These four pairs of mastication muscles are the temporalis, masseter and the external and internal pterigoideus.

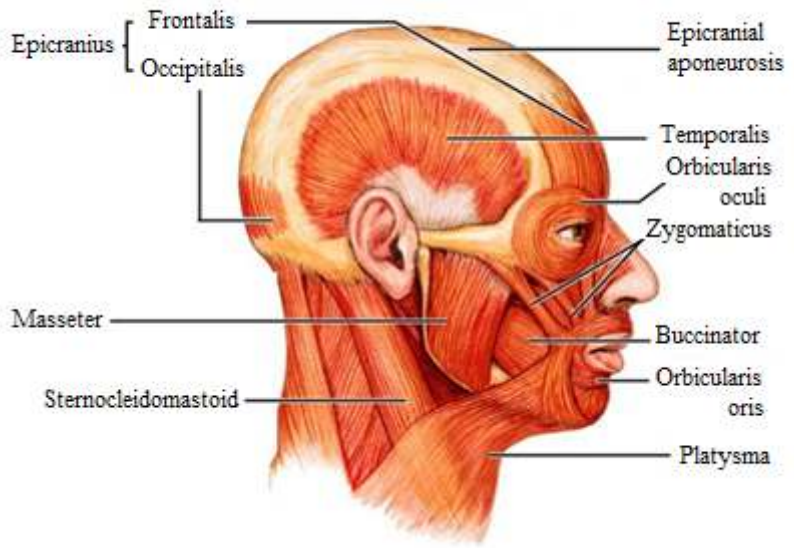

Figure 20 Facial muscles.

The temporalis, masseter, and pterygoideus internus raise the mandible against the maxilla. The Pterygoideus externus aid's in opening the mouth, but its main action is to draw forward the condyle and articular disk so that the mandible is protruded and the inferior incisors projected in front of the upper; this action is assisted by the Pterygoideus internus. The mandible is retracted by the posterior fibers of the Temporalis. If the Pterygoideus internus and externus of one side act, the corresponding side of the mandible is drawn forward while the opposite condyle remains comparatively fixed and side-to-side movements. Such occurs during the grinding of food.

The Temporalis

The Temporalis is a broad, radiating muscle, situated at the side of the head. It arises from the whole of the temporal fossa (except that portion of it which is formed by the zygomatic bone) and from the deep surface of the temporal fascia. Its fibers converge as they descend, and end in a tendon, which passes deep to the zygomatic arch and is inserted into the medial surface, apex, and anterior border of the coronoid process, and the anterior border of the ramus of the mandible nearly as far forward as the last molar tooth on [Gray, H., et al. 1995], thus its importance because it is responsible for elevating and retracting the mandible. The temporal

muscle is actually a composite like structure made of a composition of several layers of skeletal muscle, tendon and fascia. The first layer, starting the dissection from the out to the inside of the head, is of fascia connected to the subcutaneous tissue. The next layer is the muscle, followed by tendon and again muscle until bone is reached. On the upper fraction of the temporalis, the tendon is not visible but becomes stronger as the zygomatic arch is reached. As for the muscle, it's generally thinner on the upper fraction and tends to get thicker as it descends between the skull and the tendon, and to get thinner between the tendon and the fascia.

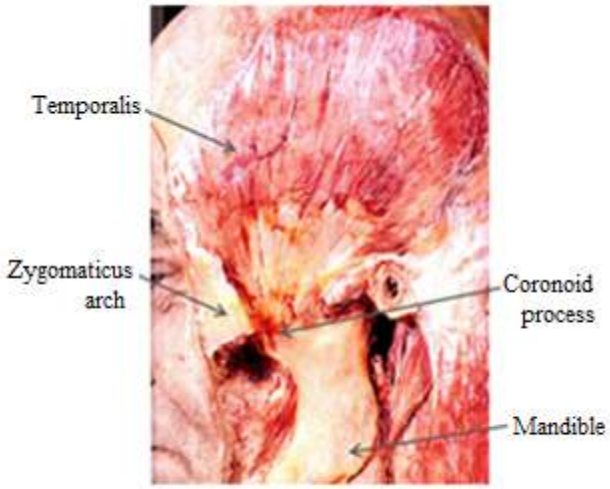

Figure 21 A temporalis after masseter withdrawal, the temporal fascia and part of the zygomatic arch [Gosling, J.A., et al., 2008].

The Masseter

The masseter is a thick, somewhat quadrilateral muscle, consisting of two portions, superficial and deep. The superficial portion, the larger, arises by a thick, tendinous aponeurosis from the zygomatic process of the maxilla, and from the anterior two-thirds of the lower border of the zygomatic arch; its fibers pass downward and backward, to be inserted into the angle and lower half of the lateral surface of the ramus of the mandible. The deep portion is much smaller, and more muscular in texture; it arises from the posterior third of the lower border and from the whole of the medial surface of the zygomatic arch; its fibers pass downward and forward, to be inserted into the upper half of the ramus and the lateral surface of the coronoid

process of the mandible. The deep portion of the muscle is partly concealed, in front, by the superficial portion; behind, it is covered by the parotid gland [Gray, H., et al. 1995].

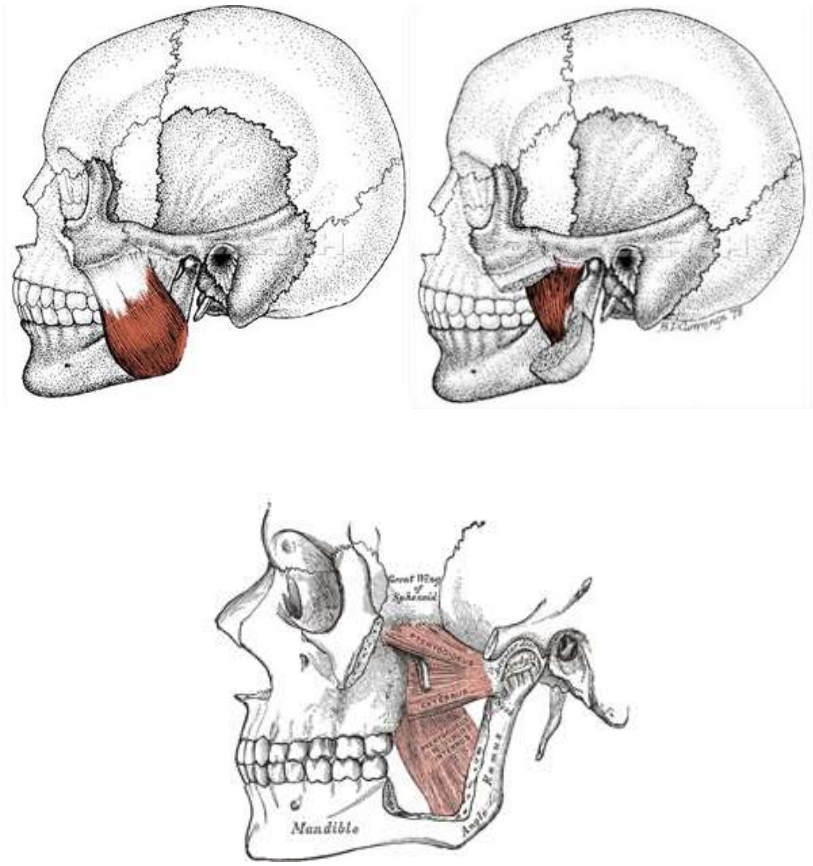

Figure 22 First it's the masseter, and below are the pterigoideus [Gray, H., et al. 1995].

The Pterygoideus

The Pterygoideus externus (External pterygoid muscle) is a short, thick muscle, somewhat conical in form, which extends almost horizontally between the infratemporal fossa and the condyle of the mandible. It arises by two heads; an upper from the lower part of the lateral surface of the great wing of the sphenoid and from the infratemporal crest; a lower from the lateral surface of the lateral pterygoid plate. Its fibers pass horizontally backward and lateralward, to be inserted into a depression in front of the neck of the condyle of the

mandible, and into the front margin of the articular disk of the temporomandibular articulation [Gray, H., et al. 1995] .

The Pterygoideus internus (Internal pterygoid muscle) is a thick, quadrilateral muscle. It arises from the medial surface of the lateral pterygoid plate and the grooved surface of the pyramidal process of the palatine bone; it has a second slip of origin from the lateral surfaces of the pyramidal process of the palatine and tuberosity of the maxilla. Its fibers pass downward, lateralward, and backward, and are inserted, by a strong tendinous lamina, into the lower and back part of the medial surface of the ramus and angle of the mandible, as high as the mandibular foramen [Gray, H., et al. 1995].

2.2. Fasciae

According to the guidelines drawn from the International Fascia Research Congress in 2009, the fascia is a connective soft tissue system that pervades and surrounds muscles, bones, organs, nerves, blood vessels and other structures. It is a continuous three-dimensional network of tissue that extends throughout the body and is responsible for maintaining the integrity of the structure, providing support and protection and also acts as a shock absorber. After injury, it is the fascia that creates an environment for tissue repair. The name fascia can refer to dense planar fascial sheets (such as the Fascia lata) as well as joint capsules, organ capsules, muscular septa, ligaments, retinacula, aponeuroses, tendons, myofascia, neurofascia, and other fibrous collagenous tissues.

In general, fasciae in the musculoskeletal system exhibits two different mechanical and functional types; the muscular fasciae adjacent to spaces that are filled with loose areolar connective tissue and, sometimes, adipose tissue which enables the sliding and gliding of muscles and tendons against each other and against other structures. There also exists intermuscular and epimysial fasciae that serve as areas of insertion for neighboring muscle fibers, which, in this way, can mechanically reach a skeletal element via those fasciae without necessarily being attached directly to the bone [Van Mameren, et al., 1984] .

The head is covered by the galea aponeurotica, a type of planar fascia and right above the temporalis muscle is the temporalis fascia contiguous with the galea aponeurotica. In modern anatomy, an aponeurosis is often considered a flat tendon. This sheet-like geometry is likely to have different mechanical properties from those of tendon, because of differences in morphology, thus it will be subject of study. The aponeurosis may have extra- as well intramuscular elements. Muscle fibers attach to the intramuscular parts and are thus connected via the aponeurosis to tendon and to bone [Langevin, H.M., et al. 2009].

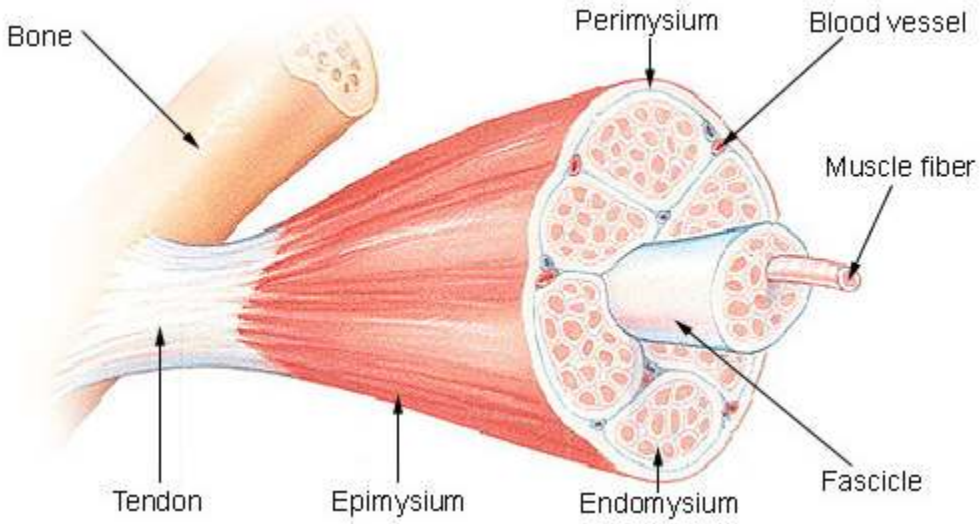

Figure 23 Skeletal muscle's structure [Netter, F.H., 2001].

The fascial structures vocabulary recommended on [Langevin, H.M., et al. 2009] are condensed in the following table,

Table 1 Fascial main structures present on the skeletal muscle.

Fascial Structure	Discription
Epimysium	A multi-layered, irregularly arranged collagen fiber sheet that envelopes muscles and that may contain layers of both dense and areolar connective tissue.
Intra- and extramuscular aponeurosis	A multilayered structure with densely laid down bundles of collagen with major preferential directions. The epimysium also covers the aponeuroses, but is not attached to them. Muscle fibers are attached to intramuscular aponeuroses by their myotendinous junctions.
Perimysium	A dense, multi-layered, irregularly arranged collagen fiber sheet that envelopes muscle fascicles. Adjacent fascicles share a wall of the tube (like the cells of a honeycomb).
Endomysium	Fine network of irregularly arranged collagen fibers that form a tube enveloping and connecting each muscle fiber. Adjacent muscle fibers share a wall of the tube (like the cells of a honeycomb).
Non-dense (areolar) connective tissue	Connective tissue containing sparse, irregularly arranged collagen fibers.

The term fascia is not recommended to be given in such a way that includes tendons and ligaments, for that is simply acknowledging that these structures are forms of connective tissue although they should present different mechanical properties as we will try to demonstrate on the 4th Chapter.

2.3. Tendons

Normal healthy tendons are mostly composed of parallel arrays of collagen fibres closely packed together. The dry mass of normal tendons, which makes up about 30% of the total mass in water, is composed of about 86% collagen, 2% elastin, 1–5% proteoglycans, and 0.2% inorganic components such as copper, manganese, and calcium [Tindball, J.G., et al., 1991].

The dense connective tissue features parallel collagen bundles to each other and aligned with fibroblasts. This connective tissue has its origin form collagen fibers in response to traction forces exerted in a particular direction. In this case fibroblasts that respond to forces that normally act on the tissues and induce fiber orientation in order to offer maximum resistance to these forces [James, H., et al., 2006].

Tendons represent a typical example of a dense modeled structure and are elongated and cylindrical connecting the striated muscles to bones. Because of its richness in collagen fibers, tendons structures are white and are made from thick and dense collagen bundles [Lin, T.W., et al., 2004].

Tendon cells are morphologically classified as fibrocytes, since they contain elongated nuclei parallel to the collagen fibers and thin cytoplasm with few extensions, which often involve bundles of collagen. The bundles of collagen, the primary bundles, aggregate into larger bundles, secondary beams which are surrounded by loose connective tissue containing blood vessels and nerves [Junqueira, L.C., et al., 2005].

Finally, the tendon is surrounded externally by a sheath of dense. In some tendon sheath that is divided into two layers: one attached to the tendon and connected to other nearby structures, between these two layers is formed a cavity containing a viscous liquid containing water and protein and acts as a lubricant, facilitating the sliding tendon within the sheath.

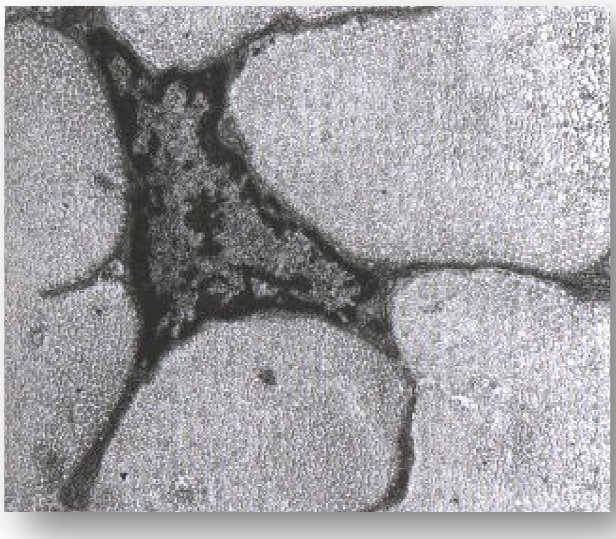

Figure 24 Electron micrography of tendon cross section [Junqueira, L.C., et al., 2005].

Tendon cells can be morphologically classified as fibrocytes, since they contain elongated nuclei parallel to the collagen fibers and thin cytoplasm with few extensions, which often involve bundles of collagen. The collagen bundles of tendons (primary bundles) aggregate into larger bundles (secondary bundles) which are surrounded by loose connective tissue containing blood vessels and nerves [Junqueira, L.C., et al., 2005].

The fascial tendon is surrounded externally by a sheath of dense connective tissue, divided into two layers: one attached to the tendon and another connected to the nearby structures: Between these two layers there is a cavity containing a viscous liquid rich in water and proteins which acts as a lubricant, smoothing the sliding tendon within the sheath [Junqueira, L.C., et al., 2005].

3. Hyperelastic Models

The constitutive models allow the demonstration of the behavior observed in a real material under specific conditions making use of mathematical models. Constitutive equations are a discipline of non-linear mechanics which determines the stress condition of any point for different types of solid bodies. For hyperelastic materials the constitutive equations are based on Helmholtz's equation of strain energy per unit volume [Lai, M.W., et al. 1993].

3.1. Nonlinear strain Measures

On linear stress-strain analysis the deformation of a continuum body is measured in terms of small strain tensor ε [Bonet, J., et al. 1997]. On a two-dimensional example the strain terms are calculated assuming very small u_x , u_y displacements.

$$\varepsilon_{xx} = \frac{\partial u_x}{\partial x} \tag{3.1}$$

$$\varepsilon_{yy} = \frac{\partial u_y}{\partial y} \tag{3.2}$$

$$\varepsilon_{xy} = \frac{1}{2}\left(\frac{\partial u_x}{\partial y} + \frac{\partial u_y}{\partial x}\right) \tag{3.3}$$

But when the body is subjected to large displacements however we must distinguish the initial coordinates from the final ones of particles by using capital letters X, Y for the initial positions and lower case x, y for final coordinates. Considering the following draft if an attempt was to be done using the above equations on this nonlinear case, the solution would contradict physical reality.
P is a particle at the beginning and P' is the same particle after deformation occurred; u is relative to the P particle traveled distance.

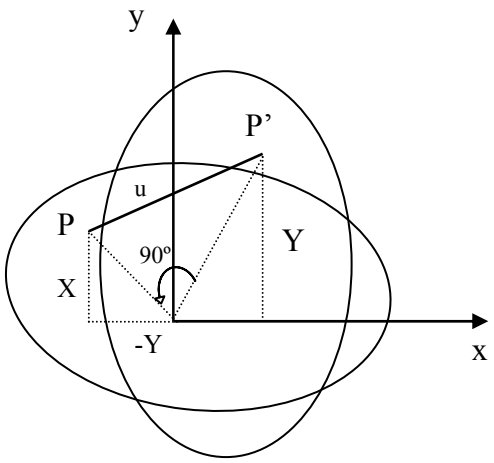

Figure 25 Two-dimensional body, 90 degrees rotation.

The displacements of any particle P are as follows,

$$u_x = -Y - (X) \tag{3.4}$$

$$u_Y = X - Y \tag{3.5}$$

And therefore the equations' application will result in,

$$\varepsilon_{xx} = \varepsilon_{yy} = -1;\ \varepsilon_{xy} = 0 \tag{3.6}$$

Which are incorrect as the body experiences no strains during rotation. Working around the problem we can extend the definition of Green's strain,

$$\varepsilon_G = \frac{l^2 - L^2}{2L^2} \tag{3.7}$$

Were l is the initial length and L is the stretched final length. Consider a small element dX initially parallel to the x axis that is deformed to a ds length as shown in the next picture,

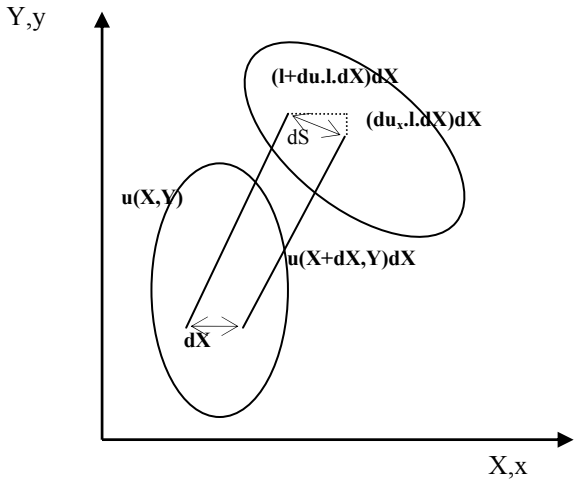

Figure 26 A two-dimensional body's general deformation.

The final length can be calculated from the displacement as,

$$ds^2 = \left(d\mathbf{X} + \frac{\partial x_x}{\partial X} d\mathbf{X}\right)^2 + \left(\frac{\partial u_y}{\partial X} d\mathbf{X}\right)^2 \tag{3.8}$$

Based on the 1-D Green strain equation (number above), the x component of the 2-D Green strain can now be defined as,

$$E_{xx} = \frac{ds^2 - d\mathbf{X}^2}{2d\mathbf{X}^2} \tag{3.9}$$

$$= \frac{1}{2}\left[\left(1 + \frac{\partial u_x}{\partial X}\right)^2 + \left(\frac{\partial u_y}{\partial X}\right)^2 - 1\right] \tag{3.10}$$

$$= \frac{\partial u_x}{\partial X} + \frac{1}{2}\left[\left(\frac{\partial u_x}{\partial X}\right)^2 + \left(\frac{\partial u_y}{\partial X}\right)^2\right] \tag{3.11}$$

And

$$E_{yy} = \frac{\partial u_x}{\partial Y} + \frac{1}{2}\left[\left(\frac{\partial u_x}{\partial Y}\right)^2 + \left(\frac{\partial u_y}{\partial Y}\right)^2\right] \tag{3.12}$$

$$E_{xy} = \frac{1}{2}\left(\frac{\partial u_x}{\partial Y} + \frac{\partial u_y}{\partial X}\right) + \frac{1}{2}\left(\frac{\partial u_x}{\partial X}\frac{\partial u_x}{\partial Y} + \frac{\partial u_y}{\partial X}\frac{\partial u_y}{\partial Y}\right) \tag{3.13}$$

Applying simple rotation to a body $E_{xx} = E_{yy} = E_{xy} = 0$, which now is physically correct.

3.1.1. Deformation Gradient

Kinematics is the study of motion and deformation without reference to the cause [Bonet, J., et al. 1997] and where the analysis of the deformation's gradient tensor is crucial. The deformation gradient is a tensor involved in all equations relating quantities before deformation to corresponding quantities after deformation [Bonet, J., et al. 1997].

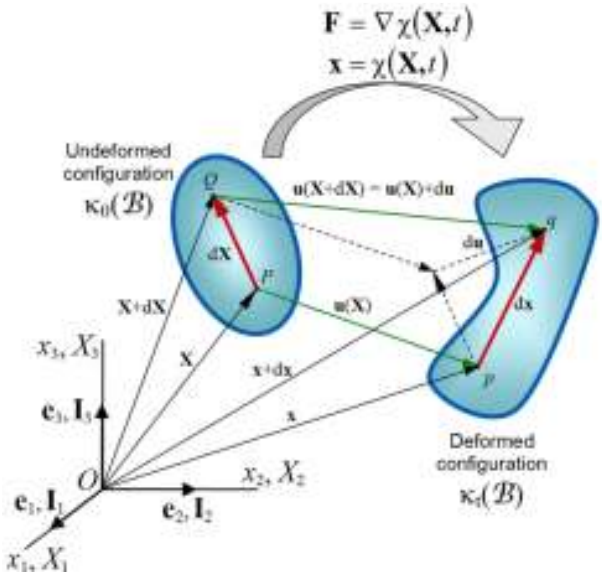

Figure 27 General motion in a particle's neighborhood.

Consider the particle P with initial position defined by the vector $\mathbf{X} = X_I I_1$ in the undeformed configuration. After a body's displacement, the new position is given by $x = x_i \mathbf{e}_1$. Consider now a material point Q neighboring P, with position vector $\mathbf{X} + d\mathbf{X} = (X_I + dX_I)I_1$.
With respect to Figure 27,

$$\mathbf{x} + d\mathbf{x} = \mathbf{X} + d\mathbf{X} + \mathbf{u}(\mathbf{x} + d\mathbf{X}) \tag{3.14}$$

$$d\mathbf{x} = d\mathbf{X} + d\mathbf{u} \tag{3.15}$$

Here du is the relative displacement between Q and P in the deformed configuration.

For an infinitesimal element $d\mathbf{X}$ assuming continuity on the displacement field, it is possible to use a Taylor series expansion around P, neglecting higher order terms, to approximate the components of the relative displacement vector for the neighboring Q, allowing the previous equation to be written as,

$$d\mathbf{x} = d\mathbf{X} + d\mathbf{u} \tag{3.16}$$

$$= d\mathbf{X} + \nabla_X \mathbf{u} \,.\, d\mathbf{X} \tag{3.17}$$

$$= (\mathbf{I} + \nabla_x u) d\mathbf{X} \tag{3.18}$$

$$= \mathbf{F} d\mathbf{X} \tag{3.19}$$

The material deformation gradient tensor is a second order tensor $\mathbf{F}(\mathbf{X}, t) = F_{jI} e_j \otimes \mathrm{I}_K$ that represents the gradient of the functional relation $\chi(\mathbf{X}, t)$ which describes the motion of a continuum. It's related to both the reference and the current configuration by e_i and $\mathbf{E}_I$, therefore is a two-point tensor.

The deformation gradient tensor **F**, in rectangular Cartesian coordinates:

$$[\mathbf{F}] = \begin{bmatrix} \frac{\partial x_1}{\partial X_1} & \frac{\partial x_1}{\partial X_2} & \frac{\partial x_1}{\partial X_3} \\ \frac{\partial x_2}{\partial X_1} & \frac{\partial x_2}{\partial X_2} & \frac{\partial x_2}{\partial X_3} \\ \frac{\partial x_3}{\partial X_1} & \frac{\partial x_3}{\partial X_2} & \frac{\partial x_3}{\partial X_3} \end{bmatrix} \tag{3.20}$$

3.1.2. Strain

The right Cauchy-Green's deformation tensor is defined as,

$$\mathbf{C} = \mathbf{F}^T\mathbf{F} \text{ or } C_{IJ} = F_{kI}F_{kJ} = \frac{\partial x_k}{\partial X_I}\frac{\partial x_k}{\partial X_J} \tag{3.21}$$

Physically is the square of local change in distances due to deformation $dx^2 = d\mathbf{X} \cdot \mathbf{C}d\mathbf{X}$. Cauchy green's invariants are often used on strain energy density functions,

$$I_1^C \coloneqq \text{tr}(\mathbf{C}) = C_{ii} = \lambda_1^2 + \lambda_2^2 + \lambda_3^2 \tag{3.22}$$

$$I_2^C \coloneqq \frac{1}{2}[\text{tr}(\mathbf{C}^2) - (\text{tr}(\mathbf{C}))^2] = \frac{1}{2}\left[C_{IK}C_{KI} - C_{JJ}^2\right] = \lambda_1^2\lambda_2^2 + \lambda_2^2\lambda_3^2 + \lambda_3^2\lambda_1^2 \tag{3.23}$$

$$I_3^C \coloneqq \det(\mathbf{C}) = \lambda_1^2\lambda_2^2\lambda_3^2 \tag{3.24}$$

The left Cauchy-Green's or finger deformation tensor is reached by reversing the order of multiplication in the formula for the right Green-Cauchy deformation,

$$\mathbf{b} = \mathbf{F}\mathbf{F}^T \text{ or } B_{ij} = \frac{\partial x_i}{\partial X_K}\frac{\partial x_i}{\partial X_K} \tag{3.25}$$

Left Cauchy-Green tensor invariants' are also frequently used for strain-energy functions and are defined as,

$$I_1^b \coloneqq \text{tr}(\mathbf{b}) = b_{ii} = \lambda_1^2 + \lambda_2^2 + \lambda_3^2 \tag{3.26}$$

$$I_2^b \coloneqq \frac{1}{2}[\mathrm{tr}(\mathbf{b}^2) - (\mathrm{tr}(\mathbf{b}))^2] = \frac{1}{2}\left[b_{IK}b_{KI} - b_{JJ}^2\right] = \lambda_1^2\lambda_2^2 + \lambda_2^2\lambda_3^2 + \lambda_3^2\lambda_1^2 \quad (3.27)$$

$$I_3^b \coloneqq \det(\mathbf{b}) = J^2 = \lambda_1^2\lambda_2^2\lambda_3^2 \quad (3.28)$$

where J is the deformation gradient determinant.

The concept of strain is used to evaluate how much a given displacement differs locally from a rigid body displacement, one of such strains for large deformations is the Lagrangean finite strain tensor, also called the Green-Lagrangean strain tensor and is defined as,

$$\mathbf{E} = \frac{1}{2}(\mathbf{C} - \mathbf{I}) \text{ or } E_{KL} = \frac{1}{2}\left(\frac{\partial x_j}{\partial X_K}\frac{\partial x_j}{\partial X_L} - \delta KL\right) \quad (3.29)$$

3.1.3. Stress

According to Cauchy, the stress at any point in an object, assumed to be a continuum, is completely defined by the nine components σ_{ij} of a second order tensor known as the Cauchy stress tensor $\boldsymbol{\sigma}$. It gives the current force (at time t) per unit deformed area.

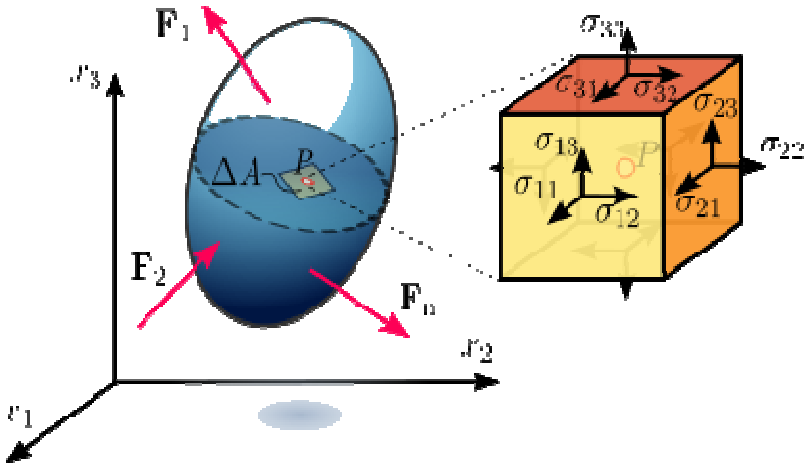

Figure 28 Stress in a loaded deformable material body assumed as a continuum.

$$[\boldsymbol{\sigma}] = \begin{bmatrix} \sigma_{11} & \sigma_{12} & \sigma_{13} \\ \sigma_{21} & \sigma_{22} & \sigma_{23} \\ \sigma_{31} & \sigma_{32} & \sigma_{33} \end{bmatrix} \tag{3.30}$$

The Cauchy stress tensor is used for stress analysis of material bodies experiencing large deformations. For large deformations, other measures of stress are required, such as the first and second Piola-Kirchhoff stress tensors, the Biot stress tensor, and the Kirchhoff stress tensor.

Simply by multiplying $\boldsymbol{\sigma}$ by the determinant of $\mathbf{F}$ gives the Kirchhoff stress tensor $\boldsymbol{\tau}$ as,

$$\boldsymbol{\tau} = J\,\boldsymbol{\sigma} \tag{3.31}$$

To express $d\mathbf{P}$ (is the elemental force vector acting on the elemental area $d\mathbf{A}$ requires a new stress tensor T called the first Piola-Kirchhoff (P-K) stress tensor giving,

$$d\mathbf{P} = \mathbf{T} \cdot d\mathbf{A} \quad \text{where} \quad d\mathbf{A}_0 = dA_0\mathbf{N} \tag{3.32}$$

This implies that for a given undeformed unit normal **N**, the first P-K stress gives the current force per unit undeformed area [Hinton, E., 1992] .

Recalling that $d\mathbf{X} = \mathbf{F}^{-1} \cdot \ d\mathbf{x}$ and transforming $d\mathbf{P}$ in the same way giving $d\widehat{\mathbf{P}} = \mathbf{F}^{-1}.\ d\mathbf{P}$, we can write,

$$d\widehat{\mathbf{P}} = \mathbf{S} \cdot d\mathbf{A}_0 \quad \text{where} \quad \mathbf{S} = \mathbf{F}^{-1}\,\mathbf{T} \tag{3.33}$$

Thus for a given undeformed unit normal **N** the second P-K gives the transformed force per unit undeformed area [Hinton, E., 1992] .

3.2. Hyperelastic Constitutive Models

A Cauchy-elastic or elastic material is one in which the Cauchy stress at each material point is determined only by the current state of deformation with respect to an arbitrary reference configuration [Ogden, R.W., 1984] .usually the undeformed configuration. The Cauchy stress in such a material doesn't depend on the deformation path or on the deformation's history. Neither does the stress depend on the time taken to achieve that deformation or the rate at which the state of deformation is reached unlike a hyperelastic material nor does Green elastic material where the work done by stresses depend on the deformation path.

A hyperelastic material is applied for ideally elastic materials for which the stress-strain relationship derives from a strain energy density function a frequent example of this kind of material is the rubber, whose stress-strain relationship can be defined as non-linearly elastic, isotropic, incompressible and generally independent of strain rate.

In order to obtain the hyperelastic material's constitutive equation the following strain-energy function is generated,

$$W = W(\mathbf{F}) - p(J - \mathbf{I}) \tag{3.34}$$

Where p is a Lagrangean multiplier identifiable with hydrostatic pressure and can be determined by equilibrium equation e boundaries.

By the hyperelastic material definition the 1st P-K tensor is,

$$\mathbf{T} = -p\mathbf{F}^{-T} + \frac{\partial W(\mathbf{F})}{\partial \mathbf{F}} \tag{3.35}$$

And the 2nd P-K tensor is,

$$\mathbf{S} = -p\mathbf{F}^{-1}\mathbf{F}^{-T} + \mathbf{F}^{-1}\frac{\partial W(\mathbf{F})}{\partial \mathbf{F}} = -p\mathbf{C}^{-1}\frac{\partial W(\mathbf{C})}{\partial \mathbf{C}} \tag{3.36}$$

3.2.1. St. Venant-Kirchhoff Model

The simplest hyperelastic material model is the Saint Venant-Kirchhoff (V-K) model which is just an extension of the linear elastic material model to the nonlinear regime. The strain-energy function density function for the St. V-K model is,

$$W(\mathbf{E}) = \frac{\lambda}{2}[\mathrm{tr}(\mathbf{E})]^2 + \mu\,\mathrm{tr}(\mathbf{E}^2) \tag{3.37}$$

And the 2nd P-K stress tensor can be obtained by the relation,

$$\mathbf{S} = \frac{\partial W}{\partial \mathbf{E}} \tag{3.38}$$

$$\mathbf{S} = \lambda \, \mathrm{tr}(\mathbf{E})\mathbf{I} + 2\mu\mathbf{E} \tag{3.39}$$

Where **S** is the 2nd P-K stress tensor, **E** is the Lagrangean Green strain and λ, μ are the Lamé constants.

3.2.2. Ogden Material Model

This model is frequently used to characterize the behavior of complex materials such as rubbers, polymers, and biological tissue which are generally considered to be isotropic, incompressible and strain rate independent [Ogden, R.W., 1984]. Ogden's strain-energy density function can be expressed in terms of the principal stretches as,

$$W(\lambda_1, \lambda_2, \lambda_3) = \sum_{p=1}^{N} \frac{\mu_p}{\alpha_p} \left(\lambda_1^{\alpha_p} + \lambda_2^{\alpha_p} + \lambda_3^{\alpha_p} - 3 \right) \tag{3.40}$$

Where *N* is a positive integer number which controls the number of terms in the equation, μ_p is the shear modulus and α_p are dimensionless constants. Under the assumption of incompressibility one can rewrite as,

$$W(\lambda_1, \lambda_2) = \sum_{p=1}^{N} \frac{\mu_p}{\alpha_p} \left(\lambda_1^{\alpha_p} + \lambda_2^{\alpha_p} + \lambda_1^{-\alpha_p} \lambda_2^{-\alpha_p} - 3 \right) \tag{3.41}$$

In general the shear modulus results from,

$$2\mu = \sum_{p=1}^{N} \mu_p \alpha_p \text{ with } \mu_p \alpha_p > 0\,, \qquad p = 1, \dots, N \tag{3.42}$$

For particular values, the Ogden model will reduce to either the Neo-Hookean solid ($N = 1$, $\alpha = 2$) or the Mooney-Rivlin material ($N = 2$, $\alpha_1 = 2$, $\alpha_2 = -2$).

From the hyperelastic definition,

$$\sigma_i = p + \lambda_i \frac{\partial W}{\partial \lambda_i} \tag{3.43}$$

Which applied to Ogden's model and added to boundary condition's $\sigma_2 = \sigma_3 = 0$ and the pressure p determined from incompressibility,

$$\sigma_\alpha = \sum_{p=1}^{N} \left(\mu_p \lambda_p^{\alpha_p} - \mu_p \lambda_p^{-\frac{1}{2}\alpha_p} \right) \tag{3.44}$$

Where

$$\sigma_1 = \sum_{p=1}^{N} \mu_p \left(\lambda_1^{\alpha_p} - (\lambda_1 \lambda_2)^{-\alpha_p} \right) \tag{3.45}$$

And

$$\sigma_2 = \sum_{p=1}^{N} \mu_p \left(\lambda_2^{\alpha_p} - (\lambda_1\lambda_2)^{-\alpha_p}\right) \tag{3.46}$$

Finally the Cauchy stress expression for the uniaxial extension, when *N*=1, is,

$$\sigma_{ogden} = c_1(\lambda^{c_2} - 2^{-1+c_2}\lambda^{-c_2/2}) \tag{3.47}$$

3.2.3. Mooney-Rivlin's Model

It's an Ogden's reduced version with *N*= 2, $\alpha_1 = 2$ and $\alpha_2 = -2$. Using the invariants I_1, I_2 with the condition $I_3 = \lambda_1^2\,\lambda_2^2\lambda_3^2 = 1$ [Holzappfel, G.A., 2004]. The resulting strain-energy function is,

$$W = c_1(\lambda_1^2 + \lambda_2^2 + \lambda_3^2 - 3) + c_2(\lambda_1^{-2} + \lambda_2^{-2} + \lambda_3^{-2} - 3) \tag{3.48}$$

Or

$$W = c_1(I_1^C - 3) + c_2(I_2^C - 3) \text{ with the constants } c_1 = \frac{\mu_1}{2}, c_2 = \frac{\mu_2}{2} \tag{3.49}$$

Adopting eq. 3.42, the shear modulus μ may be specified as,

$$\mu = 2\left(\frac{\partial\psi}{\partial I_1} + \frac{\partial\psi}{\partial I_2}\right) = 2(c_1 + c_2) > 0 \tag{3.50}$$

The relation for the shear stress is linear with the constant inclination $2(c_1 + c_2)$.
To conclude the Cauchy stress expression for the uniaxial extension is,

$$\sigma_{Mooney} = 2\left(\lambda^2 - \frac{1}{\lambda}\right)(c_1 + c_2\frac{1}{\lambda}) \tag{3.51}$$

3.2.4. Neo-Hooke Model

It's also an Ogden's reduced version now with *N*= 1, $\alpha_1 = 2$. The strain-energy resulting equation is,

$$W = c_1(\lambda_1^2 + \lambda_2^2 + \lambda_3^2 - 3) \tag{3.52}$$

And,

$$W = c_1(I_1^C - 3) \text{ with } c_1 = \frac{\mu_1}{2} \tag{3.53}$$

The shear modulus is $\mu_1 = \mu$ according to eq. 3.42.

The strain-energy function involves a single parameter only and provides a mathematically simple and reliable constitutive equation for the nonlinear deformation behavior of isotropic rubber-like materials. It relies on phenomenological considerations and includes typical effects known from nonlinear elasticity within the small strain domain [Holzappfel, G.A., 2004].

Lastly the Cauchy stress expression for the uniaxial extension is,

$$\boldsymbol{\sigma}_{Neo-Hooke} = 2(\lambda^2 - \frac{1}{\lambda})c_1 \tag{3.54}$$

3.2.5. Yeoh Model

The phenomenological material model Yeoh is motivated in order to simulate the mechanical behavior of carbon-black filled rubber. These fine filler particles are added to the elastomers in order to improve their physical properties which are mainly tensile and abrasion resistant [Yeoh, O.H., 1993]. From the relation for the shear stress,

$$\mu = 2\left(\frac{\partial \psi}{\partial I_1} + \frac{\partial \psi}{\partial I_2}\right) = 2(c_1 + c_2) > 0 \tag{3.55}$$

Yeoh made a simplifying assumption that $\frac{\partial \psi}{\partial I_2}$ is equal to zero and proposed a strain energy function where the second strain invariant does not appear,

$$\Psi = c_1(I_1 - 3) + c_2(I_1 - 3)^2 + 6c_3(I_1 - 3)^3 \tag{3.56}$$

With $c_1, c_2\ and\ c_3$ are constants that must satisfy certain restrictions. The strain energy function is either zero or positive and for an incompressible material $I_1 \geq 3$. The convex function increases monotonically with I_1 and $\frac{\partial \psi}{\partial I_1}$ has no real roots.

Now with the strain energy function it can be concluded that,

$$\mu = 2c_1 + 4c_2(I_1 - 3) + 6c_3(I_1 - 3)^2 > 0 \tag{3.57}$$

The shear modulus involves first-order and second-order terms in $(I_1 - 3)$ when $c_1 >, c_3 > 0$ and $c_2 < 0$

To conclude the Cauchy stress expression for the uniaxial extension,

$$\boldsymbol{\sigma}_{Yeoh} = 2\left(\lambda^2 - \frac{1}{\lambda}\right)(c_1 + 2c_2(I_1 - 3) + 3c_3(I_1 - 3)^2) \tag{3.58}$$

4. Force Transmission

The various constitutive equations presented on chapter 3 that follow the phenomenological approach, are able to successfully fit mathematical equations to experimental data and so describing the macroscopic nature of materials as continua. However these phenomenological based functions are not capable of relating the deformation mechanism to the microscopic structure of the material for this reason on this chapter a different approach is taken in order to describe the muscle's behavior within the nonlinear regime and the large deformations' theory.

To understand the available literature on the subject of force transmission within the skeletal muscles one must first study the myotendinous junction (MTJ). Most muscle injuries occur at the MTJ, a famous one is the known as the Achilles tendon which is formed by the confluence of the medial gastrocnemius, lateral gastrocnemius, and soleus muscles

4.1. Within Skeletal Muscle Force Transmission

Historically, skeletal muscle has been modeled for biomechanical analysis as a network of parallel cells passing from a tendinous origin to a tendinous insertion, with each cell consisting of an array of parallel myofibrils running uninterrupted along the length of cell [Monti, R.J., et al., 1999], (see Figure 29).

The MTJ is the location at which the network of myofibrils terminates in the cell membranes at the end of a cylindrical muscle fiber and is assumed to be the primary site to force transmission on skeletal muscles hence it's a very important structure to characterize the mechanical properties responsible for transmitting forces form the myofibrils to the tendon.

Figure 29 The Myotendinous junction.

Examining the anatomy of the MTJ in order to better understand how it functions; the numerous folds serve not only to increase the surface area but also to transmit the force applied to the myofibrils as a shear force rather than a tensile force on the membrane [Monti, R.J., et al., 1999]. Microscopically the linking connections between the contractile fibrils are made of protein complexes including vinculin and dystrophin by [Tindball, J.G., et al., 1991].

Physiological evidences first provided [Street S.F., 1983] demonstrate that only a portion of the force is transmitted from the myofibrils to the MTJ because of the lateral transmission mechanism in which the forces are transmitted laterally through the cell membrane or extracellular matrix of the myofibrils. It was verified that not only passive but also active forces are transmitted by the sarcolemma of single fibbers by means of an experimental procedure in which two preparations of a

single fibber in which both had one end surrounded by a bundle of transected fibbers as shown on Figure 30,

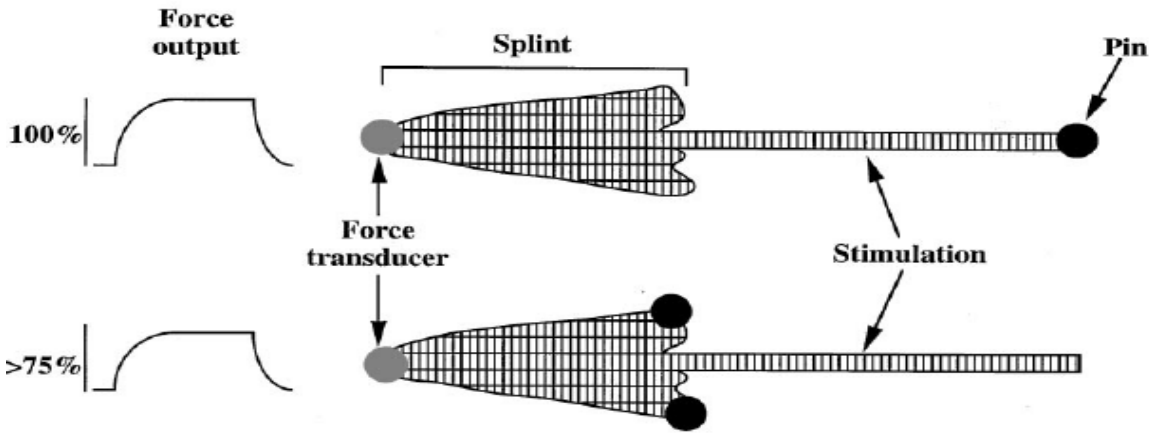

Figure 30 Diagrammatic representation of the experiments performed [Street S.F., 1983].

The experiment showed that when not held at its free end a fibber could transmit to the tendon on the distal end of the splint 76-100% of the force it transmitted when held at both ends which proved that if force transmission was primarily focused at MTJs. Thus MTJ relied on the ability of a muscle to pull its attachments closer together, then a cell held only at one end should merely shorten and not be able to transmit force to the held end [Monti, R.J., et al., 1999]. On the contrary what happens is that the cells are linked at various points along the sarcolemma, and they apply forces by pulling against one another.

The author [Street S.F., 1983] has also presented cytoarquitectural data which helped explain the large proportion of the force that is transmitted through the splint. Imagine a linear cell that ran along the full length of the muscle; that meant that only the peripheral cells would be able to transmit forces to the membrane then the force produced by a splinted fibber at one end would dependent on the number of myofibrils at the periphery of the cell, instead if the myofibrils branch and blend with one another that would allow the central myofibrils to transmit forces throughout the net increasing MTJ's viability.

Also recent experiments support the theory that there is linkage between myofibrils and extracellular matrix; in bundles of skeletal muscle fibers stretched to the point of MTJ's failure, sarcomeres in those fibbers which failed remained stretched. If in those fibbers there were no lateral connections, passive elements within sarcomeres would return them to their resting length when MTJ failed. Therefore, there must be some link between myofibrils to maintain similar sarcomere lengths [Law, D.J., et al., 1993] .

4.1.1. Muscle -Tendon association

Forces appear to be transmitted through the muscles via the MTJ and the intramuscular connective tissue to the tendon, although it isn't quite clear yet how the musculotendinous system depends upon the connective tissue to store mechanical energy and release it in appropriate time. One possibility is rather than the tendon, the aponeurosis and the components of the interfiber matrix being strictly transmitters of muscle force, they may act in concert with muscle to improve the total output by storing and releasing energy [Monti, R.J., et al., 1999].

Several experiments done on kangaroos' hoping [Morgan, et al., 1978], show that there is in fact some elastic energy storage occurring on the tendons and connective tissues by measuring energy loss with full tendon in place and with portion of the tendon excluded from the experimental system at strains up to 3,7% and as much as 60% of the total output could be attributed to the tendon. Demonstrating the potential of tendon to serve as a sink for strain energy [Bennett, M.B., et al. 1986] showed for various other species that in some cases as much as 90% of strain energy was recovered during repetitive stretch-shortening cycles at frequencies and stresses during locomotion.

Other evidences collected using ultrasonic imaging during in vivo movements of the skeletal muscle [Fukunaga, T., et al. 1997], revealed fascicle length decreasing during "static" contractions which could indicate strain of elastic elements in the muscle-tendon complex. Figure 31 shows the significance of this strain without the change of length of the musculotendinous unit.

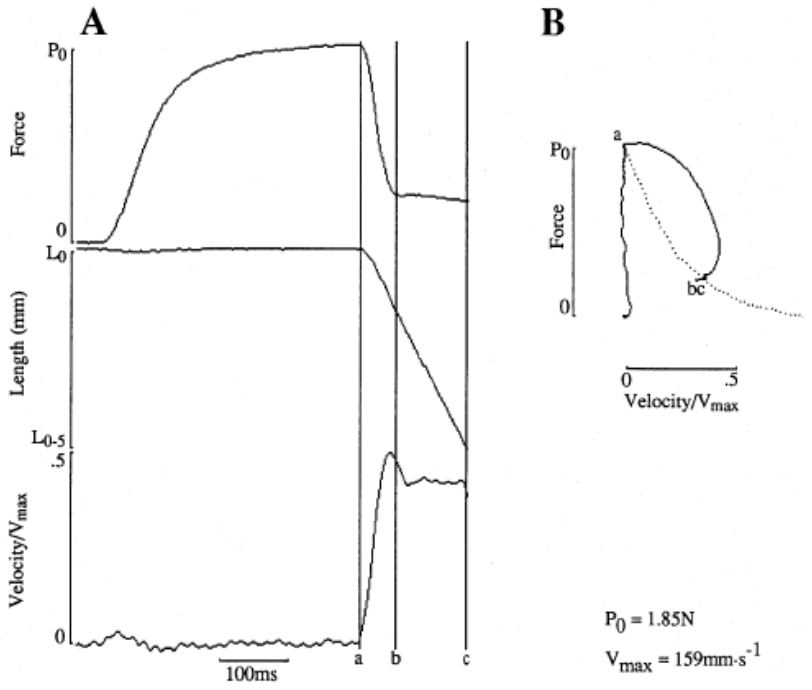

Figure 31 Isometric contraction of a whole rat soleus in situ. The muscle is allowed to shorten at a constant velocity similar to those occurring in locomotion (fig. A). The iso-velocity curve (fig. B) displays the storage of strain energy in a muscle that never received a stretch [Monti, R.J., et al., 1999].

Currently there are two theories that explain this energy release; the first one says that although the musculotendinous unit is isometric, the muscle shortens, thereby lengthening the series elastic element and introducing strain energy; and the second one that contraction of the muscle causes a realignment of the intramuscular connective tissue which releases energy when it returns to its resting arrangement [Monti, R.J., et al., 1999]. Both conditions have been proved by different experimental data, [Gregor, R. J., et al. 1988] and [Fukunaga, T., et al. 1997] for the first condition and [Trotter, J.A., 1993] for the second one therefore it is appropriate to suggest that all connective tissue in the musculotendinous complex is a portion of the series elastic element [Trotter J. A., 1990].

4.1.2. Structure and Functional Roles of Endomysium

The interstitial space between two adjacent cells is occupied as previously discussed by the endomysium, a substantial reticular layer built of a comprised network of collagen fibrils and fibbers in a proteoglycan matrix that runs across the whole muscle fascicle [Swatland, H.J., 1975] and whose thickness varies according to the total length of the muscle.
Transmission electron micrography of intact endomysium in situ confirms that all the collagen fibbers in the network layer lie in the plane of the layer [Purslow, P.P., 2010] and the thick reticular region of the endomysium is often described as a random or quasi-random network of irregular wavy fibers although this is not entirely true for there's a preferable direction for collagen fibber orientations that also changes with muscle length [Purslow, P.P., et al., 1994] and [Trotter, J.A., 1991] the mechanical importance of this is that the planar network will be very complaint in tension along the fibber direction and can easily deform to follow changing muscle lengths in vivo which potentially could provide overload protection at high deformations.

The endomysium is the only structure that links muscle fibers together within fascicles [Purslow, P.P., 2010] and on undamaged conditions the orientation and curvilinearity of the collagen fibers make the endomysium very complaint in tension, however within normal activity muscles are frequently injured and that fact may increase the role of force transmission in tension by the endomysium according to [Trotter, J.A., 1992].

4.2. Endomysium Through Thickness Shear Properties

The original concept on force transmission through the intramuscular connective tissue (IMCT) given by [Trotter, J.A., 1993] is the shear through the endomysium which is the most important mechanism explaining efficient linkage even as most fibers aren't directly connected to an aponeurosis of tendon, therefore due to narrow thickness of the membrane, even large translaminar

shear strains, would only contribute miniscule tensile elongations of the order of 1μm throughout the length of the fiber.

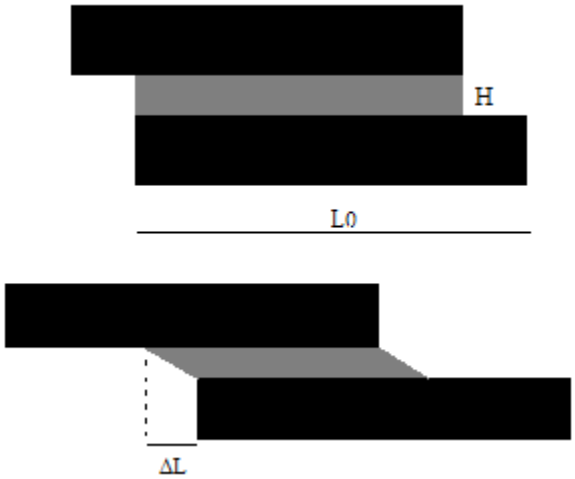

Figure 32 Diagram on shear displacement between two fibers and the endomysium. ΔL is very small comparing to initial and final length of the fiber, and L0/H is typically of 104 [Trotter, J.A., 1992].

In order to quantify *Pruslow's* theory [Purslow, P.P., 2002], the scheme above must be considered, where E_f is the axial stiffness of the fibers with L Length, joined by and endomysial matrix of G shear modulus and H thickness.

Assuming a simple linear model where F is the force generated along the direction of muscle action and W is the width, the stress is,

$$\tau_{xy} = \frac{F}{LW} \text{ is the shear stress} \tag{4.1}$$

And

$$\gamma_{xy} = \frac{\Delta L}{H} \text{ is the shear strain} \tag{4.2}$$

They can be related to the endomysium shear modulus *G*,

$$\mu = \frac{\tau_{xy}}{\gamma_{xy}} = \frac{F\ H}{L\ W\ \Delta L} \tag{4.3}$$

Also the shear displacement can also be related to ΔL using an apparent longitudinal tensile displacement related to the applied longitudinal forces, resulting into an apparent tensile modulus E_{app},

$$E_{app} = \frac{\sigma}{\varepsilon} = \frac{F/_{HW}}{\Delta L/_{L}} = \frac{F\ L}{\Delta L\ H\ W} \tag{4.4}$$

$$E_{app} = \frac{F\ L}{\Delta L\ H\ W} \times \frac{H}{L} \times \frac{L}{H} \tag{4.5}$$

$$E_{app} = \frac{F\ H}{\Delta L\ L\ W} \times \frac{L}{H} \times \frac{L}{H} \tag{4.6}$$

$$E_{app} = \mu \times \left(\frac{L}{H}\right)^2 \tag{4.7}$$

As the length is always several cm's longer than the thickness *H*, the calculated apparent young modulus is several order higher than true shear modulus of the endomysium. This fact means tensile contribution to deformation is much more important than endomysial shear contribution to overall assembly deformation.

Even though local shear strains are present in the endomysium, the overall picture for the entire composite structure is that fiber's young modulus will be numerically higher and E_{app}. We can represent the shear element as a tensile element in series with the fibers,

Figure 33 Schematic diagram on the composite structure.

$$\varepsilon_c = \varepsilon_f + \varepsilon_{app} \tag{4.8}$$

Where by definition

$$\frac{\sigma_c}{E_c} = \frac{\sigma_f}{E_f} + \frac{\sigma_{app}}{E_{app}} \tag{4.9}$$

As $\sigma_c = \sigma_f = \sigma_{app}$ because structures are in series, the composite tensile modulus E_c is given by;

$$\frac{1}{E_c} = \frac{1}{E_f} + \frac{1}{E_{app}} \tag{4.10}$$

This mathematical expression demonstrates the previous argument that the apparent modulus is overcome by the fibers' tensile modulus as it is expected the same behavior with bundles of fibers.

4.3. The endomysium Through-Thickness Shear Properties Non-Linear Mechanics approach

In order to simplify the problem may be divided it into two simpler sub-problems, of pure shear and the uniaxial tension case. Pure shear is determined starting from a rectangular element, whose deformation gradient is as follows,

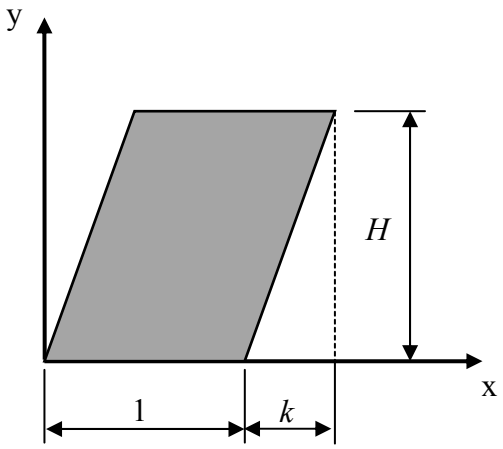

Figure 34 illustration of pure shear, 2D.

$$[\mathbf{F}] = \begin{bmatrix} 1 & \frac{k}{H} & 0 \\ 0 & 1 & 0 \\ 0 & 0 & 1 \end{bmatrix} = 1, \quad \det(\mathbf{F}) = 1 \tag{4.11}$$

The second order tensor **F**, is also set from the uniaxial stretching case,

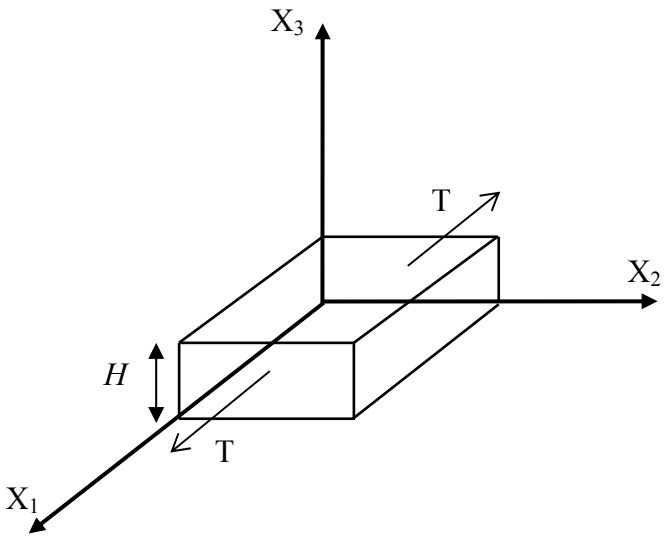

Figure 35 The uniaxial stretching.

$$[\mathbf{F}] = \begin{bmatrix} \frac{k}{H} & 0 & 0 \\ 0 & \frac{1}{\sqrt{\frac{k}{H}}} & 0 \\ 0 & 0 & \frac{1}{\sqrt{\frac{k}{H}}} \end{bmatrix}, \quad \det(\mathbf{F}) = 1 \tag{4.12}$$

For each case, the Cauchy-Green deformation tensor is given in terms of deformation gradient, followed by the material or Lagrangian tensor, **E**.

As shown earlier on this chapter the Cauchy stress tensor can be obtained by,

$$\boldsymbol{\sigma} = \mathbf{F}\,\mathbf{S}\,\mathbf{F}^{T} \tag{4.13}$$

Resorting to the definition,

$$\sigma_{xx} = \frac{F}{W\,H} \Leftrightarrow \frac{F}{W} = H\,\sigma_{xx} \tag{4.14}$$

And,

$$\tau_{xy} = \frac{F}{W\,L} \Leftrightarrow \frac{F}{W} = L\,\tau_{xy} \tag{4.15}$$

Matching eq. 1.14 with eq. 4.15, and solving in order of λ, we have the following result,

$$\lambda = \frac{2\mu(-H^4k^3 +)H^4kL^2 + L^5H^2 + L^5k^2}{H^4k^3 - 3H^4kL^2 + 2H^4L^3 - L^5k^2} \tag{4.16}$$

Remembering that λ, μ and E can be related by,

$$\lambda = \frac{2\,\mu - E}{E - 3\,\mu} \tag{4.17}$$

The final equation is,

$$E = \frac{2\mu(H^4k^3 - 3H^4kL^2 + 2H^4L^3 - L^5k^2 - 3\mu H^4k^3 + 3\mu H^4kL^2 + 3\mu L^5H^2 + 3\mu L^5k^2)}{H^4k^3 - 3kH^4L^2 + 2H^4L^3 - L^5k^2 - 2\mu H^4k^3 + 2\mu H^4L^2 + 2\mu L^5H^2 + 2\mu L^5k^2} \tag{4.18}$$

Eq. 4.18, depends on L, H, on the material constant μ and on the stretch k.

Recalling eq. 4.7, according to [Purslow, P.P., 2002] based on the linear solid mechanics' theory, Young modulus E varies linearly with the shear modulus μ and is of a quadratic order to H and L. Recurring to the large deformation's theory, L and H are now raised to higher orders, the material constants μ has no longer a linear behavior and the stretch k, absent on eq. 4.18 function, attends the author's equation, perfectly expected due to the non-linear theory's appliance.

5. Establishment of the Mechanical Properties of the temporal Muscle

The experimental procedure consisted of several successive stages: collecting the samples at the National Institute of Forensic Medicine INML followed by the experimental protocol on BML the Biomechanics' Laboratory at the Institute of Mechanical Engineering. All data and observations were collected and registered at the time; an example of the lab report was added on the appendix.

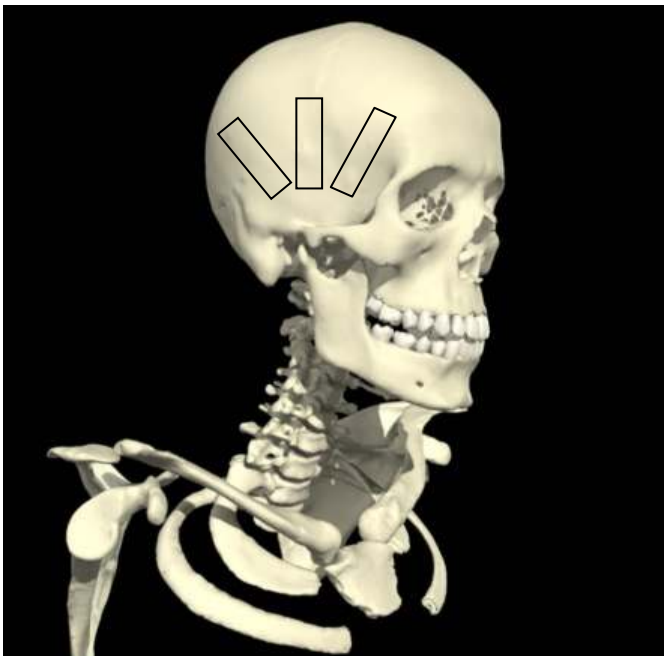

Figure 36 The squares lying on the skull represent the samples' direction and approximate geometry. Although they are not scaled [McMinn, 2002].

Each individual sample was surgically dissected respecting the fibers direction whenever possible, as shown on Figure 36.

The temporalis tissue used to perform the mechanical tests was collected from twelve cadavers; Table 2 provides a characterization of the patients,

Table 2 Samples characteristics.

Collected Sample	**Gender**	**Age**	**Remaining teeth on the Upper Left side**	**Remaining teethon the Bottom Left side**	**Remaining teethon the Upper Right side**	**Remaining teethon the Bottom Right side**
I	Fem.	36	all	all	all	all
II	Masc.	61	all but 17	all but 27,28	all but 44,45,46	all but 36
III	Masc.	61	none	none	44,45,46	31,32, 37,38
IV	Fem.	34	all	all	all	all
V	Masc.	20	all but 14	all	all but 47,48	all
VI	Masc.	50	none	none	41,42, 43,44	31,32, 33,34
VII	Fem.	80	none	none but 23	none but 42	none but 32
VIII	Masc.	43	11,12, 13,14	21,22,24	all but 47	all
IX	Masc.	63	11,12, 13,14	21,23,27	41,42, 43,44	31,32,33
X	Masc.	46	none	none but 21,22	43	none but 32
XI	Masc.	52	none	none	41,42, 43,44,45	31,32, 33,34,35

The nomenclature used to distinguish the teething is based on the model used by INML professionals. From numbers 11 to 18 and 41 to 48 it's considered the left side of the mouth; as

such the remaining numbers belong to the right side of the mouth. The temporalis tissue excised during autopsy was preserved in a saline solution bath. The saline bath temperature was kept at 10ºC until the mechanical tests were performed. The storage time did not exceed 12 h, and for most of the samples it did not exceed 6h.

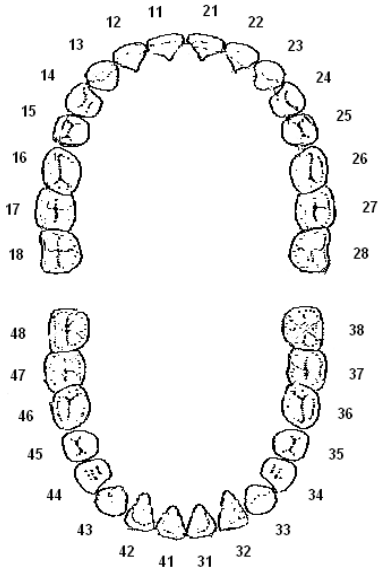

Figure 37 Dental disposition's draft.

All samples were dissected and separated into muscle, fascia and tendon and after careful preparation, every specimen was divided according to a parallelepiped geometry and the fibers direction is preferably parallel to the edge, wherever's possible, avoiding sharp defects on the cut.

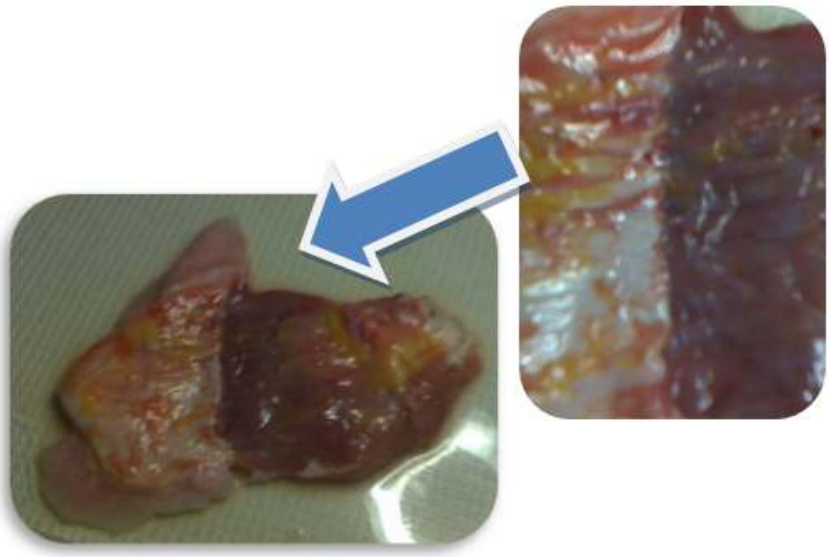

Figure 38 Samples' dissection. The fascia is being carefully removed. The muscle is lying under need.

All tissue remaining are reserved in the refrigerator and are later collected by a company specializing in the treatment of hospital waste.

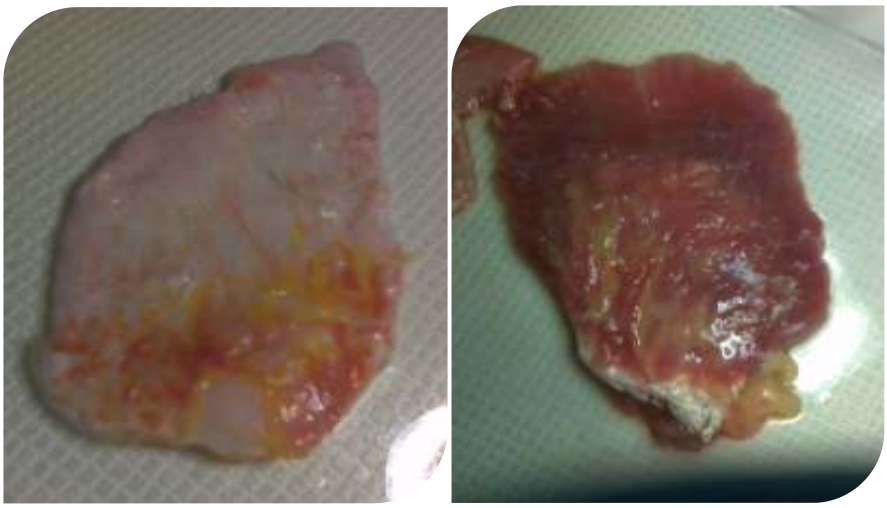

Figure 39 An example of the fascia on the left and the muscle with the visible tendon (in white) on the right picture.

The samples are fixed in the stainless steel bond with the aid of velcro and sandpaper, afterwards placed in the machinery. Images were gathered front and sides of all samples, now prepared for the uniaxial test.

The BM laboratory is equipped with a uniaxial tensile testing machine monitored with a LBVM sensor. The load (N) and displacement (mm) data were acquired using a load cell (Force max. ¼ 200 N) and the LBVM displacement sensor, respectively. The testing process did not involve the preconditioning of the tissues; however, in practice, the weight of the inferior grips (330 g) acts as a preloading. This ensures that the samples are stretched so that the initial length, width and thickness may be measured using image analysis. All the tests were performed at room temperature (<20ºC).

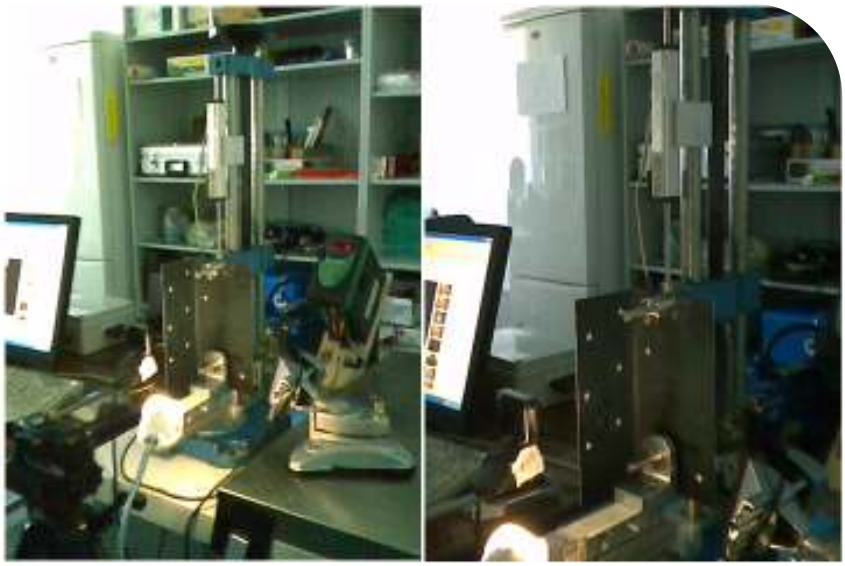

Figure 40 The test equipment.

All recorded data are stored on .txt file format, to be subsequently handled in order to obtain the force/displacement graphics. As the test occurs the camera record from the beginning in order to obtain a complete archive of each exam.

The collected data on BML equipment were processed using various software tools. With the help of *Matblab* it some key points were chosen to describe the graphic force /displacement; since the equipment at the LBM gathers excess data and becomes necessary to restrict this information. With the help of the tool *ginput* found in Matlab a few points are chosen on the graphic which later will be used to integrate graphical information lighter than its predecessor. It is believed that the quality loss that might be associated with this operation was not here because the main focus was to characterize the slope of the linear zone of each graph and thus the amount of points needed to characterize the slope of a straight is lower compared to the number of points obtained in the laboratory.

To calculate the stress (MPa) and strain, the cross-section of each sample was estimated using frontal and lateral images (see Figure 41). The measurements were performed using the grip dimensions as reference using Autodesk Inventor software to measure the picture's dimensions.

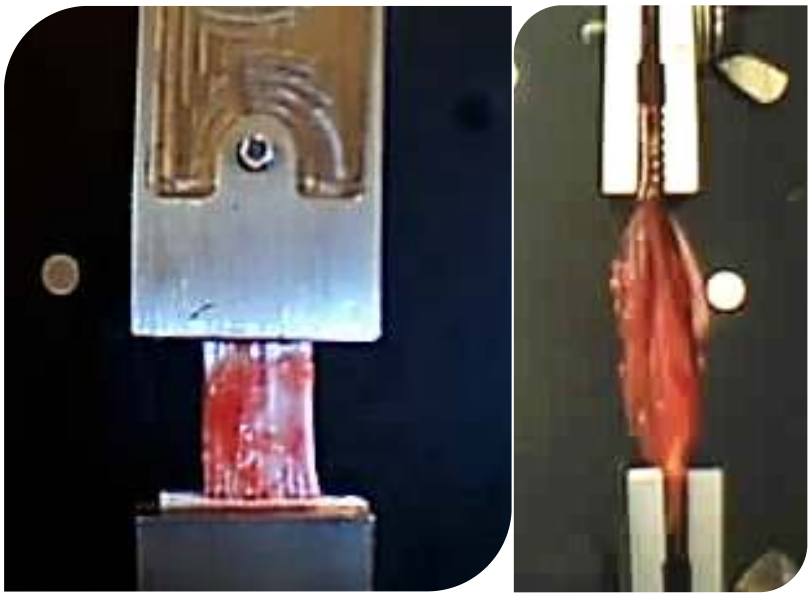

Figure 41 Examples of the front and side images taken just before testing.

Because it is expected to have acquired different results for different types of soft tissues from now on all results will be divided into three fractions; muscles, tendons and fasciae. As the results within each type are scattered and therefore difficult to interpret, it becomes necessary to divide them into groups and the premise to do so was to divide them according to gender and age;
Groups distinguished by gender and also by age;

- Group A : Male 20-50
- Group B: Male 50-80
- Group C : Female 20-50
- Group D: Female 50-80

And distinguishing only by age, groups E and F:

- Group E: Age to 20-50
- Group F: Age to 50-80

The *Pedro Martins*'s algorithm, presented at [Martins, P., 2009], was employed to compute the constants associated with each stress-strain graphic to each constitutive model that was already presented on chapter 3.

5.1. Muscles

A total of sixty samples of the initial seventy six tests were admitted to be included in this study. The sixteen removed tests were so due to reasons connected with the poor quality of the uniaxial tensile.

For each stress/strain pair of values was assigned a number for easier handling.

Table 3 Corresponding number for muscles.

Number	*Correspondent Sample*	*Gender*	*Age*
1 to 6	VIII	Fem.	36
7 to 10	IX	Masc.	61
11 to 18	X	Masc.	61
19 to 25	XI	Fem.	34
26 to 29	I	Masc.	20
30 to 37	II	Masc.	50
38 to 47	III	Fem.	80
48 to 53	IV	Masc.	43
54 to 60	V	Masc.	63
61 to 69	VI	Masc.	46
70 to 76	VII	Masc.	52

After the sample's distribution through groups A to F, and all constants c_1, c_2 and c_3 (for *Yeoh*'s case) calculated to the four previously studied constitutive models; *Ogden*, *Mooney-Rivlin, Neo-Hooke* and *Yeoh*. All constants means were also determined to each group and with the respective constitutive function the mean's graphics were plotted.

All results for *Mooney-Rivlin*, *Neo-Hooke* and *Yeoh* models are shown ahead, both calculated constants and the experimental versus numerical plots. However *Ogden* based results are absent due to clear incompatibility of the numerical plots and the experimental data.

5.1.1. Mooney-Rivlin Model Constants

The calculated constants based on Mooney-Rivlin material model and on the experimental data resulted on the following tables; Table 4, Table 5, Table 6, Table 7 and Table 9.

Table 4 *Mooney-Rivlin* Constants group of Male from 20 to 50 samples.

Sample	*Mooney-Rivlin Constants – Group A*	
Number	C_1	C_2
1	0,0294	0,0339
2	4,001	-1,3591
3	0,0031	0,0899
4	-0,0149	0,0884
5	-0,0399	0,1189
6	-0,031	0,1431
11	0,2299	-0,0531
12	0,1669	0,0026
13	0,1649	0,1744
14	-0,0722	0,1779
15	0,4471	0,0601
16	0,2455	0,1709
17	0,1044	0,3617
18	-0,0088	0,1521
54	-0,086	0,1715
55	-0,1281	0,2844
56	0,0019	0,0906
57	0,0098	0,0218
59	0,0104	0,1285
60	-0,0252	0,1279
61	0,0204	0,0373
62	-0,0743	0,2601
63	0,0019	0,2427
64	-0,1781	0,2959

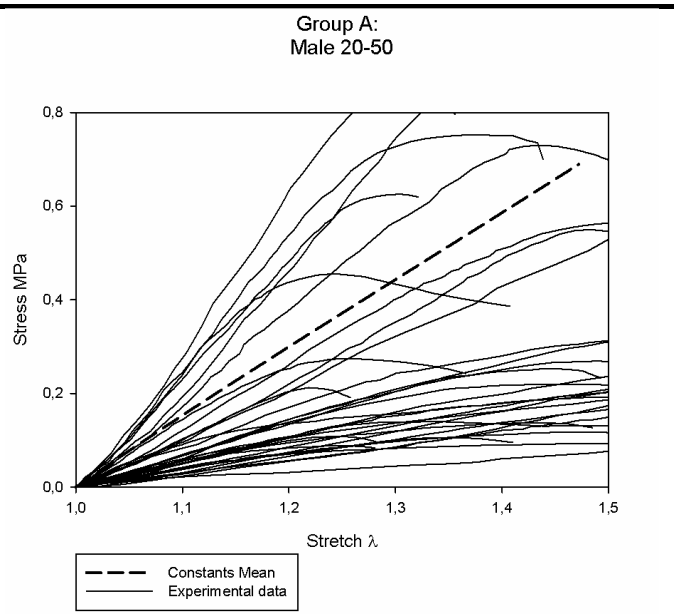

65	-0,1657	0,4457
67	0,0471	0,2138
68	-0,0268	0,151
69	-0,0333	0,1463
Mean	**0,164264**	**0,099257**

Table 5 *Mooney-Rivlin* Constants group of Male from 50 to 80 samples.

Sample	*Mooney-Rivlin Constants – Group B*	
Number	C_1	C_2
7	-0,0084	0,0364
8	0,2184	-0,1054
19	-0,017	0,0446
21	0,029	0,022
23	-0,04	0,1029
24	-0,0346	0,1045
25	0,0025	0,0433
30	0,502	-0,3667
31	-0,1084	0,3833
35	-0,2058	0,3144
36	-0,2178	0,358
39	0,1616	-0,1537
40	2,4959	-2,4105
42	0,4161	-0,2969
43	0,8324	-0,7745
44	0,7558	-0,5411
45	0,4728	-0,3436
46	0,4686	-0,3991
47	1	-1
Mean	**0,358211**	**-0,26553**

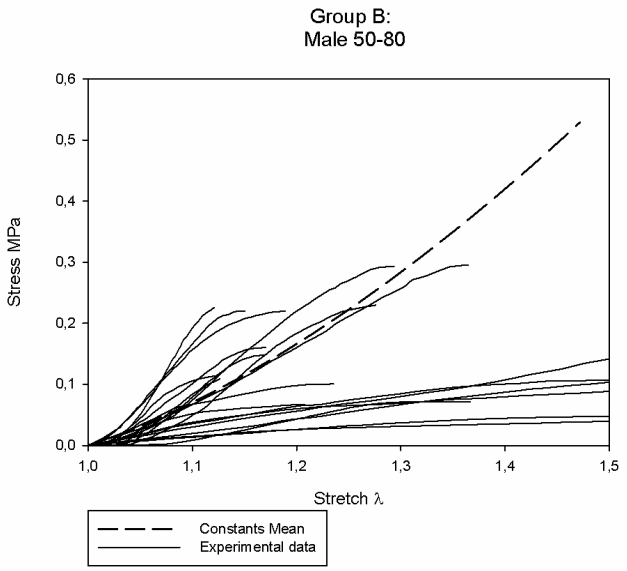

20 to 50 years old male group experimental data is built from twenty of the sixty samples of muscles; it is a bigger group compared to the 50 to 80 years old group, composed of twenty samples.

Notice the almost exclusive linearity of the constants mean plot, for the older group and also its slope tendency to occupy the graphic's middle following the higher inclination curves. Matching it up to the older group it can be observed a slight tendency to have a convex plot, tracking the higher sloped data curves

The higher stress value achieved by the mean's curves is identical.

Table 6 *Mooney-Rivlin* Constants group of Female from 20 to 50 samples.

Sample	*Mooney-Rivlin Constants – Group C*	
Number	C_1	C_2
48	0,0078	0,1193
49	-0,2636	0,7488
52	-0,1135	0,2339
54	-0,0504	0,1276
53	0,0838	-0,045
29	0,003	0,504
Mean	**-0,05548**	**0,281433**

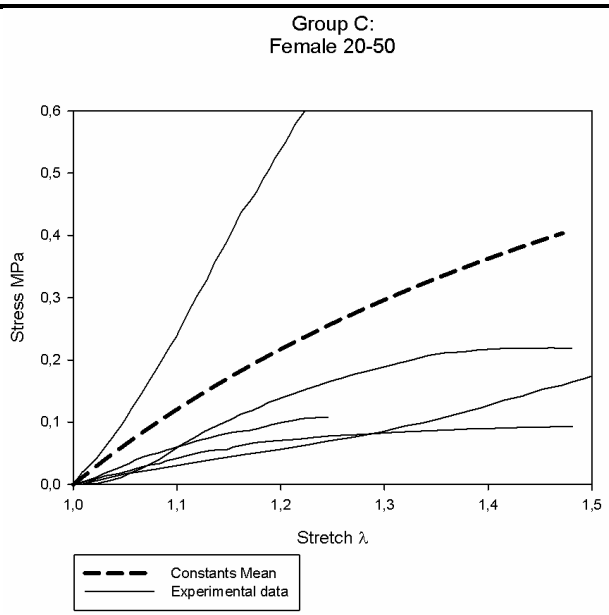

Table 7 *Mooney-Rivlin* Constants group of Female from 50 to 80 samples.

Sample	*Mooney-Rivlin Constants – Group D*	
Number	C_1	C_2
70	-0,0235	0,0706
71	-0,1701	0,3895
72	-0,2276	0,3861
73	-0,1295	0,219
74	0,0117	0,0518
75	-0,0046	0,1298
76	0,1568	-0,0003
Mean	**-0,05526**	**0,178071**

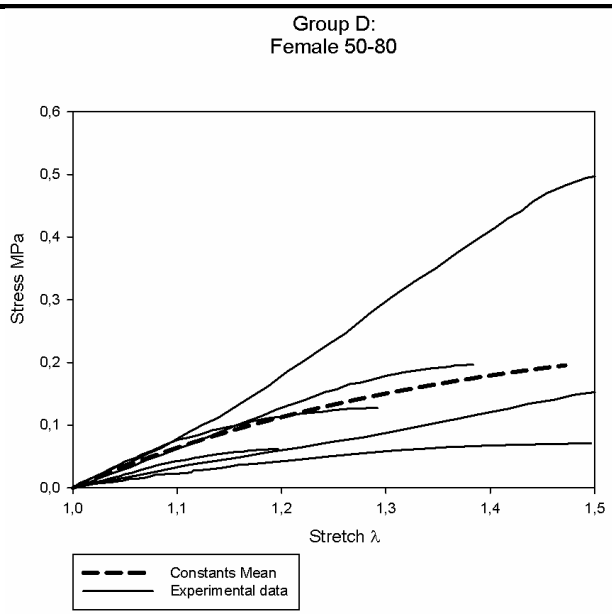

The 20 to 50 years old female group's experimental data is composed of six from the sixty samples of muscles and its size is match to the 50 to 80 years old female group, with its seven samples.

There is no linearity on any of the curves, instead both mean's plots are concave, which is completely opposite to what happens on the male graphs. The younger one maximum stress value is apparently slightly higher than the corresponding value to the older curve.

Table 8 *Mooney-Rivlin* Constants group of all samples from 20 to 50 years old.

Sample	*Mooney-Rivlin Constants – Group E*	
Number	C_1	C_2
1	0,0294	0,0339
2	4,001	-1,3591
3	0,0031	0,0899
4	-0,0149	0,0884
5	-0,0399	0,1189
6	-0,031	0,1431
11	0,2299	-0,0531
12	0,1669	0,0026
13	0,1649	0,1744
14	-0,0722	0,1779
15	0,4471	0,0601
16	0,2455	0,1709
17	0,1044	0,3617
18	-0,0088	0,1521
29	0,0078	0,1193
48	-0,2636	0,7488
49	-0,1135	0,2339
51	-0,0504	0,1276
52	0,0838	-0,045
53	0,003	0,504
54	-0,086	0,1715
55	-0,1281	0,2844
56	0,0019	0,0906
57	0,0098	0,0218
59	0,0104	0,1285
60	-0,0252	0,1279
61	0,0204	0,0373
62	-0,0743	0,2601
63	0,0019	0,2427

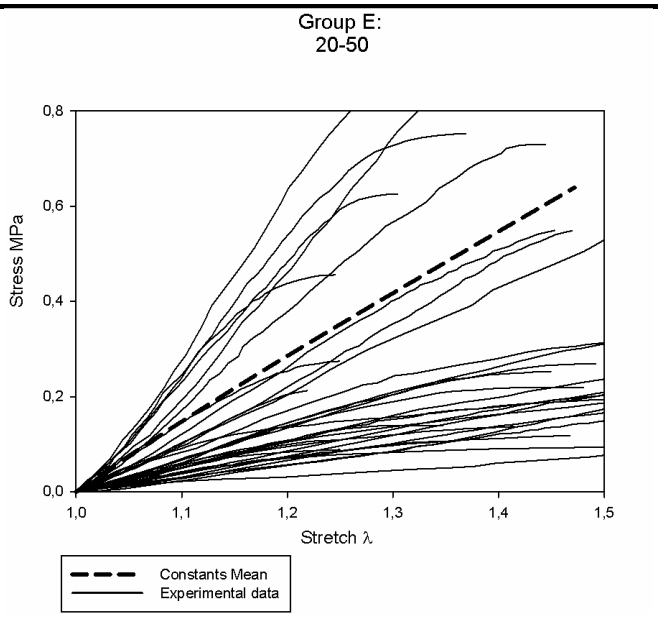

64	-0,1781	0,2959
65	-0,1657	0,4457
67	0,0471	0,2138
68	-0,0268	0,151
69	-0,0333	0,1463
Mean	**0,125485**	**0,131406**

Table 9 *Mooney-Rivlin* Constants group of all samples from 50 to 80 years old.

Sample	*Mooney-Rivlin Constants – Group F*	
Number	C_1	C_2
7	-0,0084	0,0364
8	0,2184	-0,1054
19	-0,017	0,0446
21	0,029	0,022
23	-0,04	0,1029
24	-0,0346	0,1045
25	0,0025	0,0433
30	0,502	-0,3667
31	-0,1084	0,3833
35	-0,2058	0,3144
36	-0,2178	0,358
39	0,1616	-0,1537
40	2,4959	-2,4105
42	0,4161	-0,2969
43	0,8324	-0,7745
44	0,7558	-0,5411
45	0,4728	-0,3436
46	0,4686	-0,3991
47	1	-1
70	-0,0235	0,0706
71	-0,1701	0,3895

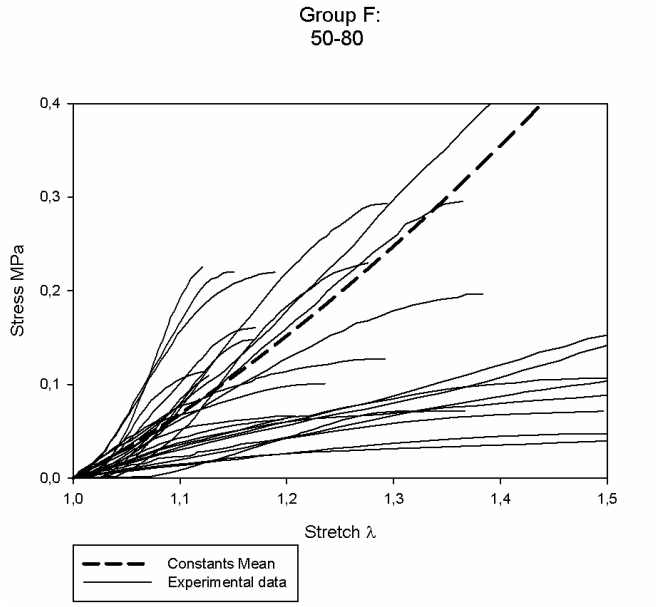

72	-0,2276	0,3861
73	-0,1295	0,219
74	0,0117	0,0518
75	-0,0046	0,1298
76	0,1568	-0,0003
Mean	**0,246892**	**-0,1461**

Observing Table 8 , of all samples from 20 to 50 years, apparently the constants' mean plot is linear, tracking Table 4, which was expected due to the number of samples contributing from A (male) group to E group comparing to the only 6 samples from group C (female); furthermore the mean plot maximum stress value is clearly of the same order of A group.

Table 9 mean plot tendency is linear , tracking preferably the higher inclination experimental data data plots. Which is legitimate due gain to the number of data coming from the male group contrasting to the number of data coming from the female group.

Examining all the previous tables concerning the *Mooney-Rivlin* constants it is noticed the tendency of c_2 values to decrease on groups B and D (belonging to older groups) when compared to groups A

It is noticed the tendency of c_1 values to increase value on groups B and D (belonging to older groups) when compared to groups A and C (belonging to younger groups).
Finally the graphics observation leads to a remark; the higher the inclinations the younger groups and as we approach smoother slopes, the curves tend to belong to older groups.

5.1.2. Neo-Hooke Model Constants

The calculated constants based on *Neo-Hooke* material model and on the experimental data resulted on the following tables; Table 10,Table 11, Table 12 and Table 13.

Table 10 *Neo-Hooke* Constants Male group of 20 to 50 samples.

Sample	*Neo-Hooke Constants - Group A*
Number	C_1
1	0,0492
2	2,8685
3	0,0609
4	0,0557
5	0,0483
6	0,0856
11	0,1911
12	0,1691
13	0,2974
14	0,0626
15	0,4954
16	0,3867
17	0,3606
18	0,1036
54	0,0412
55	0,0736
56	0,0554
57	0,0219
59	0,1004
60	0,0553
61	0,0442
62	0,1062
63	0,1371
64	0,0704
65	0,2113
67	0,2021
68	0,0567
69	0,0741
Mean	**0,0946**

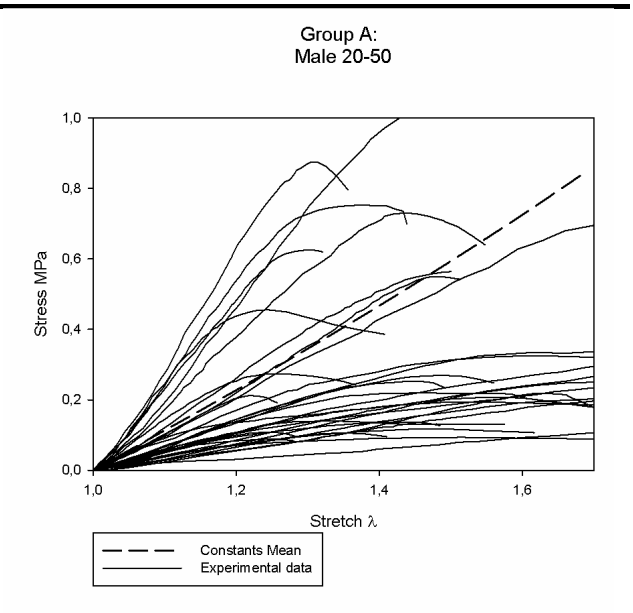

Table 11 *Neo-Hooke* Constants Male group of 50 to 80 samples.

Sample	*Neo-Hooke Constants - Group B*
Number	C_1
7	0,0186
8	0,1356
19	0,0132
21	0,0428
23	0,0248
24	0,042
25	0,0314
30	0,12863
31	0,2293
35	0,069
36	0,0876
39	0,0358
40	0,2873
42	0,1733
43	0,1429
44	0,2671
45	0,1666
46	0,1371
47	0,1191
Mean	**0,1536**

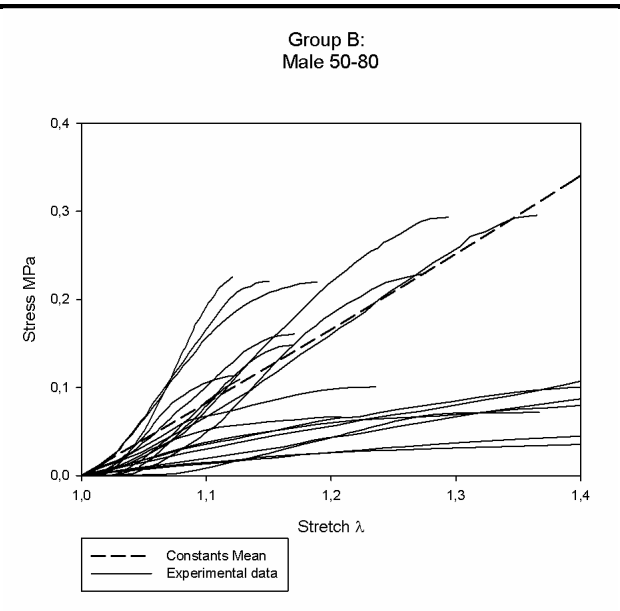

Notice the almost exclusive linearity of the constants mean plot for the both groups. On A group there is tendency of the slopes' mean curve to occupy the middle of the graphic and group B mean plot to follow higher inclination curves.

Group B higher mean plot values are about 55% lower than group A's; the younger group shows twice the stress values for the same applied stretch than the older one.

Table 12 *Neo-Hooke* Constants Female group of 20 to 50 samples.

Sample	*Neo-Hooke Constants - Group*
Number	C_1
29	0,0998
48	0,3763
49	0,085
50	0,3956
52	0,0538
53	0,4053
Mean	**0,2360**

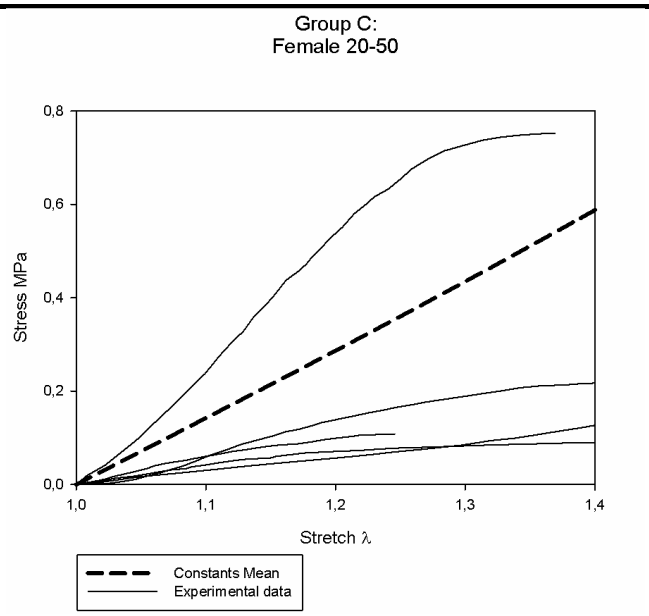

Table 13 *Neo-Hooke* Constants Female group of 50 to 80 samples.

Sample	*Neo-Hooke Constants - Group D*
Number	C_1
70	0,0292
71	0,1321
72	0,0924
73	0,0615
74	0,0441
75	0,0968
76	0,1566
Mean	**0,0875**

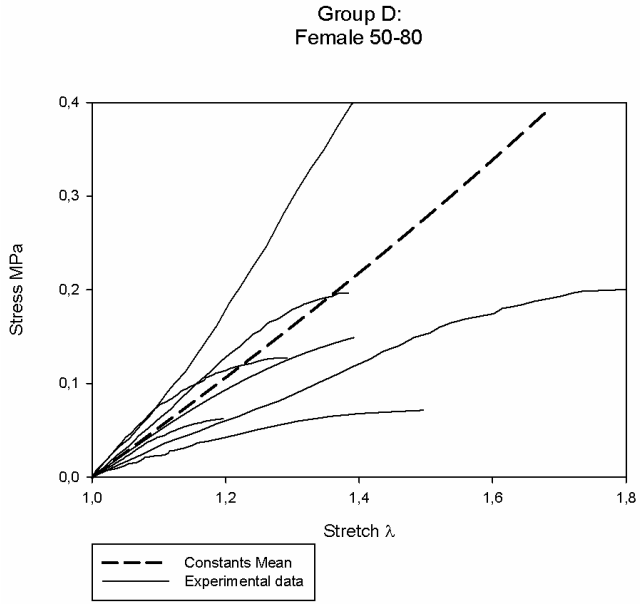

Both Table 12 and Table 13 mean plots have a tendency towards linearity which was expected for a *Neo-Hooke* based plot due to this material model only depending on one constant, c_1, which controls the curves slope.

Again the same event happens concerning the stress values for the same stretch, group C is 50% higher than D group; the younger group has twice the stress value than the older group.

Table 14 *Neo-Hooke* Constants group of sample from 20 to 50 years old.

Sample	*Neo-Hooke Constants - Group E*
Number	C_1
1	0,0492
2	2,8685
3	0,0609
4	0,0557
5	0,0483
6	0,0856
11	0,1911
12	0,1691
13	0,2974
14	0,0626
15	0,4954
16	0,3867
17	0,3606
18	0,1036
29	0,0998
48	0,3763
49	0,085
50	0,3956
52	0,0538
53	0,4053
54	0,0412
55	0,0736
56	0,0554
57	0,0219

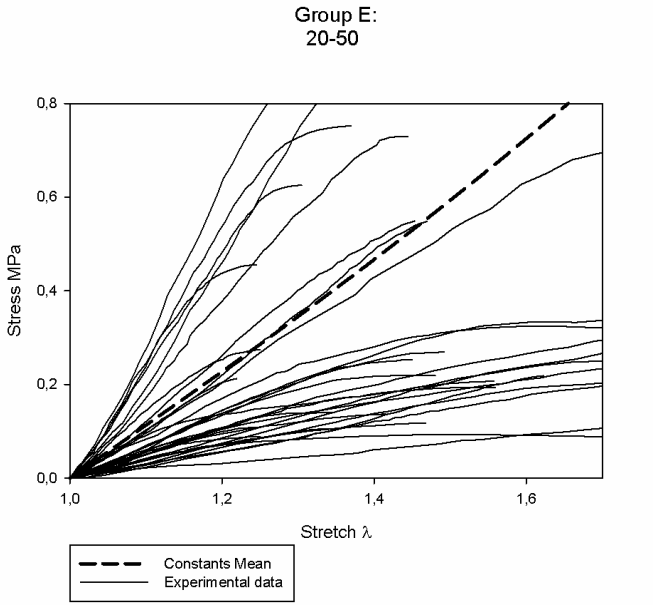

59	0,1004
60	0,0553
61	0,0442
62	0,1062
63	0,1371
64	0,0704
65	0,2113
67	0,2021
68	0,0567
69	0,0741
Mean	**0,0946**

Table 15 *Neo-Hooke* Constants group of sample from 50 to 80 years old.

Sample	*Neo-Hooke Constants - Group F*
Number	C_1
7	0,0186
8	0,1356
19	0,0132
21	0,0428
23	0,0248
24	0,042
25	0,0314
30	0,12863
31	0,2293
35	0,069
36	0,0876
39	0,0358
40	0,2873
42	0,1733
43	0,1429
44	0,2671

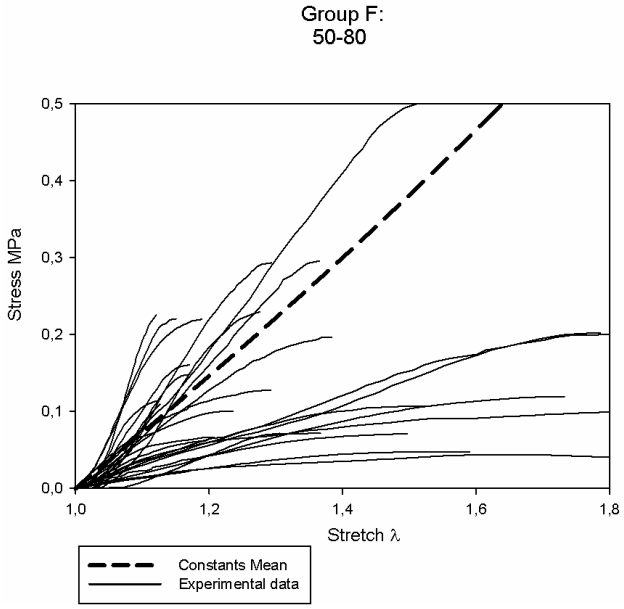

45	0,1666
46	0,1371
47	0,1191
70	0,0292
71	0,1321
72	0,0924
73	0,0615
74	0,0441
75	0,0968
76	0,1566
Mean	**0,1205**

Examining all the previous tables concerning the *Neo-Hooke* constants it is noticed the tendency of c_1 values to increase from male only groups A to B (younger to older) and the opposite happens for the female groups.
The phenomenon that occurs do the male samples is reflected on the major groups, E and F, which contain a higher percentage of male contribution than female ones.

Finally the graphics observation leads to the conclusion that the higher the inclinations the younger groups and as we approach smoother slopes, the curves tend to belong to older groups.

5.1.3. Yeoh Model Constants

The calculated constants based on *Yeoh* material model and on the experimental data resulted on the following tables; Table 17, Table 18, Table 19, Table 20 and Table 21.

Table 16 *Yeoh* Constants group of Male from 20 to 50 samples.

Sample	*Yeoh Constants – Group A*		
Number	C_1	C_2	C_3
1	0,0553	0,0013	-0,0040
2	2,2858	6,6761	-20,6693
3	0,0719	-0,0016	-0,0040
4	0,0678	-0,0485	0,0466
5	0,0657	-0,0302	0,0067
6	0,096	-0,0081	-0,1052
11	0,1636	0,0911	-0,0886
12	0,1523	0,3203	-1,5457
13	0,3009	0,0654	-0,148
14	0,0887	-0,0591	0,0255
15	0,4334	0,6397	-1,6379
16	0,3557	0,4248	-1,3518
17	0,3643	0,1069	-0,1368
18	0,1192	-0,0091	-0,0239
54	0,0725	-0,0726	0,0427
55	0,1382	-0,1264	0,0691
56	0,0674	-0,0022	-0,0014
57	0,0245	0,0000	-0,0003
59	0,1123	0,0010	-0,0152
60	0,0873	-0,0304	0,0080
61	0,0455	0,0039	-0,0031
62	0,1511	-0,0552	0,0123
63	0,1802	-0,0113	-0,0013
64	0,1018	-0,1890	0,2206
65	0,2396	-0,0289	-0,6570
67	0,2108	0,036	-0,0742
68	0,0897	-0,0136	0,001
69	0,0912	-0,0174	-0,0102
Mean	**0,222596**	**0,273675**	**-0,93019**

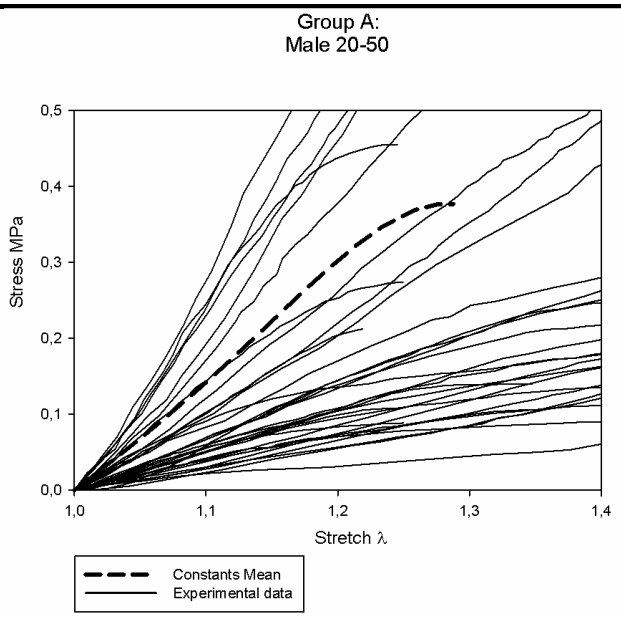

Table 17 *Yeoh* Constants group of Male from 50 to 80 samples.

Sample	*Yeoh Constants – Group B*		
Number	C_1	C_2	C_3
7	0,0229	-0,0055	-0,0015
8	0,1042	0,1685	-0,2582
19	0,0235	-0,0143	0,0054
21	0,0426	0,0047	-0,0031
23	0,0521	-0,0276	0,0079
24	0,0581	-0,0279	0,0084
25	0,0361	-0,0003	-0,0029
30	0,0956	3,6849	-48,7283
31	0,2205	0,7755	-7,0546
35	0,0927	-0,1957	0,0639
36	0,1226	-0,2635	0,4018
39	0,0068	0,1911	-0,3563
40	0,0553	8,7288	-93,4971
42	0,0956	0,6408	-1,5547
43	0,0443	2,1515	-13,2193
44	0,1799	2,8714	-26,8311
45	0,1081	1,4941	-10,4261
46	0,0421	0,8665	-2,1954
47	0,0063	3,292	-25,626
Mean	**0,074174**	**1,280789**	**-12,0667**

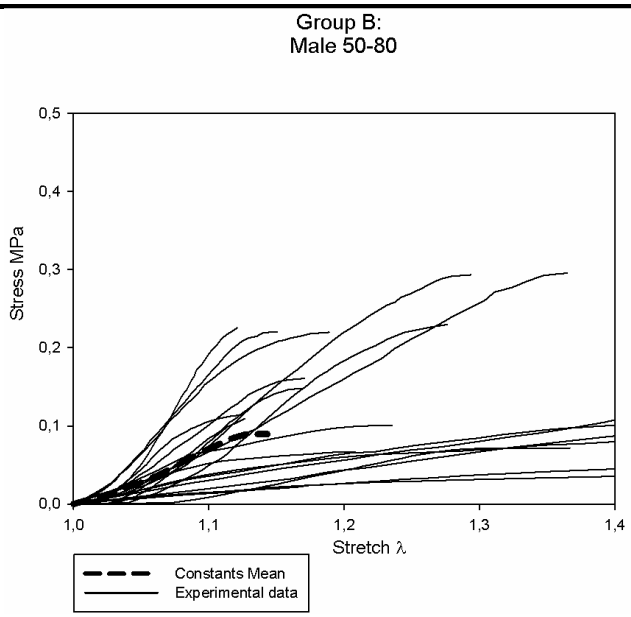

Table 16, mean plot is slightly concave on the edge, trying to track the same effect on some of the experimental data curves. Its inclination corresponds to the mean of the general curves data slopes.

Group B mean plot shows an interesting deflection, tacking the beginning of the experimental curves and again on the end with a concave portion. This happened due to *Yeoh*'s model being a three constant dependent (hence a 3 order equation).

The younger group stress value for a 1,12 stretch value is almost 60% higher than the older stress value at the same stretch.

Table 18 *Yeoh* Constants group of Female from 20 to 50 samples.

Sample	*Yeoh Constants – Group C*		
Number	C_1	C_2	C_3
48	0,3952	0,3199	-2,8416
49	0,1091	-0,1772	0,2885
52	0,0415	0,0173	-0,0073
54	0,0725	-0,0726	0,0427
53	0,4007	0,314	-0,9007
29	0,1032	0,0416	-0,1092
Mean	**0,2114**	**0,0660**	**-0,5000**

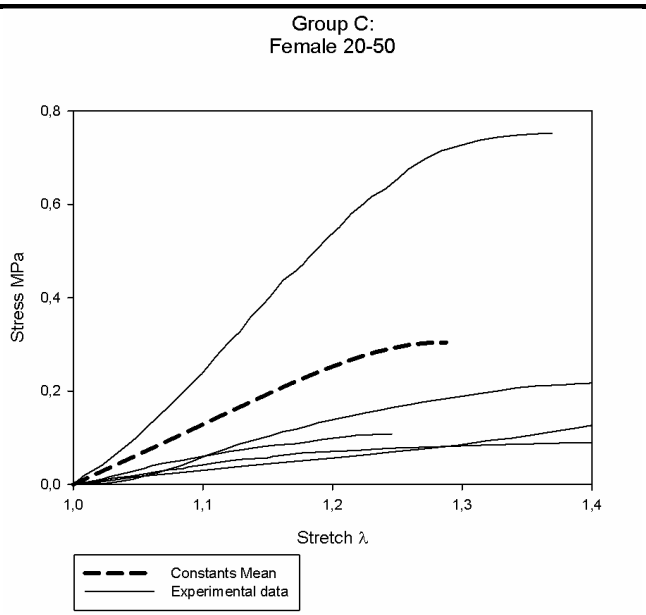

Table 19 *Yeoh* Constants group of Female from 50 to 80 samples.

Sample	*Yeoh Constants – Group D*		
Number	C_1	C_2	C_3
70	0,0398	-0,0196	0,0055
72	0,1371	-0,2536	0,3223
73	0,0758	-0,1012	-0,0915
74	0,0490	0,0015	-0,0029
75	0,104	0,0158	-0,0891
76	0,1294	0,0904	-0,0754
Mean	**0,0844**	**-0,0376**	**0,0115**

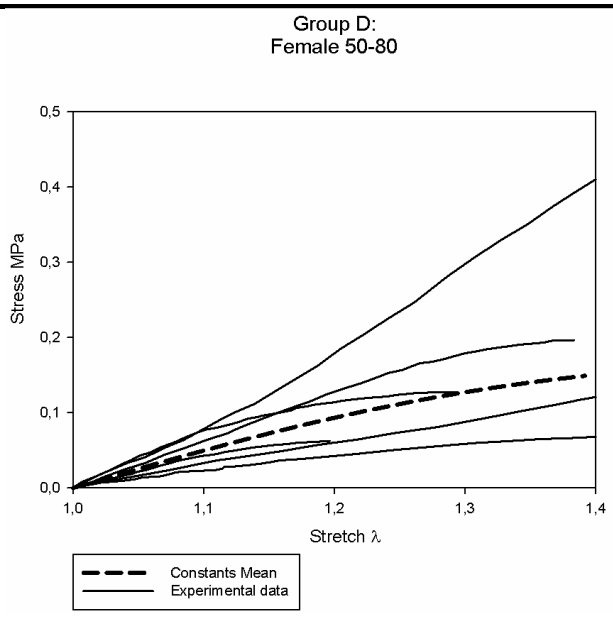

Table 18 and Table 19 mean plots are concave, both of them. D group seems to track the experimental plots better though.

Stress values wise, the younger group is three times higher than the older group, for a 1,25 stretch value.

Table 20 *Yeoh* Constants group of all samples from 20 to 50 years old.

Sample	*Yeoh Constants – Group E*		
Number	C_1	C_2	C_3
1	0,0553	0,0013	-0,0040
2	2,2858	6,6761	-20,6693
3	0,0719	-0,0016	-0,0040
4	0,0678	-0,0485	0,0466
5	0,0657	-0,0302	0,0067
6	0,096	-0,0081	-0,1052
11	0,1636	0,0911	-0,0886
12	0,1523	0,3203	-1,5457
13	0,3009	0,0654	-0,148
14	0,0887	-0,0591	0,0255
15	0,4334	0,6397	-1,6379
16	0,3557	0,4248	-1,3518
17	0,3643	0,1069	-0,1368
18	0,1192	-0,0091	-0,0239
29	0,1032	0,0416	-0,1092
48	0,3952	0,3199	-2,8416
49	0,1091	-0,1772	0,2885
52	0,0415	0,0173	-0,0073
53	0,4007	0,314	-0,9007
54	0,0725	-0,0726	0,0427
55	0,1382	-0,1264	0,0691
56	0,0674	-0,0022	-0,0014
57	0,0245	0,0000	-0,0003
59	0,1123	0,0010	-0,0152
60	0,0873	-0,0304	0,0080

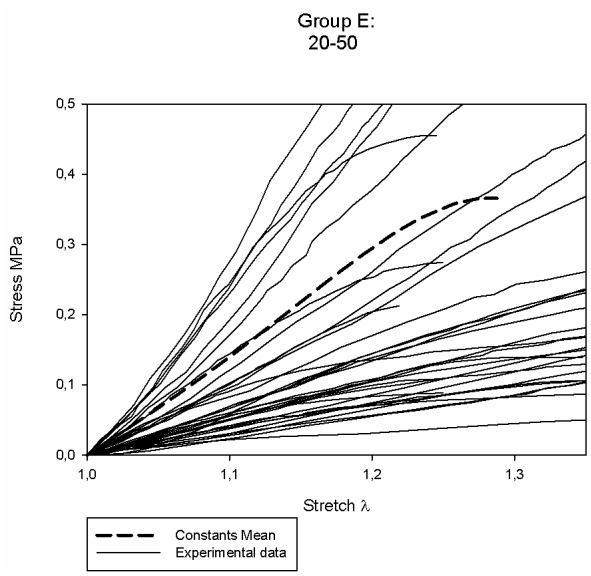

61	0,0455	0,0039	-0,0031
62	0,1511	-0,0552	0,0123
63	0,1802	-0,0113	-0,0013
64	0,1018	-0,1890	0,2206
65	0,2396	-0,0289	-0,6570
67	0,2108	0,036	-0,0742
68	0,0897	-0,0136	0,001
69	0,0912	-0,0174	-0,0102
Mean	**0,2204**	**0,2451**	**-0,8698**

Table 21 *Yeoh* Constants group of all samples from 50 to 80 years.

Sample	*Yeoh Constants – Group F*		
Number	C_1	C_2	C_3
7	0,0229	-0,0055	-0,0015
8	0,1042	0,1685	-0,2582
19	0,0235	-0,0143	0,0054
21	0,0426	0,0047	-0,0031
23	0,0521	-0,0276	0,0079
24	0,0581	-0,0279	0,0084
25	0,0361	-0,0003	-0,0029
30	0,0956	3,6849	-48,7283
31	0,2205	0,7755	-7,0546
35	0,0927	-0,1957	0,0639
36	0,1226	-0,2635	0,4018
39	0,0068	0,1911	-0,3563
40	0,0553	8,7288	-93,4971
42	0,0956	0,6408	-1,5547
43	0,0443	2,1515	-13,2193
44	0,1799	2,8714	-26,8311
45	0,1081	1,4941	-10,4261
46	0,0421	0,8665	-2,1954

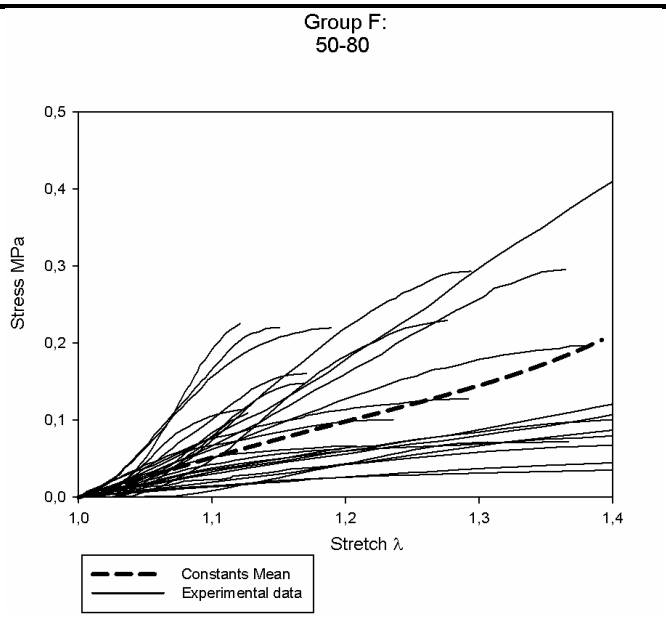

47	0,0063	3,292	-25,626
70	0,0398	-0,0196	0,0055
72	0,1371	-0,2536	0,3223
72	0,1371	-0,2536	0,3223
73	0,0758	-0,1012	-0,0915
74	0,0490	0,0015	-0,0029
75	0,104	0,0158	-0,0891
76	0,1294	0,0904	-0,0754
Mean	**0,0880**	**-0,0433**	**0,0670**

The previous tables examination leads to some observations concerning the *Yeoh* constants; for the male groups it is noticed the tendency of c_1, c_3 values to decrease from A to B (younger to older group) and c_2 to increase value from A to B.

For the female groups it is noticed the tendency of c_1, c_2 values to decrease from A to B (younger to older group) and c_3 to increase value from A to B.

The phenomenon that occurs do the male samples is reflected on the major groups, E and F that contain a higher percentage of male contribution than female ones.

Once more the male groups show a tendency for a linear plot against the female concave groups, nevertheless the maximum stress values are identical for equivalent age ranges.

Finally the graphics observation leads to the conclusion that the higher the inclinations the younger groups and as we approach smoother slopes, the curves tend to belong to older groups.

5.2. Fasciae

A total of nineteen samples of the initial twenty tests were admitted to be included in this study. The one result removed was so, due to reasons connected with the poor quality of the uniaxial tensile test.

For each stress/strain pair of values was assigned a number for easier handling.

Table 22 Corresponding number for Fasciae

Number	*Correspondent Sample*	*Gender*	*Age*
1 and 2	IX	masc.	63
3 and 4	X	masc.	46
5	I	fem	36
6	II	masc.	61
8 to 12	III	masc.	61
13 and 14	IV	fem	34
15 and 16	V	masc.	20
17 and 18	VI	masc.	51
19 and 20	VII	fem.	80

5.2.1. Mooney-Rivlin Model Constants

The calculated constants based on *Mooney-Rivlin* material model and on the experimental data resulted on the following tables;. Table, Table 24, Table 25, Table 26, Table 27 and Table 28.

Table 23 *Mooney-Rivlin* Constants group of Male from 20 to 50 samples.

Sample	*Mooney-Rivlin Constants – Group A*	
Number	C_1	C_2
3	0,7073	1,0892
4	0,7614	0,819
15	0,1978	1,2411
16	0,4887	0,9672
Mean	**0,5388**	**1,029125**

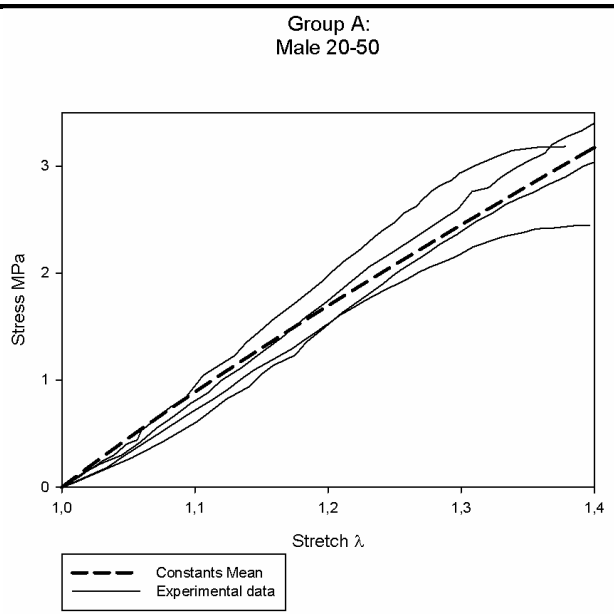

Table 24 *Mooney-Rivlin* Constants group of Male from 50 to 80 samples.

Sample	*Mooney-Rivlin Constants – Group B*	
Number	C_1	C_2
1	-1,1565	3,4943
2	-0,3305	1,712
6	3,3966	-1,9002
8	11,048	-8,6471
9	8,5078	-3,458
10	18,214	-11,8955
11	4,0579	-3,9685
12	9,2984	-6,5102
18	-0,0519	0,9065
17	0,5271	0,3681
Mean	**5,35109**	**-2,98986**

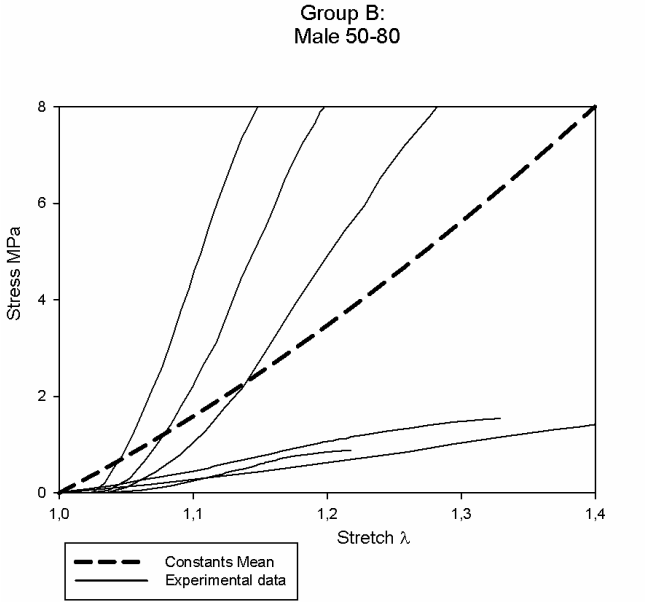

Table 23 ‘s group A is built from four of the twenty valid samples of fascia and the mean plot apparently fits very well all experimental curves at the linear portion, as for the initial portion that

doesn't happen that well. Group B shows a convex mean plot, that apparently doesn't track the experimental data as nicely as for A group.

The older group is slightly higher than twice the value of the younger group's stress for 1,3 stretch. It's actually the opposite of what happened for the muscles on same conditions.

Table 25 *Mooney-Rivlin* Constants group of Female from 20 to 50 samples.

Sample	*Mooney-Rivlin Constants – Group C*	
Number	C_1	C_2
5	-0,6089	1,4343
14	-2,8111	5,419
13	0,1541	1,5208
Mean	**-1,08863**	**2,791367**

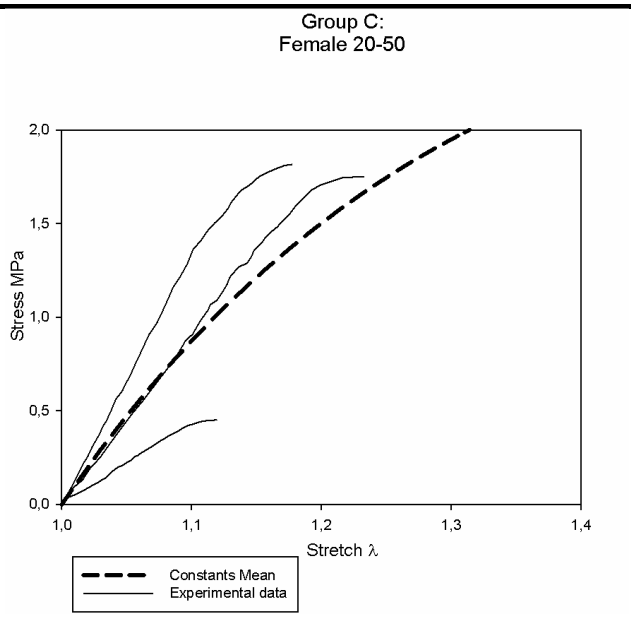

Table 26 *Mooney-Rivlin* Constants group of Female from 50 to 80 samples.

Sample	*Mooney-Rivlin Constants – Group D*	
Number	C_1	C_2
19	0,8781	0,7744
20	0,3433	1,1788
Mean	**0,6107**	**0,9766**

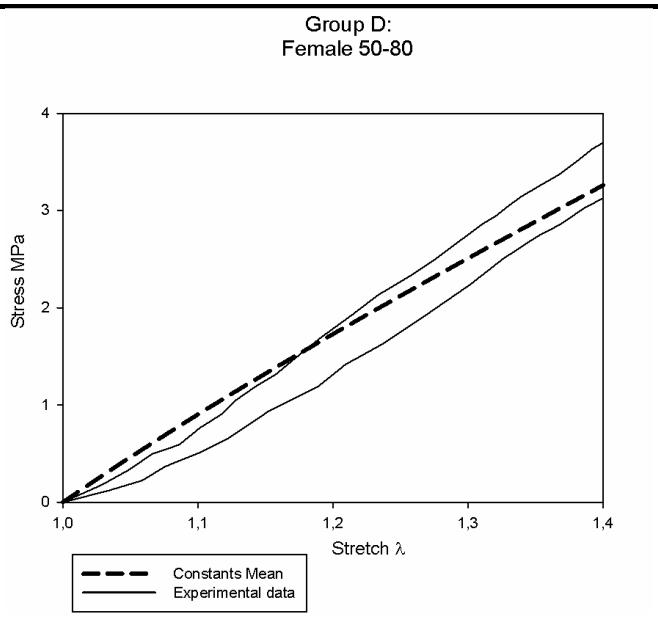

Table 25 is built from three of the twenty samples from the fascia tests, and Table 26 from four of them. Group C, the younger one, is concave against D group's tendency to linearity.
The differences between stress values at the 1,3 stretch point can be appreciated, for the older group is about 0,5 MPa higher than the youger group.

Table 27 *Mooney-Rivlin* Constants group of samples from 20 to 50 years old.

Sample	*Mooney-Rivlin Constants – Group E*	
Number	C_1	C_2
3	0,7073	1,0892
4	0,7614	0,819
5	-0,6089	1,4343
13	0,1541	1,5208
14	-2,8111	5,419
15	0,1978	1,2411
16	0,4887	0,9672
Mean	**-0,15867**	**1,784371**

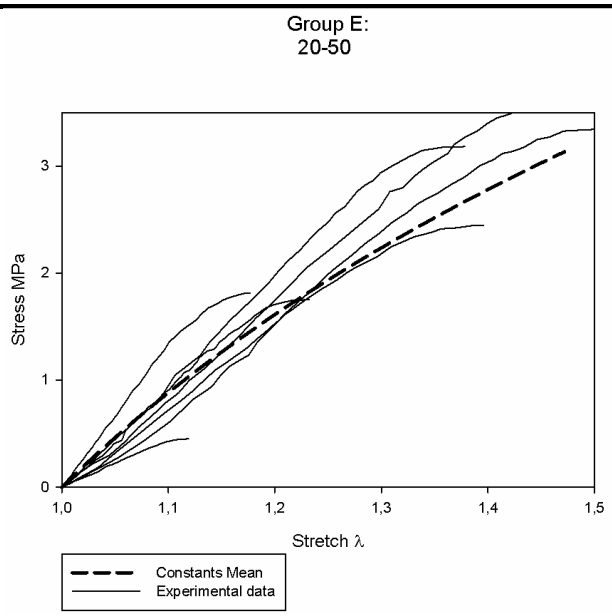

Table 28 *Mooney-Rivlin* Constants group of samples from 50 to 80 years old.

Sample	*Mooney-Rivlin Constants – Group F*	
Number	C_1	C_2
1	-1,1565	3,4943
2	-0,3305	1,712
6	3,3966	-1,9002
8	11,048	-8,6471
9	8,5078	-3,458
10	18,214	-11,8955
11	4,0579	-3,9685
12	9,2984	-6,5102
17	0,5271	0,3681
18	-0,0519	0,9065
19	0,8781	0,7744
20	0,3433	1,1788
Mean	**4,561025**	**-2,32878**

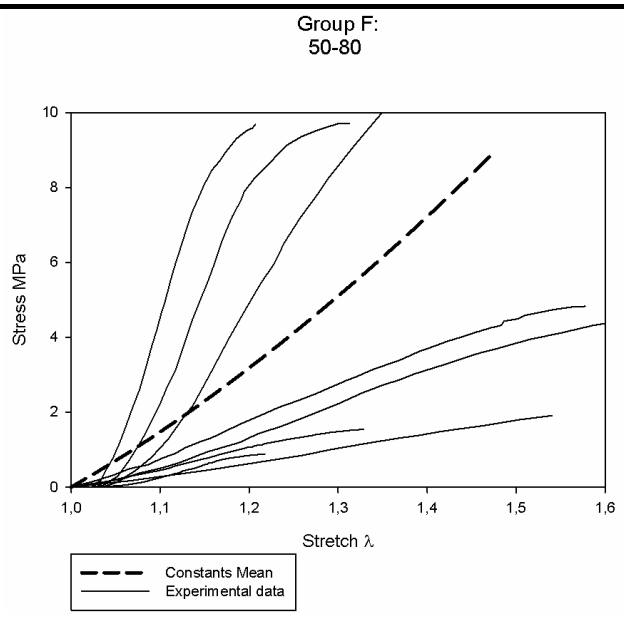

Regarding all plots, it can be noticed the tendency of c_2 values to decrease on groups B and D (belonging to older groups) when compared to groups A and C (belonging to younger groups) and c_1 to increase value on groups B and D (belonging to older groups) when compared to groups A and C (belonging to younger groups).

E and F graphics observation leads to the conclusion that the higher the inclinations the older groups and as we approach smoother slopes, the curves tend to belong to younger groups; older groups show in general two times higher stress values for one same stretch value.

5.2.2. Neo-Hooke Model Constants

The calculated constants based on *Neo-Hooke* material model and on the experimental data resulted on the following tables; Table 29, Table 30, Table 31, Table 32, Table 33 and Table 34.

Table 29 *Neo-Hooke* Constants group of Male from 20 to 50 samples.

Sample	*Neo-Hooke Constants - Group A*
Number	C_1
3	1,5643
4	1,3654
15	1,1669
16	1,1882
Mean	**1,3212**

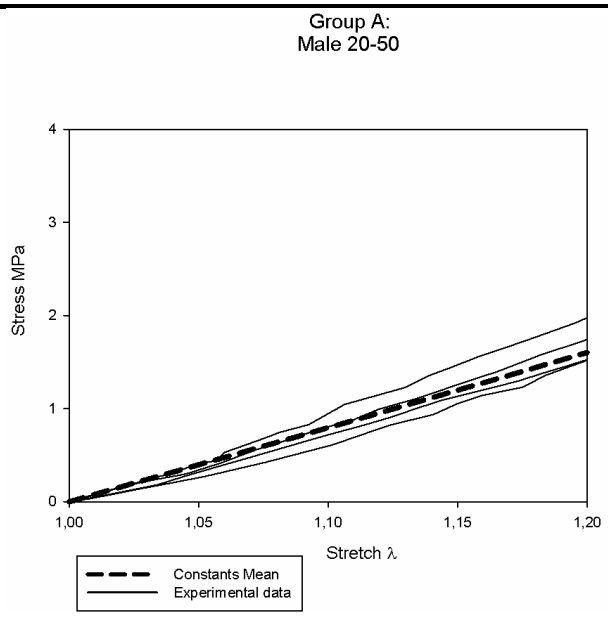

Table 30 *Neo-Hooke* Constants group of Male from 50 to 80 samples.

Sample	*Neo-Hooke Constants - Group B*
Number	C_1
1	1,2814
2	0,8557
6	1,7882
8	3,7247
9	5,6844
10	7,99
11	0,6303
12	4,3818
17	0,8223
18	0,4218
Mean	**2,75806**

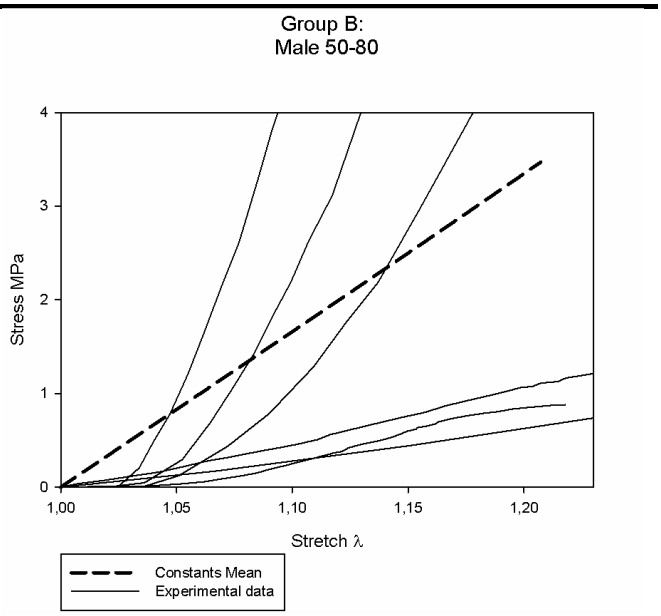

Table 29‘s mean plot apparently fits the linear portion, as for the initial portion that doesn’t happen that well. Group B shows also a linear mean plot, that seemingly doesn’t track the experimental data as nicely as for A group.

The older group (B), is twice the value of the younger group stress value, for 1,3 stretch. Again is the opposite of what happens for the muscles on same conditions; following the *Mooney-Rivlin* results for fasciae respectively to Group A and B.

Table 31 *Neo-Hooke* Constants group of Female from 20 to 50 samples.

Sample	*Neo-Hooke Constants - Group C*
Number	C_1
5	0,7103
13	1,4657
14	1,9857
Mean	**1,387233**

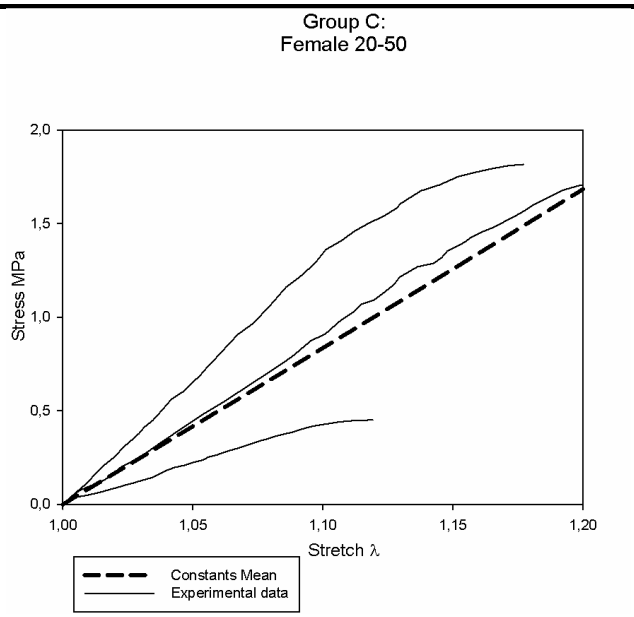

Table 32 *Neo-Hooke* Constants group of Female from 50 to 80 samples.

Sample	*Neo-Hooke Constants - Group D*
Number	C_1
19	1,4147
20	1,0888
Mean	**1,25175**

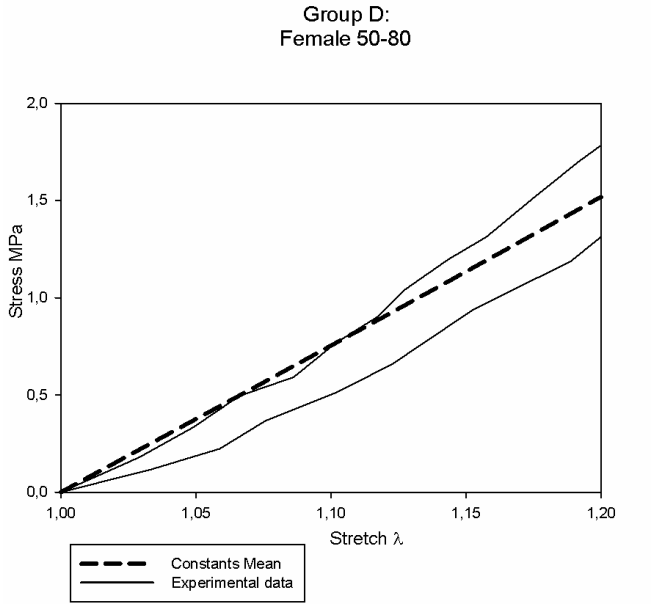

Both group C and D mean plots are practically linear and are equally inclined as the stress values to a 1,3 stretch value are similar.

The mean plots shape are expected has the Neo-Hooke model is only based in one constant, defining the slope.

Table 33 *Neo-Hooke* Constants group of samples from 20 to 50 years old.

Sample	*Neo-Hooke Constants - Group E*
Number	C_1
3	1,5643
4	1,3654
5	0,7103
13	1,4657
14	1,9857
15	1,1669
16	1,1882
17	0,8223
18	0,4218
Mean	**1,187844**

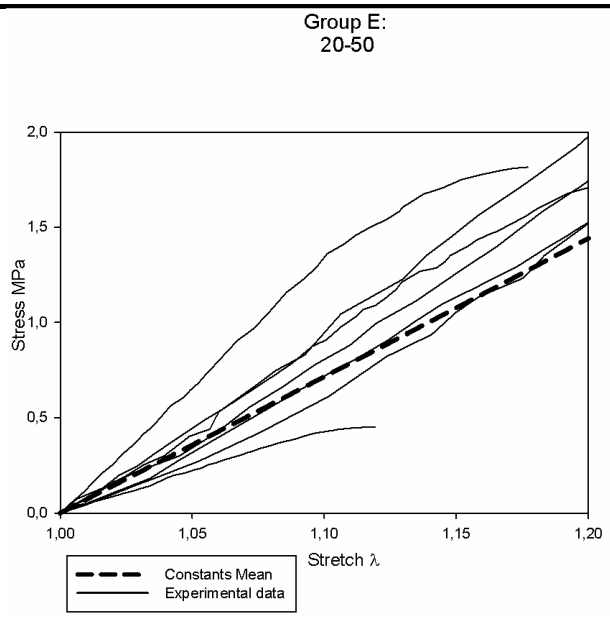

Table 34 *Neo-Hooke* Constants group of samples from 50 to 80 years old.

Sample	*Neo-Hooke Constants - Group F*
Number	C_1
1	1,2814
2	0,8557
6	1,7882
8	3,7247
9	5,6844
10	7,99
11	0,6303
12	4,3818
19	1,4147
20	1,0888
Mean	**2,884**

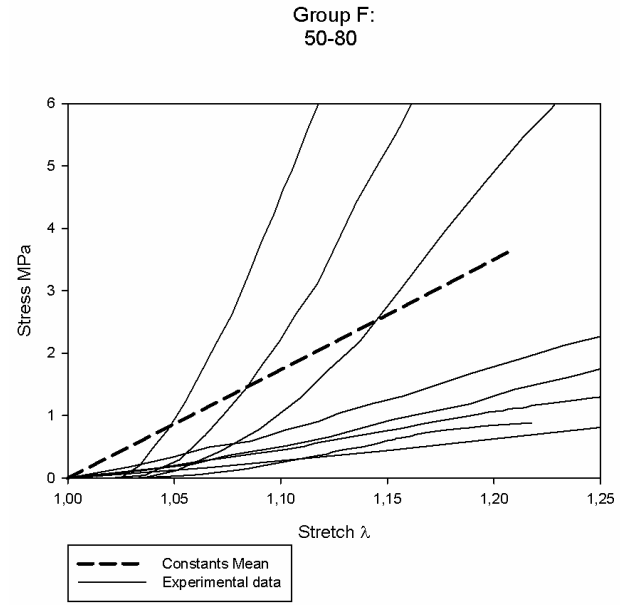

Examining the previous tables concerning the *Neo-Hooke* constants for the male samples it is noticed the tendency of c_1 values to increase from younger to older groups and to for the female the tendency is for c_1 to decrease from the younger to the older samples.
This phenomenon is reflected on the major groups, E and F that contain a higher percentage of male contribution than female ones.
F group, Table 33, representing the older samples has a stress value 2,5 times higher than group E, Table 34.

5.2.3. Yeoh Model Constants

The calculated constants based on *Yeoh* material model and on the experimental data resulted on the following tables; Table 35, Table 36, Table 37, Table 38, Table 39 and Table 40.

Table 35 *Yeoh* Constants group of Male from 20 to 50 samples.

Sample	*Yeoh Constants – Group A*		
Number	C_1	C_2	C_3
15	1,1888	0,4654	-1,3087
16	1,1454	0,5172	-0,6929
3	1,4924	0,9991	-2,2823
4	1,3283	0,5395	-0,8598
Mean	**1,288725**	**0,6303**	**1,28593**

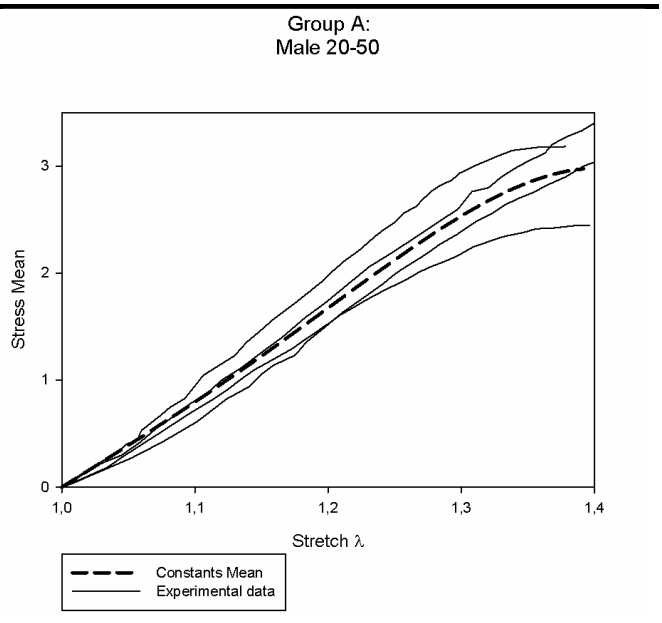

Table 36 *Yeoh* Constants group of Male from 50 to 80 samples.

Sample	*Yeoh Constants – Group B*		
Number	C_1	C_2	C_3
1	1,9098	-0,8193	0,2119
2	1,1058	-0,218	-0,0228
6	1,0736	9,1117	-30,7877
8	1,6529	25,2781	-86,1824
9	2,9435	25,7059	-60,479
10	3,9158	68,6565	-309,837
11	0,0362	7,6214	-28,04
12	2,049	9,5187	-10,9693
18	0,608	-0,0523	0,0007
17	0,7445	0,8708	-2,1095
Mean	**1,60391**	**14,56735**	**-52,8215**

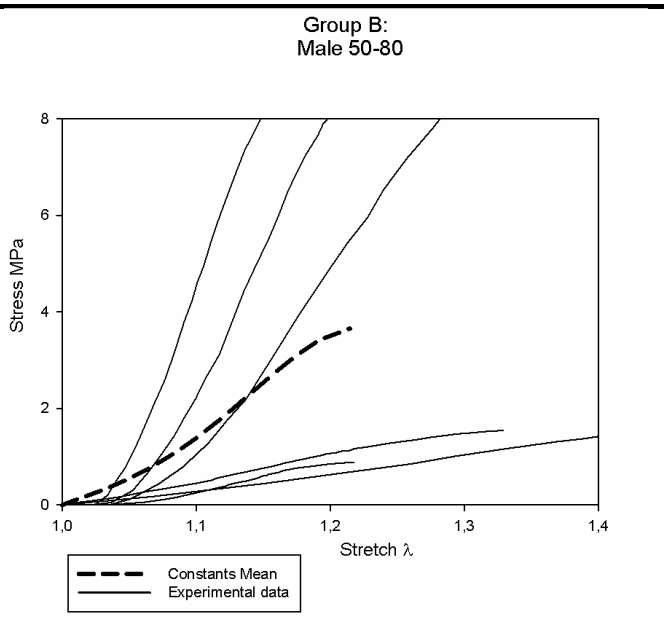

Group A is slightly concave at the end portion, following the experimental data end portions. Group B tracks poorly all data curves, but still continues to be concave. Stress values wise both plots are identical.

Table 37 *Yeoh* Constants group of Female from 20 to 50 samples.

Sample	*Yeoh Constants – Group C*		
Number	C_1	C_2	C_3
5	0,7157	2,2104	-55,9817
13	1,4637	1,2879	-9,8836
14	2,2323	-0,0073	-25,9312
Mean	**1,470567**	**1,163667**	**-30,5988**

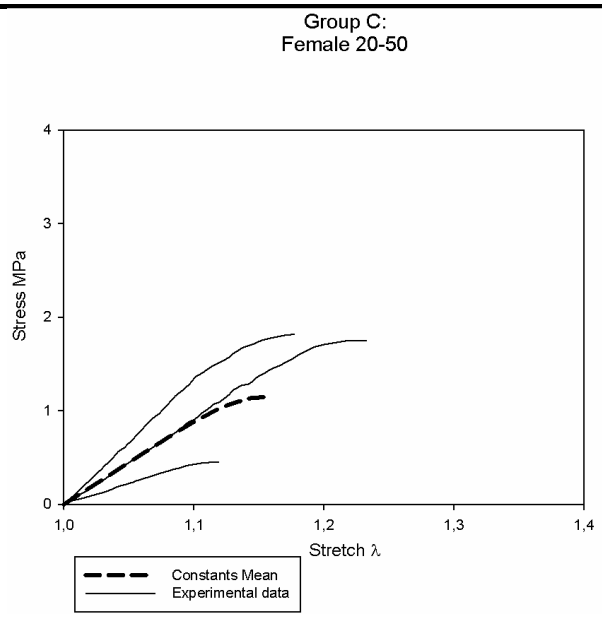

Table 38 *Yeoh* Constants group of Female from 50 to 80 samples.

Sample	*Yeoh Constants – Group D*		
Number	C_1	C_2	C_3
19	1,3725	0,348	-0,35
20	1,1302	0,1879	-0,1488
Mean	**1,25135**	**0,26795**	**-0,2494**

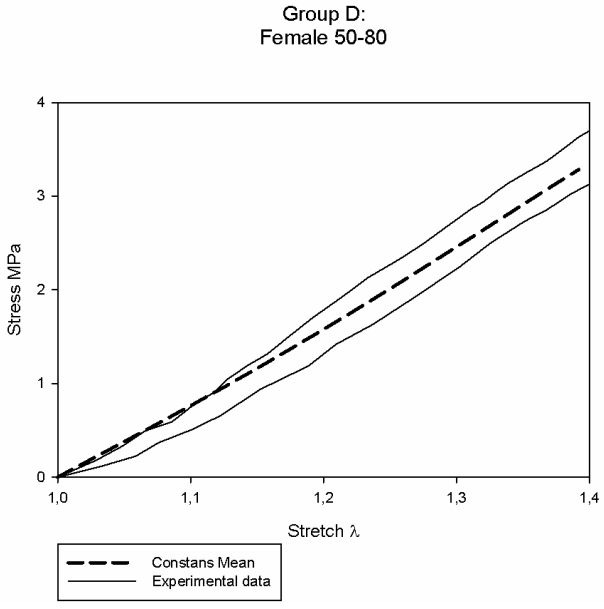

Notice Table 35 where the means plot is concave and Table 36 ‘s linear. For a stretch of 1,2 value, the older group (D) is somewhat 40% higher than the younger group stress value.

Table 39 *Yeoh* Constants group of samples from 20 to 50 years old.

Sample	*Yeoh Constants – Group E*		
Number	C_1	C_2	C_3
3	1,4924	0,9991	-2,2823
4	1,3283	0,5395	-0,8598
5	0,7157	2,2104	-55,9817
13	1,4637	1,2879	-9,8836
14	2,2323	-0,0073	-25,9312
15	1,1888	0,4654	-1,3087
16	1,1454	0,5172	-0,6929
Mean	**1,366657**	**0,858886**	**-13,8486**

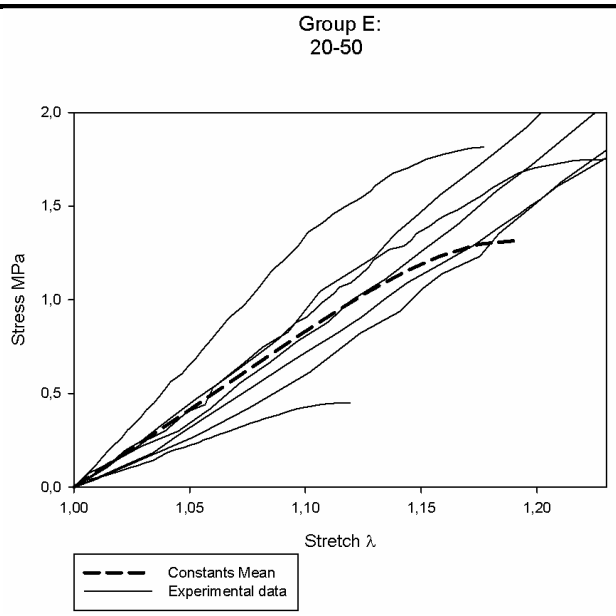

Table 40 *Yeoh* Constants group of samples from 50 to 80 years old.

Sample	*Yeoh Constants – Group F*		
Number	C_1	C_2	C_3
1	1,9098	-0,8193	0,2119
2	1,1058	-0,218	-0,0228
6	1,0736	9,1117	-30,7877
8	1,6529	25,2781	-86,1824
9	2,9435	25,7059	-60,479
10	3,9158	68,6565	-309,837
11	0,0362	7,6214	-28,04
12	2,049	9,5187	-10,9693
19	1,3725	0,348	-0,35
20	1,1302	0,1879	-0,1488
18	0,608	-0,0523	0,0007
17	0,7445	0,8708	-2,1095
Mean	**1,54515**	**12,18412**	**-44,0595**

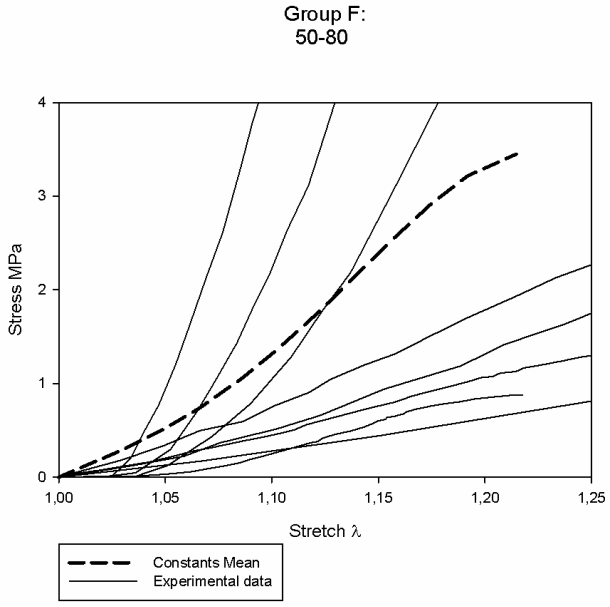

On both mean plots of E and F groups, non-linearity is patent. Tendency for concave mean curves on female groups (especially older ones). Linearity or convex style for male mean plots.

Concerning the *Yeoh* constants for the male samples, it is noticed the tendency of c_1, c_3 values to decrease from group A to B (younger to older groups) and c_2 to increase value at the same circumstance. For the female samples, the tendency to c_1, c_2 values is to decrease from group A to B (younger to older groups) and c_3 to increase value at the same circumstance.
The phenomenon that occurs do the male samples is reflected on the major groups, E and F that contain a higher percentage of male contribution than female ones.

Finally the graphics observation leads to the conclusion that the higher the inclinations the older groups and as we approach smoother slopes, the curves tend to belong to younger groups; twice the oldest stress value for the youngest group.

5.3. Tendons

A total of twenty six samples of the initial twenty eight tests were admitted to be included in this study. The two removed tests were so, due to reasons connected with the poor quality of the uniaxial tensile test.

For each stress/strain pair of values was assigned a number for easier handling.

Table 41 Corresponding number for tendons

Number	*Correspondent Sample*	*Gender*	*Age*
1 to 3	VIII	Masc.	43
4 and 5	IX	Masc.	63
6 and 7	X	Masc.	46
8 and 9	XI	Masc.	52
10 to 12 + 15	III	Masc.	61
13 and 14	IV	Fem.	34
18 and 19	V	Masc.	20
20 to 24	VI	Masc.	50
25 to 28	VII	Fem.	80

5.3.1. Mooney-Rivlin Model Constants

The calculated constants based on *Mooney-Rivlin* material model and on the experimental data resulted on the following tables; Table 42, Table 43, Table 44, Table 45, Table 46 and Table 47.

Table 42 *Mooney-Rivlin* Constants group of Male from 20 to 50 samples.

Sample	*Mooney-Rivlin Constants – Group A*	
Number	C_1	C_2
1	0,5338	1,4831
2	3,5054	-0,7841
3	0,3751	0,5539
6	0,1531	0,4529
7	0,6056	1,5227
18	-0,427	2,1129
19	0,29	1,6847
20	0,7584	1,6433
21	1,2027	0,6773
22	1,3697	0,0748
23	-1,1008	4,0721
24	-1,2608	3,3182
Mean	**0,500433**	**1,400983**

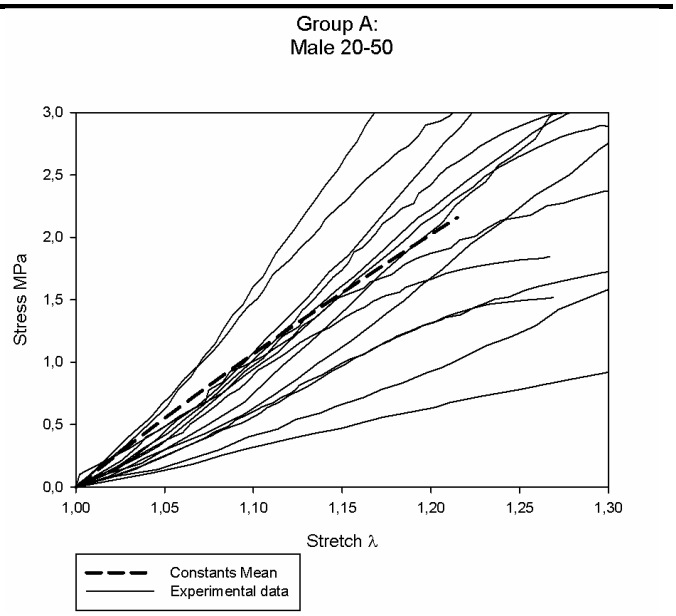

Table 43 *Mooney-Rivlin* Constants group of Male from 50 to 80 samples.

Sample	*Mooney-Rivlin Constants – Group B*	
Number	C_1	C_2
4	0,208	0,5978
5	0,8239	0,9651
9	-0,0191	1,9279
10	65,2291	-65,5753
11	36,4606	-36,396
12	35,48	-35,7409
15	24,4196	-24,1767
16	3,9479	-1,9424
Mean	**20,81875**	**-20,0426**

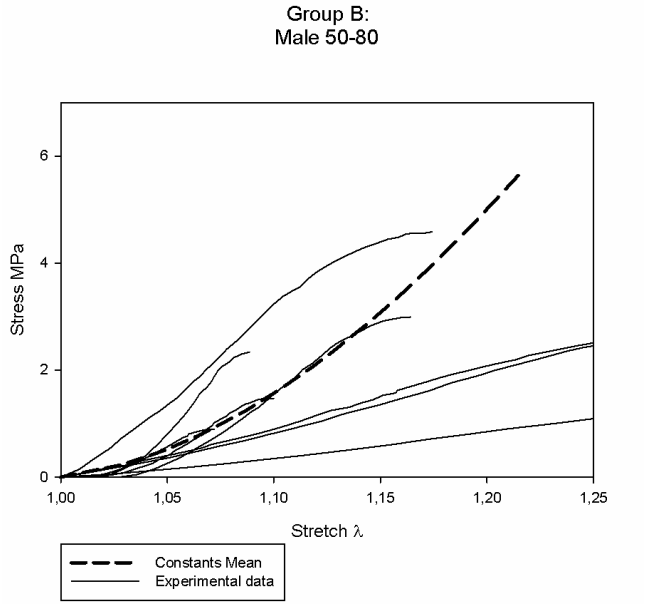

20 to 50 years old male group experimental data is built from twelve of the twenty six samples of tendons; it is a bigger group compared to the 50 to 80 years younger group, composed of eight samples.

Notice the almost exclusive linearity of the constants mean plot, for the younger group, shows a good tendency of accompanying the higher data plots focus on the graphic. The older group shows a tendency for a convex curve style, as it had already happened for the fascia results.

The higher stress value achieved by the mean curves is very different for the older group shows twice he stress value for a 1,2 stretch value than the younger group .

Table 44 *Mooney-Rivlin* Constants group of Female from 20 to 50 samples.

Sample	*Mooney-Rivlin Constants – Group C*	
Number	C_1	C_2
13	0,5662	0,5516
14	0,8551	0,2229
Mean	**0,71065**	**0,38725**

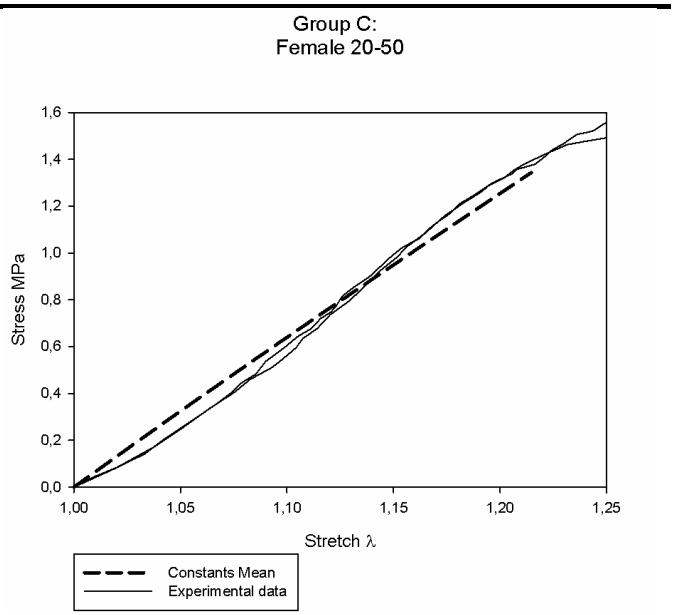

Table 45 *Mooney-Rivlin* Constants group of Female from 50 to 80 samples.

Sample	*Mooney-Rivlin Constants – Group D*	
Number	C_1	C_2
25	2,1651	-1,2442
26	1,7268	-0,4005
27	2,223	-1,1044
28	1,3501	-0,3807
Mean	**1,86625**	**-0,78245**

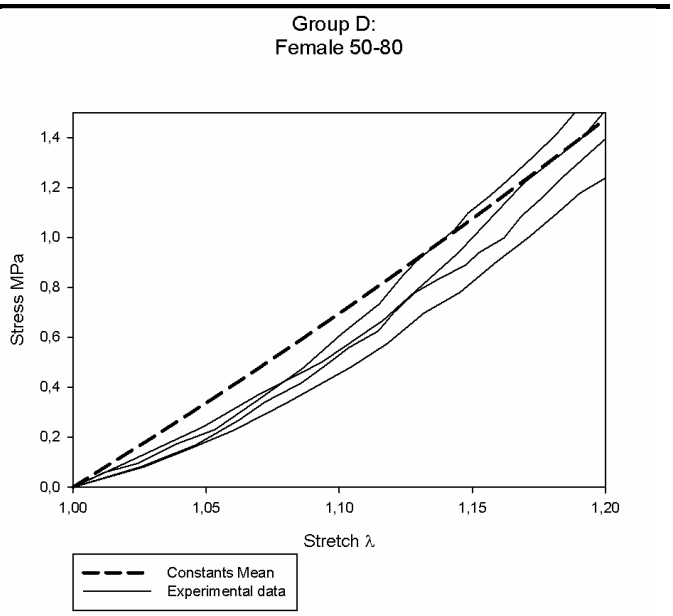

Table 44 is built form fourteen male and female samples and Table 45 groups is composed of twelve of the twenty six available samples of tendons.

Both mean plots are almost linear and the stress value hit by the older group, of female 50 to 80 samples, is slightly higher than the younger group.

Table 46 *Mooney-Rivlin* Constants group of samples from 20 to 50 years old.

Sample	*Mooney-Rivlin Constants – Group E*	
Number	C_1	C_2
1	0,5338	1,4831
2	3,5054	-0,7841
3	0,3751	0,5539
6	0,1531	0,4529
7	0,6056	1,5227
13	0,5662	0,5516
14	0,8551	0,2229
18	-0,427	2,1129
19	0,29	1,6847

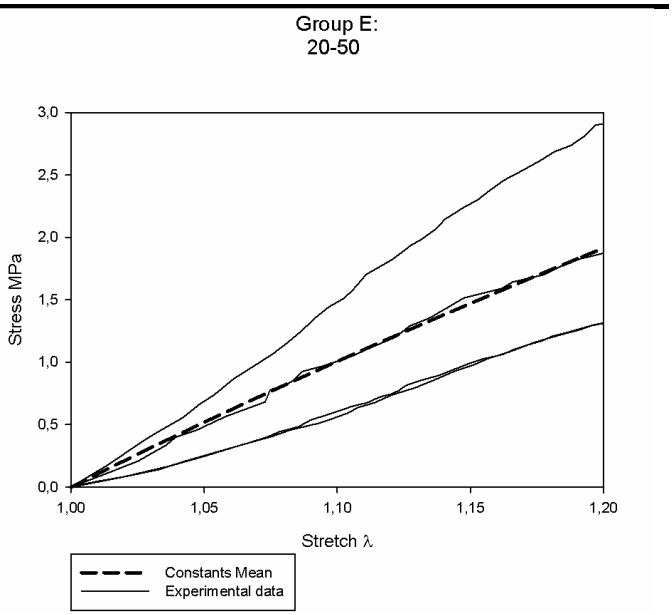

20	0,7584	1,6433
21	1,2027	0,6773
22	1,3697	0,0748
23	-1,1008	4,0721
24	-1,2608	3,3182
Mean	**0,530464**	**1,256164**

Table 47 *Mooney-Rivlin* Constants group of samples from 50 to 80 years old.

Sample	*Mooney-Rivlin Constants – Group F*	
Number	C_1	C_2
4	0,208	0,5978
5	0,8239	0,9651
9	-0,0191	1,9279
10	65,2291	-65,5753
11	36,4606	-36,396
12	35,48	-35,7409
15	24,4196	-24,1767
16	3,9479	-1,9424
25	2,1651	-1,2442
26	1,7268	-0,4005
27	2,223	-1,1044
28	1,3501	-0,3807
Mean	**14,50125**	**-13,6225**

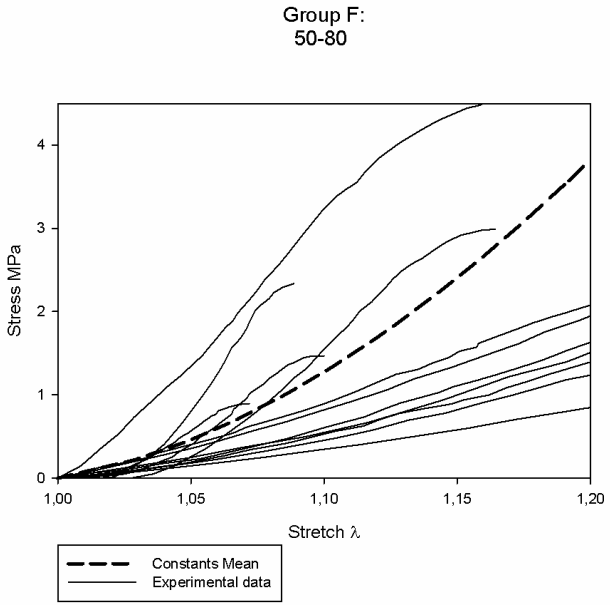

E group mean plot, of younger male and female samples, is positively linear but F group is convex following the higher percentage preference of male samples.

Examining the previous tables some observations can be draw, concerning the *Mooney-Rivlin* constants it is noticed the tendency of c_2 values to decrease on groups B and D (belonging to older groups) when compared to groups A and C (belonging to younger groups) and c_1 to increase value on groups B and D (belonging to older groups) when compared to groups A and C (belonging to younger groups).

Finally the graphics observation leads to the conclusion that the higher the inclinations the older groups and as we approach smoother slopes, the curves tend to belong to younger groups.

5.3.2. Neo-Hooke Model Constants

The calculated constants based on *Neo-Hooke* material model and on the experimental data resulted on the following tables; Table 48, Table 49, Table 50, Table 51, Table 52 and Table 53.

Table 48 *Neo-Hooke* Constants group of Male from 20 to 50 samples.

Sample	*Neo-Hooke Constants - Group A*
Number	C_1
3	1,5643
4	1,3654
15	1,1669
16	1,1882
Mean	**1,3212**

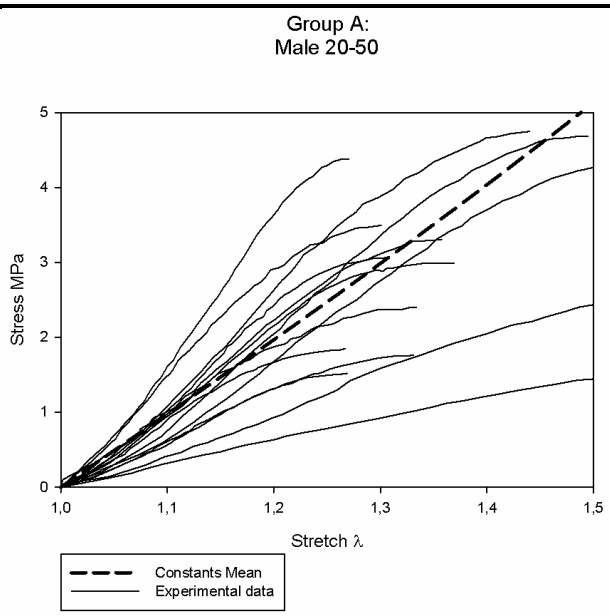

Table 49 *Neo-Hooke* Constants group of Male from 50 to 80 samples.

Sample	*Neo-Hooke Constants - Group B*
Number	C_1
1	1,2814
2	0,8557
6	1,7882
8	3,7247
9	5,6844
10	7,99
11	0,6303
12	4,3818
17	0,8223
18	0,4218
Mean	**2,75806**

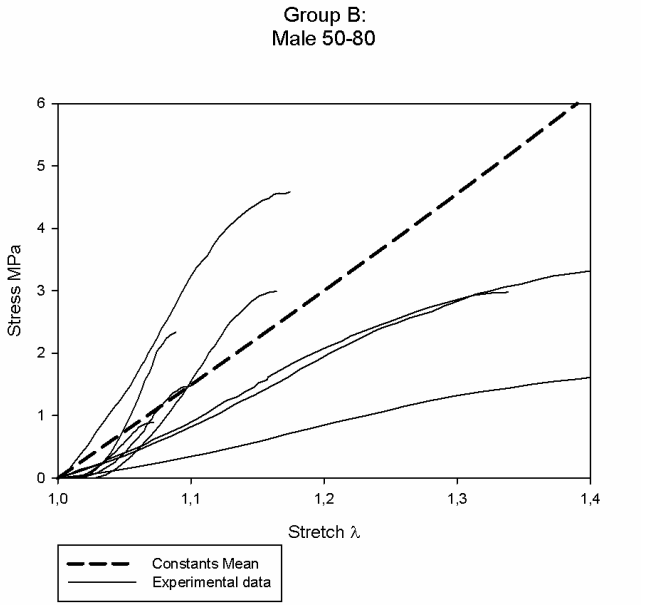

Both Table 48 and Table 49 mean plots have a tendency towards linearity which was expected for a *Neo-Hooke* based plot due to this material model only depending on one constant, c_1, which controls the curves slope.

Stress values are apparently similar for both mean plots at a stretch point.

Table 50 *Neo-Hooke* Constants group of Female from 20 to 50 samples.

Sample	*Neo-Hooke Constants - Group C*
Number	C_1
5	0,7103
13	1,4657
14	1,9857
Mean	**1,387233**

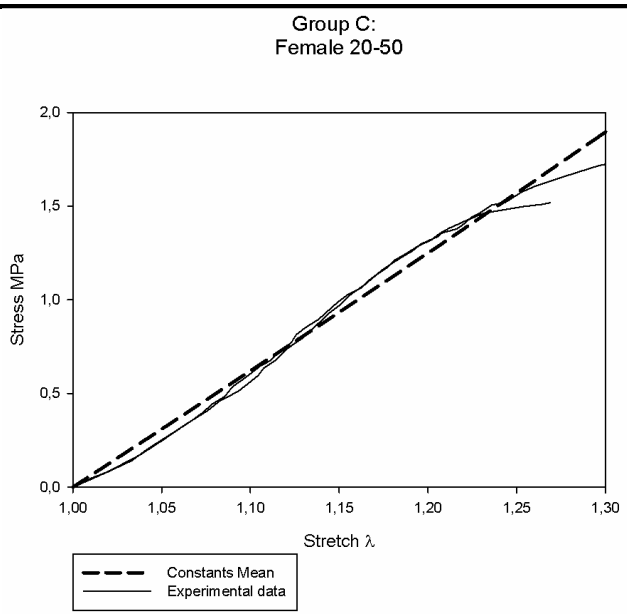

Table 51 *Neo-Hooke* Constants group of Female from 50 to 80 samples.

Sample	*Neo-Hooke Constants - Group D*
Number	C_1
19	1,4147
20	1,0888
Mean	**1,25175**

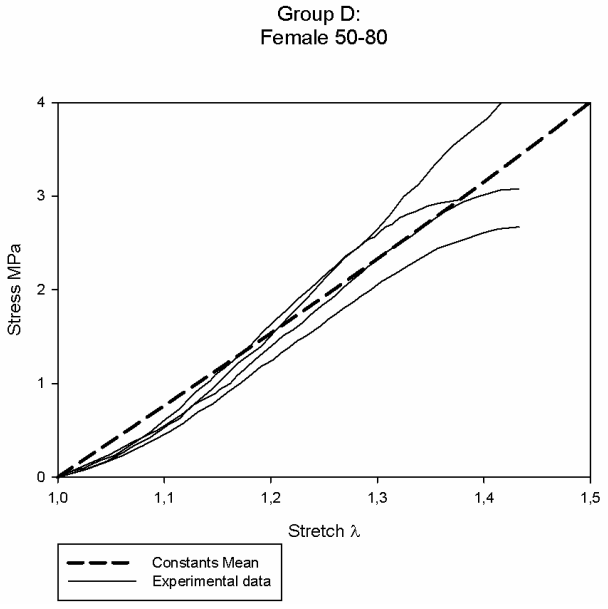

Both group C and D's mean plots have a tendency towards linearity, with deficient tracking of the experimental data.

Again the same event happens concerning the stress values for the same stretch, group C is 50% higher than D group; the younger group has twice the stress value than the older group.

Table 52 *Neo-Hooke* Constants group of samples from 20 to 50 years old.

Sample	*Neo-Hooke Constants - Group E*
Number	C_1
3	1,5643
4	1,3654
5	0,7103
13	1,4657
14	1,9857
15	1,1669
16	1,1882
17	0,8223
18	0,4218
Mean	**1,187844**

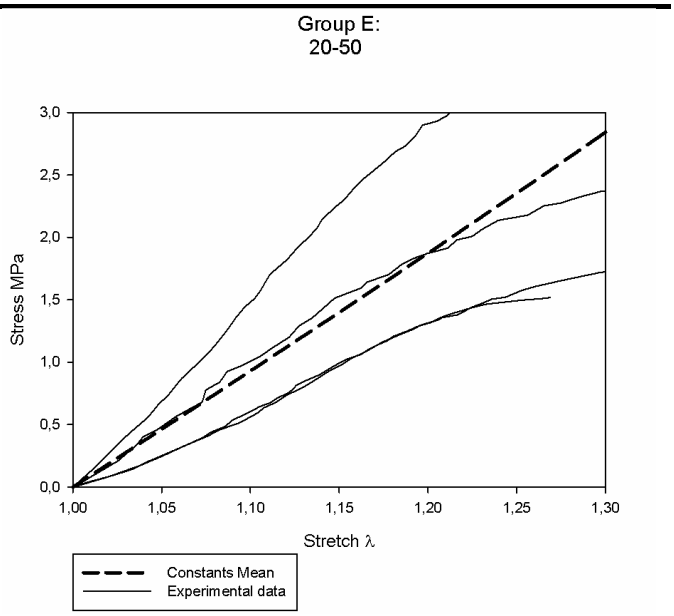

Table 53 *Neo-Hooke* Constants group of samples from 50 to 80 years old.

Sample	*Neo-Hooke Constants - Group F*
Number	C_1
1	1,2814
2	0,8557
6	1,7882
8	3,7247
9	5,6844
10	7,99
11	0,6303
12	4,3818
19	1,4147
20	1,0888
Mean	**2,884**

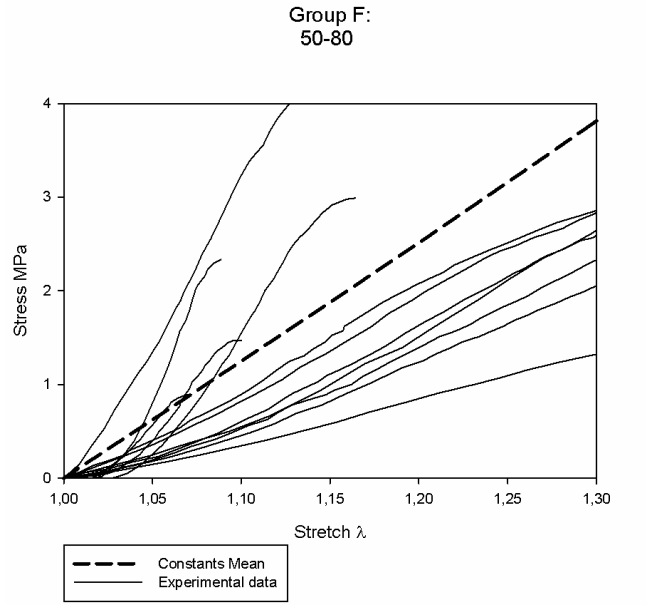

Both E and F mean plots are linear although having different inclinations; F, the older group, is about 1MPa higher for a 1,3 stretch value than E group.

With concern to the *Neo-Hooke* constants it is noticed the tendency of c_1 values to increase from groups A and B and to decrease on value for groups C to D.
The phenomenon that occurs do the male samples is reflected on the major groups, E and F that contain a higher percentage of male contribution than female ones.

5.3.3. Yeoh Model Constants

The calculated constants based on *Yeoh* material model and on the experimental data resulted on the following tables; Table 54, Table 55, Table 56, Table 57, Table 58 and Table 59.

Table 54 Yeoh Constants group of Male from 20 to 50 samples.

Sample	*Yeoh Constants – Group A*		
Number	C_1	C_2	C_3
1	1,6187	1,4565	-3,5886
2	2,2989	6,4777	-19,9206
3	0,7628	0,1379	-0,1411
6	0,5222	-0,011	-0,0562
7	1,6168	3,0469	-8,5095
13	0,9323	1,1662	-3,4171
14	0,8907	2,2206	-7,9378
18	1,3748	1,3771	-7,9626
19	1,5538	1,5974	-4,3789
20	1,903	1,3212	-2,3552
21	1,4505	1,2782	-1,4961
22	1,1837	0,934	-0,9077
23	2,4698	0,3979	-5,0208

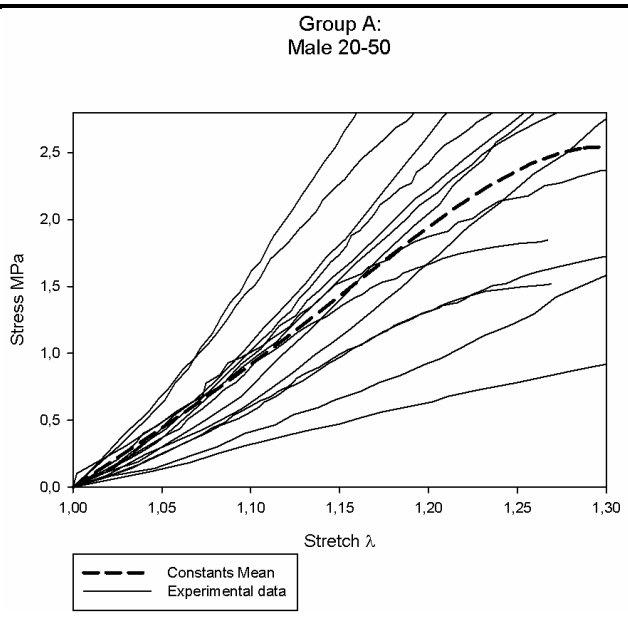

24	1,7344	-0,8046	-0,559
Mean	**1,450886**	**1,471143**	**-4,73223**

Table 55 *Yeoh* Constants group of Male from 50 to 80 samples.

Sample	*Yeoh Constants – Group B*		
Number	C_1	C_2	C_3
4	0,6334	0,3038	-0,4645
5	1,4958	1,4951	-3,8883
8	4,491	18,8388	-162,733
9	1,4911	0,4954	-1,1544
10	-0,4783	265,7304	-4676,83
11	0,1047	180,5209	-5167,3
12	-0,1218	119,8477	-1751,64
15	0,1727	56,6878	-346,911
Mean	**0,973575**	**80,48999**	**-1513,87**

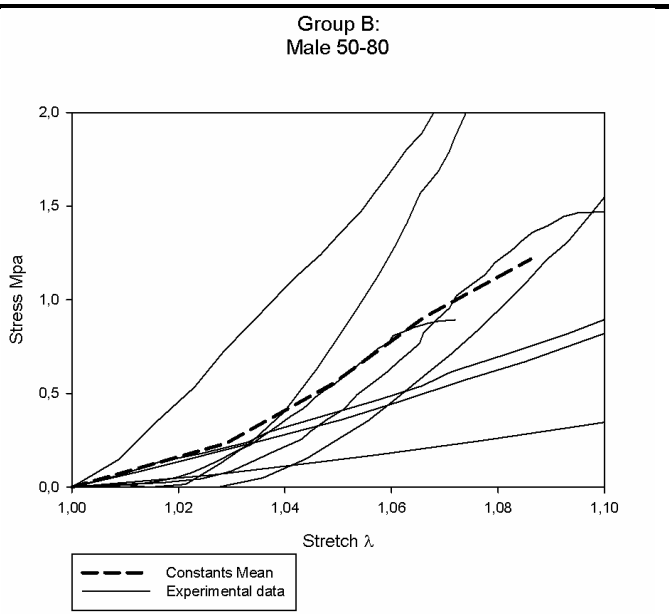

Table 54 mean plot follows experimental data in an empirically satisfactory way, with the initial non-linear portion and the concave curve type. Group B is not as interesting when tracking is in order although it follows the concave expression of A group.

The stress value is similar to both groups presenting a 1,08 stretch value.

Table 56 *Yeoh* Constants group of Female from 20 to 50 samples.

Sample	*Yeoh Constants – Group C*		
Number	C_1	C_2	C_3
13	0,9323	1,1662	-3,4171
14	0,8907	2,2206	-7,9378
Mean	**0,9115**	**1,6934**	**-5,67745**

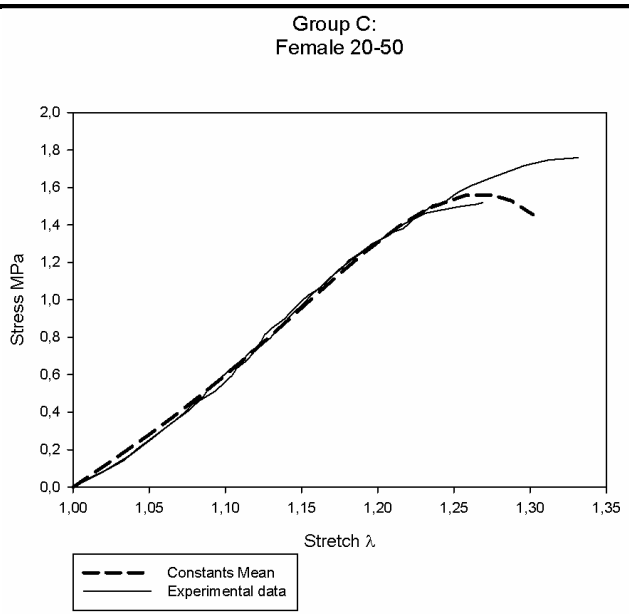

Table 57 *Yeoh* Constants group of Female from 20 to 50 samples.

Sample	*Yeoh Constants – Group D*		
Number	C_1	C_2	C_3
25	0,8453	1,5711	-1,8954
26	1,0069	1,2955	-1,0451
27	0,9583	2,2297	-3,5184
28	0,7822	1,2778	-1,5896
Mean	**0,898175**	**1,593525**	**-2,01213**

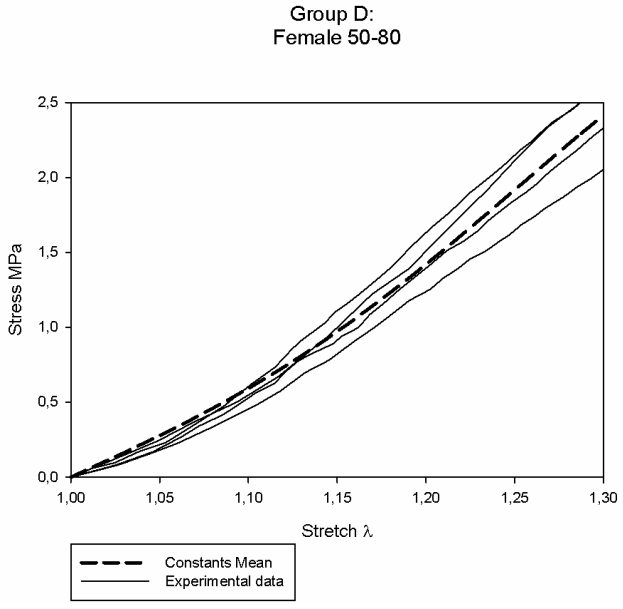

Notice both mean plots have a concave tendency, with similar stress values for a same stretch value.

Table 58 *Yeoh* Constants group of samples from 20 to 50 years old.

Sample	*Yeoh Constants – Group E*		
Number	C_1	C_2	C_3
1	1,6187	1,4565	-3,5886
2	2,2989	6,4777	-19,9206
3	0,7628	0,1379	-0,1411
6	0,5222	-0,011	-0,0562
7	1,6168	3,0469	-8,5095
13	0,9323	1,1662	-3,4171
14	0,8907	2,2206	-7,9378
18	1,3748	1,3771	-7,9626
19	1,5538	1,5974	-4,3789
20	1,903	1,3212	-2,3552
21	1,4505	1,2782	-1,4961
22	1,1837	0,934	-0,9077
23	2,4698	0,3979	-5,0208
24	1,7344	-0,8046	-0,559
Mean	**1,450886**	**1,471143**	**-4,73223**

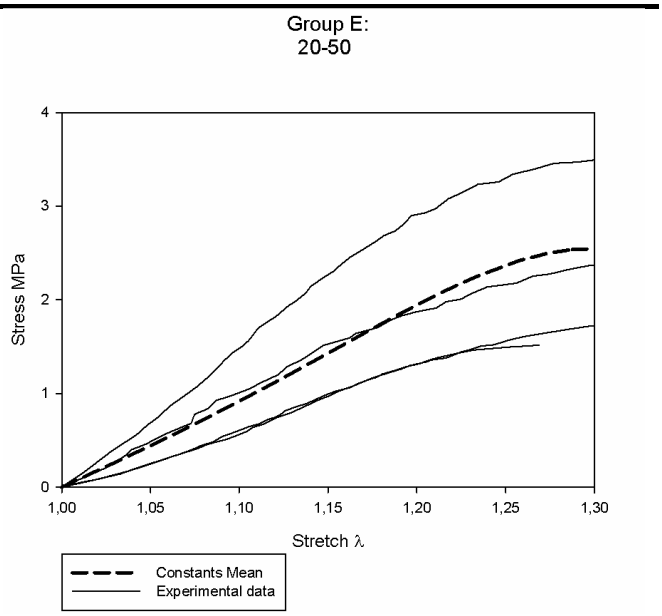

Table 59 *Yeoh* Constants group of samples from 50 to 80 years old.

Sample	*Yeoh Constants – Group F*		
Number	C_1	C_2	C_3
8	4,491	18,8388	162,733
9	1,4911	0,4954	-1,1544
4	0,6334	0,3038	-0,4645
5	1,4958	1,4951	-3,8883
10	-0,4783	265,7304	4676,83
11	0,1047	180,5209	-5167,3
12	-0,1218	119,8477	1751,64
15	0,1727	56,6878	346,911
25	0,8453	1,5711	-1,8954
26	1,0069	1,2955	-1,0451
27	0,9583	2,2297	-3,5184
28	0,7822	1,2778	-1,5896
Mean	**0,948442**	**54,19117**	**1009,91**

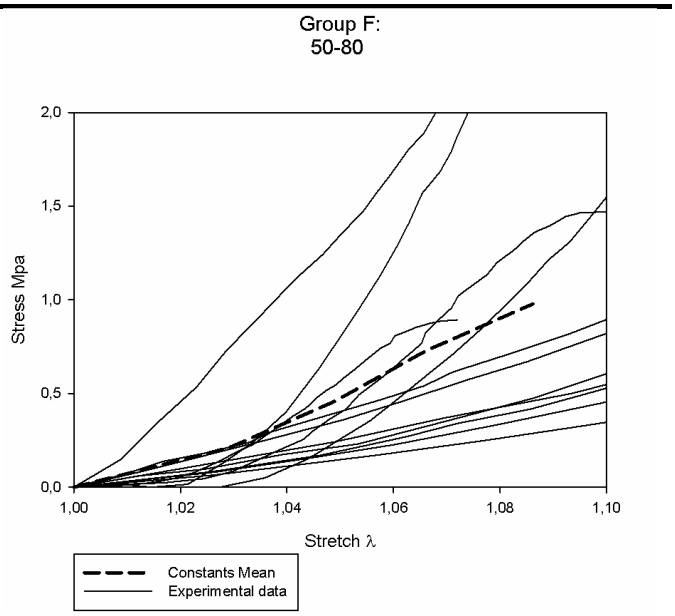

Table 58 and Table 59 follow the convex tendency for the mean curves type and the with similar stress values for a stretch.

By examining the previous tables some observations can be draw, concerning the *Yeoh* constants for the male samples, it is noticed the tendency of c_1, c_3 values to decrease from group A to B (younger to older groups) and c_2 to increase value at the same circumstance. For the female samples c_1 and c_2 decrease value from B to C groups as c_3 raises.

The phenomenon that occurs do the male samples is reflected on the major groups, E and F which contains a higher percentage of male contribution than female ones.

5.4. Final notes on the results

For muscles male groups show a tendency for linear or convex plots, the female's opposite which are mainly concave. Younger groups usually have higher stress values for a same stretch value when matching to older groups.

The fascia and tendons groups, again show that there is a tendency for linear if not convex plot types and concave (sometimes linear) curves for female groups. However stress values wise, there is tendency for higher values, at a same stretch value, for older groups and milder slopes for females. This first arguments will be discussed and validated on the next chapter.

6. Discussion

During chapter 5, the computed results on the different constitutive functions constants were presented, already differentiated according to gender and sex and accompanied with the respective plot which showed all experimental data against the calculated curve. This chapter presents a synthesis of the relevant data.

Recalling the assigned groups' designation, we have differentiating gender, groups A to D;

- Group A : Male 20-50
- Group B: Male 50-80
- Group C : Female 20-50
- Group D: Female 50-80

And distinguishing age, groups E and F:

- Group E: Age to 20-50
- Group F: Age to 50-80

An important notion such as stiffness is key to establish a qualitative notion between the next plots. Stiffness is an extensive material property, which is referred to as the resistance of an elastic body to deformation by an applied force along a given degree of freedom when a set of loading points and boundary conditions are prescribed on the elastic body.

6.1. Influence of age and gender for muscles

6.1.1. The Mooney-Rivlin model

The recommended constants to be used in case the *Mooney-Rivlin's* material model is used are as is shown on Table 60:

Table 60 Recommended constants.

	Male		Female	
	20-50	50-80	20-50	50-80
C_1	**0,164264**	**0,358211**	**-0,05548**	**-0,05526**
C_2	**0,099257**	**-0,26553**	**0,281433**	**0,178071**

C_1 shows an increase on twice its value with age for the male groups whilst for the female groups the same doesn't happen. C_2 happens to decrease its value for both genders from the younger to the older groups.

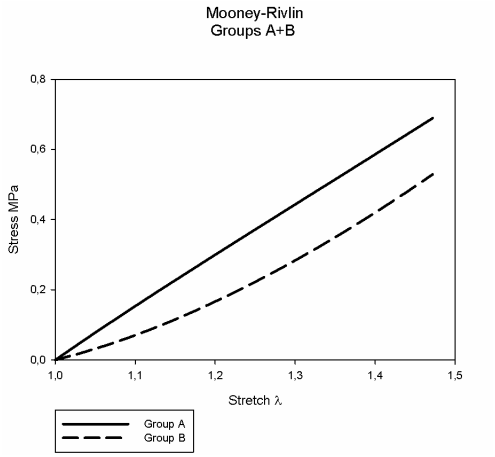

(a)Male groups

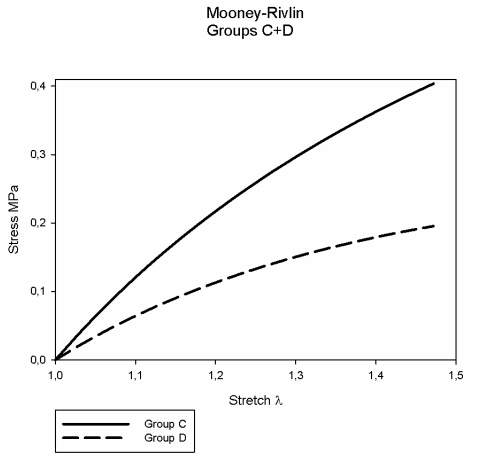

(b)Female groups

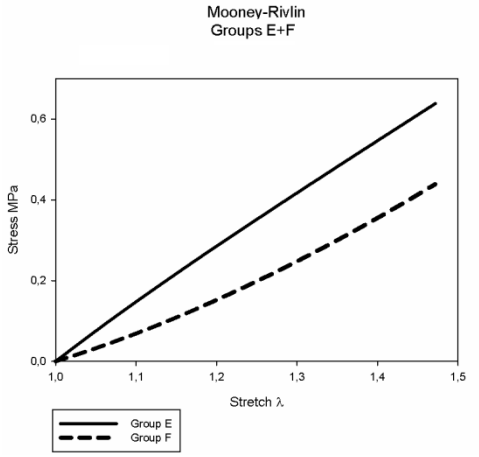

(c)Age separated groups

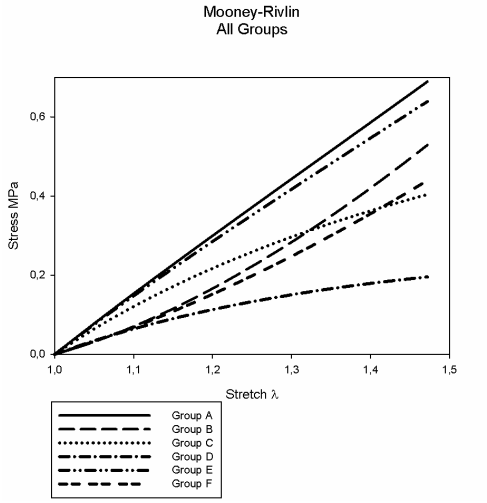

(d) all groups

Figure 42 The Money-Rivlin model for the selected groups.

Male groups mean plots are either linear shaped or convex , younger and older respectively and female plots are positively concaved.

For the *Mooney-Rivlin* model applied to muscles, age is shown to be an important factor as younger groups are shown to be stiffer than older ones, since for (a) and (b) plots the stiffness is clearly higher for younger groups (A and C). (d) plot shows that same fact;

- Male from 20 to 50 years old mean plot stress value at 1,4 stretch is 67% higher than for 50 to 80 years old group;
- Female from 20 to 50 years old mean plot stress value is 40% higher than for the older corresponding group.

Gender plays a decisive factor on stress values, for the male group's maximum stress value (to a stretch of 1,4) is consistently higher than the values of maximum stress for the female groups (to the same stretch value); by (d) plots analysis it can be shown that:

- for 20 to 50 years old, the male selection is 60% higher than the female corresponding selection;
- For 50 to 80 years old , the female plot is 40% higher that the female corresponding group.

6.1.2. The *Neo-Hooke* Model

The recommended constants to be used in case the *Neo-Hooke's* material model is used are as is shown on Table 61:

Table 61 Recommended constants.

	Male		Female	
	20-50	50-80	20-50	50-80
C_1	**0,0946**	**0,1536**	**0,2360**	**0,0875**

The *Neo-Hooke* constants are contradictory as for male groups it decreases form the younger to the older group and the opposite occurs for the female groups.

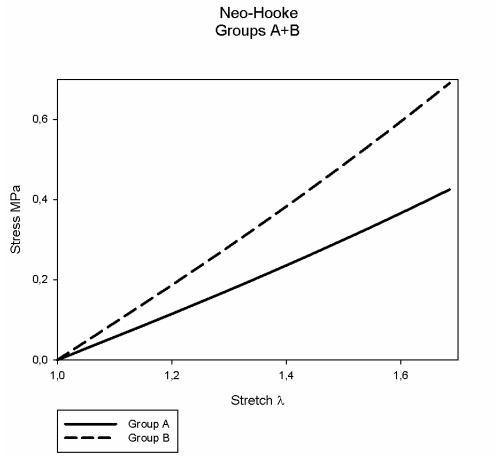

(a)Male groups

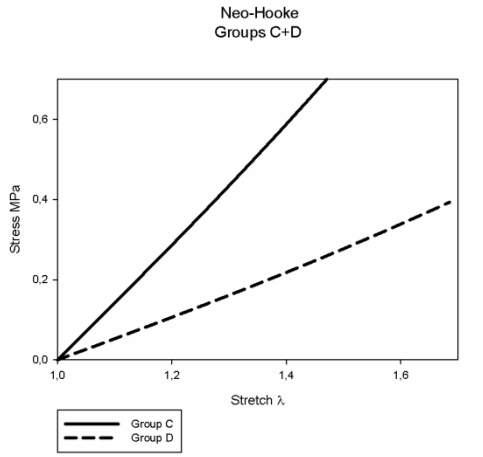

(b)Female groups

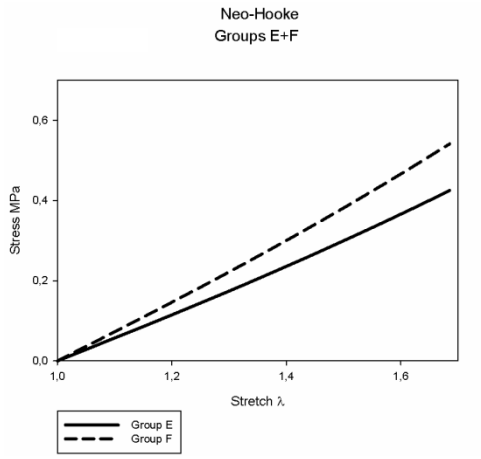

(c)Age separeted groups

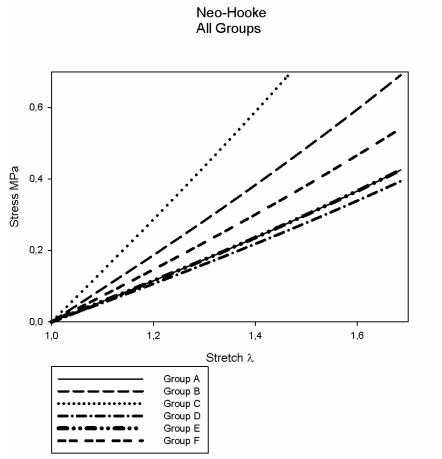

(d) All groups

Figure 43 The *Neo-Hooke* model for the selected groups.

Both for the female groups as well as for the male ones, plots present themselves linear shaped.

For the *Neo-Hooke* model applied to muscles, age doesn't seem to be an important factor as younger groups are scattered (see (a) and (b)). Plot (d) ties the question raised aback, showing that for the *Neo-Hooke* model, older groups are stiffer;

- For the male selection, 20 to 50 years old plot stress value is 60% higher than for 50 to 80 years old plot, considering a 1,6 stretch value;
- For the female groups, 20 to 50 years old stress value at 1,6 stretch is 25 % higher than the older corresponding stress value.

Gender wise ((d)plot) the results are too scattered to take any conclusion.

6.1.3. The Yeoh model

The recommended constants to be used in case the *Yeoh's* material model is used are as is shown on:

Table 62 Recommended constants.

	Male		Female	
	20-50	50-80	20-50	50-80
C_1	**0,222596**	**0,074174**	**0,2114**	**0,0844**
C_2	**0,273675**	**1,280789**	**0,0660**	**-0,0376**
C_3	**-0,93019**	**-12,0667**	**-0,5000**	**0,0115**

C_1 is consistent when matching same age groups, although C_2 and C_3 fluctuate within corresponding groups.

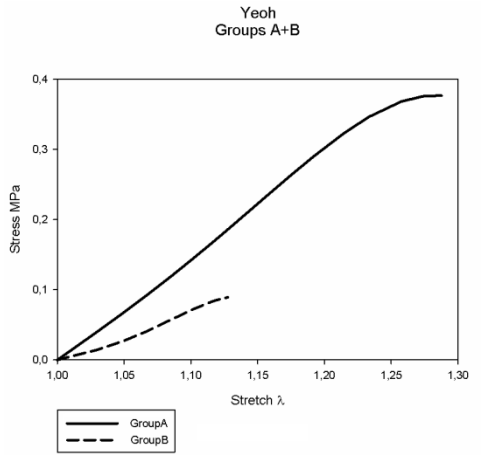

(a)Male groups

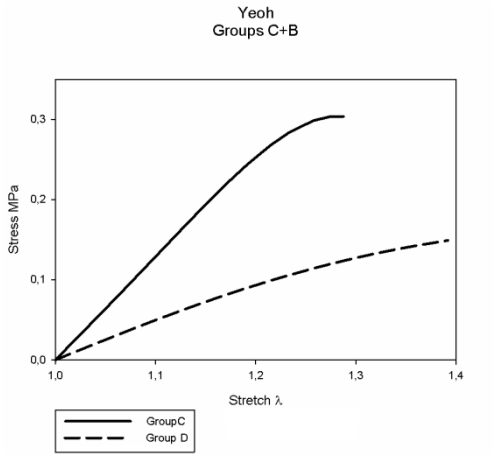

(b)Female groups

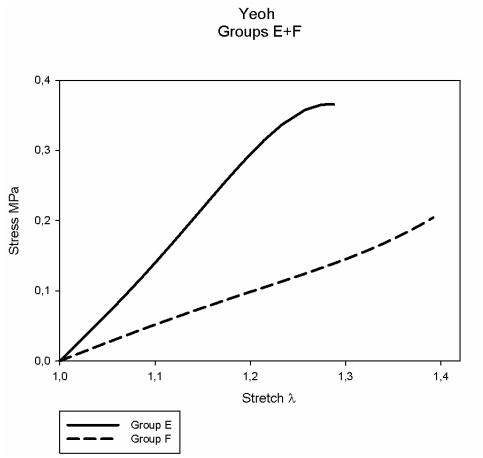

(c)Age separeted groups

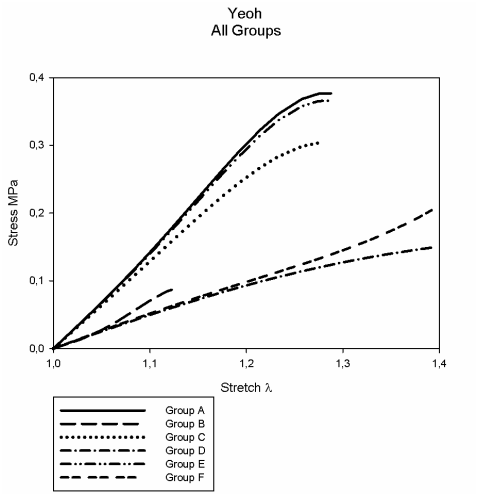

(d) All groups

Figure 44 The *Yeoh* model for the selected groups.

By (d) plots observation younger groups tend to be of concave shape and older convex.

For the *Yeoh* model applied to muscles, age is shown to be an important factor as younger groups are shown to be stiffer than older ones, since for (a) and (b) plots the stiffness is higher for younger groups (A and C); (d) plot shows that same fact;

- Corresponding to a 1,1 stretch value, stress values for male groups are 40% higher from A to B plots;
- Corresponding to a 1,1 stretch value, stress values for female groups are 30higher from C to D plots.

(d) plot shows that there is a predominance of younger plots with higher maximum stress values than older ones.

About gender, the plots observation doesn't lead to a conclusive understanding.

6.1.4. Muscle's final discussion

Within muscles there will be presented some final conclusions regarding plot shape and stress values according to the stretch in accordance with and age and gender differences;

- Shape wise; Male groups mean plots have a tendency towards either linear or convex shapes (depending either they are younger and older respectively) and female plots are mainly concaved;
- Age wise; for all tested material models age is shown to be an important factor as younger groups are shown to be stiffer than older ones. And there is a noticed tendency for a bigger gap between stress values for younger and older male groups (60 to 40% higher for younger groups) than there is in younger to older female groups (40 to 25% higher for younger plots);
- Gender wise; only for *Mooney-Rivlin*'s model does this parameter seem to play a decisive role for the male groups' maximum stress value are consistently higher than the values of maximum stress for the female groups.

6.2. Influence of the age and gender for fasciae

6.2.1. The Mooney-Rivlin model

The recommended constants to be used in case the *Mooney-Rivlin's* material model is used are as is shown on Table 63:

Table 63 Recommended constants.

	Male		Female	
	20-50	50-80	20-50	50-80
C_1	**0,5388**	**5,35109**	**-1,08863**	**0,6107**
C_2	**1,029125**	**-2,98986**	**2,791367**	**0,9766**

C_1 values range between]-2 ;6[governing the initial portion of the plots and C_2's values vary from]-3;3[dictating the slopes values.

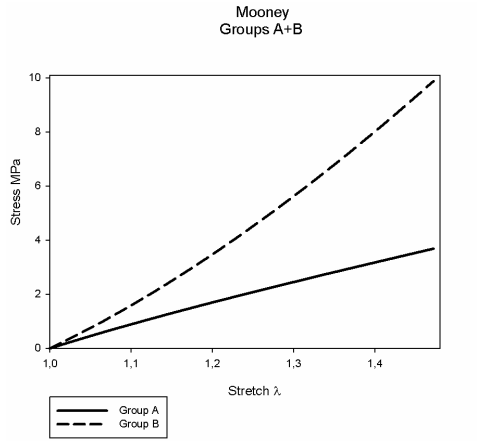

(a)Male groups

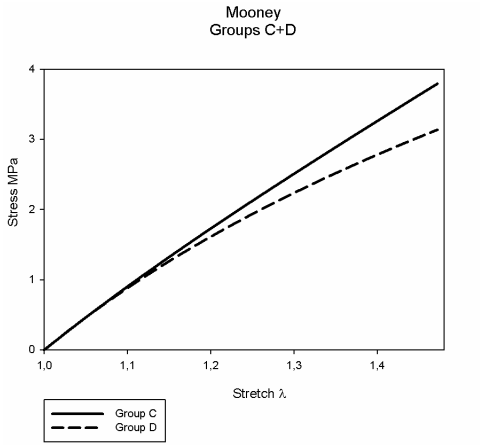

(b)Female groups

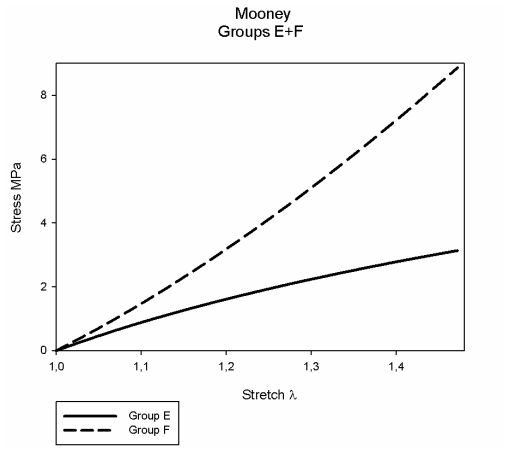

(c)Age separated groups

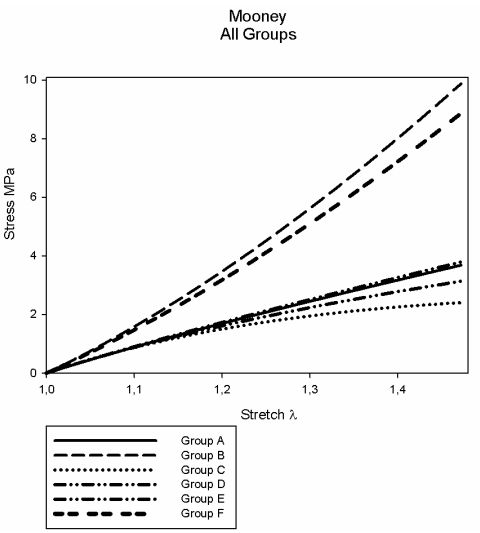

(d) all groups

Figure 45 The Money-Rivlin model for the selected groups.

Male groups' shapes are linear and convex. As for female groups are positively concave, as it had happened for the muscles' case.

For the *Mooney-Rivlin* model applied to fasciae, age is shown to be a factor as older male groups are shown to be stiffer than younger ones, since for observation of (a) and (d) plots the stiffness is clearly higher for older groups (B and F). as for the Female only plots, this difference isn't noticeable;

- Male plots have a 25% higher stress value (at a 1,4 stretch) for older samples than the younger ones.
- Female stress values for a 1,4 stretch value do not present as much difference between younger and older groups, 0.03% higher for the older considered stress value.

Gender wise, the results play a role on the stress value, for the older male group (A) the stress value (to a stretch of 1,4) is consistently higher than the values of for the female groups (to the same stretch value). The same doesn't happen however for the younger male group, which stress value wise is identical do the female groups for the same stretch; (d) plot shows that same fact;

- From 50 to 80 years old, male stress value at 1,4 stretch is 25% higher than the female corresponding value ;

6.2.2. The Neo-Hooke Model

The recommended constants to be used in case the *Neo-Hooke's* material model are as is shown on Table 64:

Table 64 Recommended constants.

	Male		Female	
	20-50	50-80	20-50	50-80
C_1	**1,3212**	**2,75806**	**1,387233**	**1,25175**

C_1 values are identical for both genders, although C_2's are not; they are 45% higher the male group (this fact will influence its slope, see ahead.).

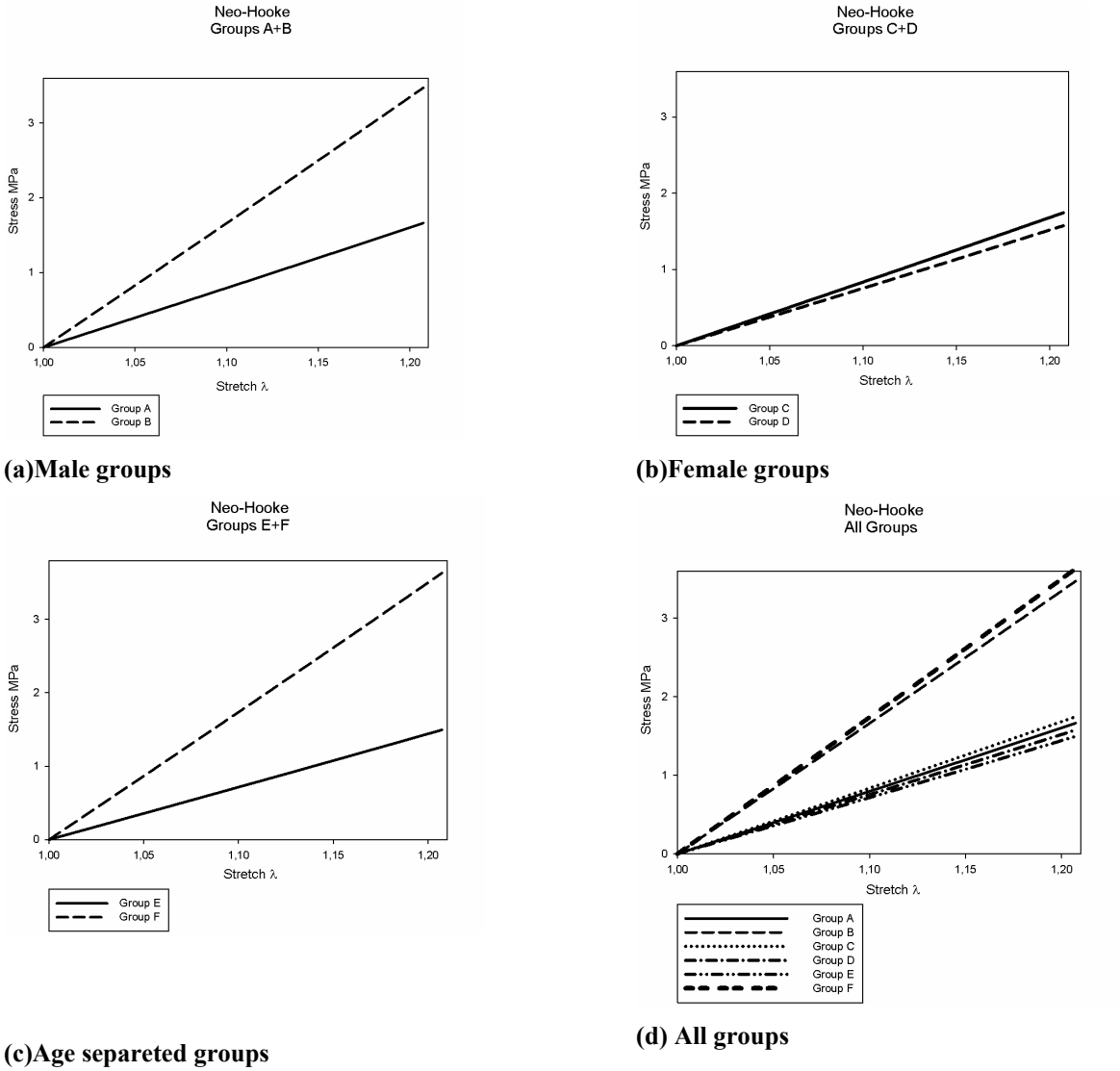

(a)Male groups

(b)Female groups

(c)Age separeted groups

(d) All groups

Figure 46 The *Neo-Hooke* model for the selected groups.

All plots present themselves as linear, independent of age and gender.

For the *Neo-Hooke* model applied to fasciae, age is shown to be a factor as older male and older general groups are shown to be stiffer then female and general younger ones, since for observation of (a) and (d) plots the stiffness is clearly higher for older groups (B and F);

- Older group, B has a stress value (at 1,15 stretch) 40% higher than the corresponding younger plot stress value.
- Stress value for female plots are similar.

Gender wise, the results aren't very different, so there is no relevance there. What really comes as important is that by (d) plots observation, F and B groups (both genders 50-80 and male 50-80 respectively) are severely detached from the rest of the groups.

6.2.3. The Yeoh model

The recommended constants to be used in case the *Yeoh's* material model is used are as is shown on Table 65:

Table 65 Recommended constants.

	Male		Female	
	20-50	50-80	20-50	50-80
C_1	**1,288725**	**1,60391**	**1,470567**	**1,25135**
C_2	**0,6303**	**14,56735**	**1,163667**	**0,26795**
C_3	**1,28593**	**-52,8215**	**-30,5988**	**-0,2494**

The presented constants vary a great deal, which makes it rather difficult to extract a linear conclusion.

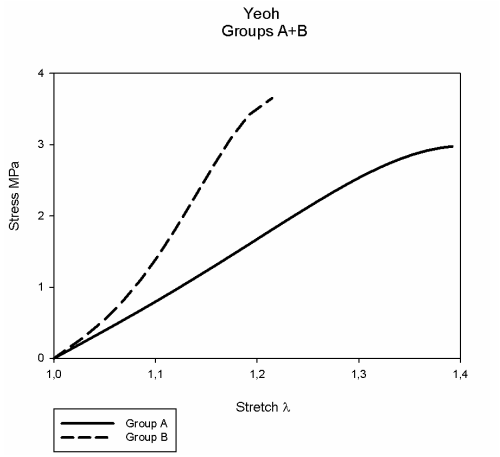

(a)Male groups

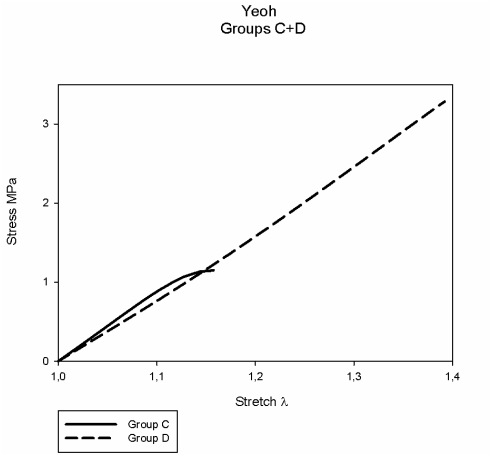

(b)Female groups

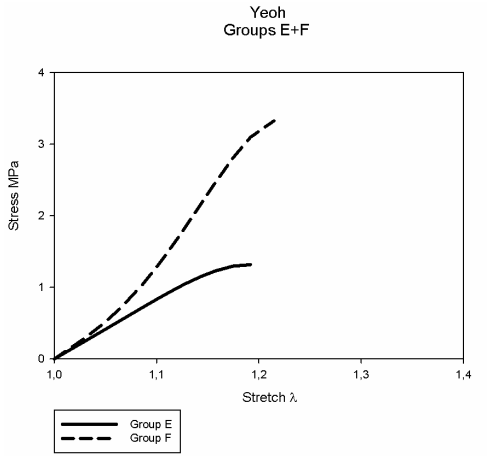

(c)Age separeted groups

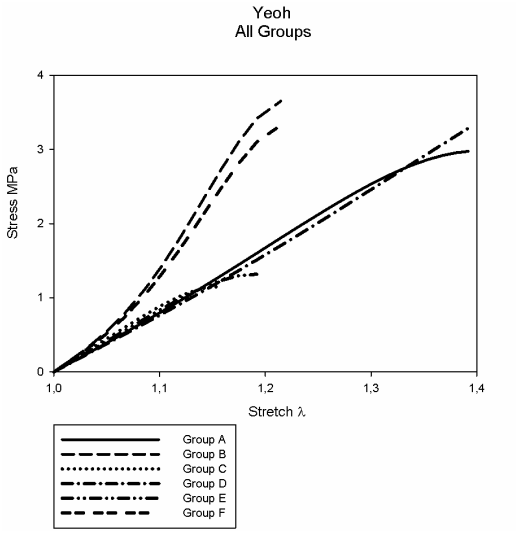

(d) All groups

Figure 47 The *Yeoh* model for the selected groups.

Yeoh's mean plots are concave, independently of their age and gender.

Concerning age, B plot (male form 50 to 80 years old) is 40% stiffer than A plot (younger), as it had occur for the other material models. Female groups have identical slopes, only different maximum stresses; older samples make for higher maximum stress than younger ones.

Again has it had occur for the previous models, by (d) plots observation, F and B groups (both genders 50-80 and male 50-80 respectively) are severely detached from the rest of the groups.

6.2.4. Fasciae' final discussion

Within fasciae there will be presented some final conclusions regarding plot shape and stress values according to the stretch in accordance with and age and gender differences;

- Shape wise; there isn't much agreement. For *Mooney-Rivlin*'s model Male groups' shapes are linear and convex. As for female groups are positively concave. For *Neo-Hooke's* model, All plots present themselves as linear, independent of age and gender and for *Yeoh*'s model mean plots are concave;
- Age wise; it is rather unanimous since age is shown to be a factor as older male groups are shown to be stiffer than younger ones, although this fact is exacerbated for the male groups. Male plots have a higher stress values for older samples, ranging from 40 to 25% higher to than the younger ones. As for the female groups there is also an understanding that female stress values for a same stretch value do not present as much difference between younger and older groups, being this range from about 0.03% higher for the older plots;
- Gender wise; there is again an unanimous answer as all models agree that for the older male group the stress value is consistently higher than the values of for the female groups . The same doesn't happen however for the younger male group, which stress value wise is identical do the female groups for the same stretch. Being F and B groups consistently severely detached from the rest of the plots.

6.3. Influence of the age and gender for tendons

6.3.1. The Mooney-Rivlin model

The recommended constants to be used in case the *Mooney-Rivlin's* material model is used are as is shown on Table 66:

Table 66 Recommended constants.

	Male		Female	
	20-50	50-80	20-50	50-80
C_1	**0,500433**	**20,81875**	**0,71065**	**1,86625**
C_2	**1,400983**	**-20,0426**	**0,38725**	**-0,78245**

C_1 values range between]-1 ;20[governing the initial portion of the plots and C_2's values vary from]-20;2[dictating the slope.

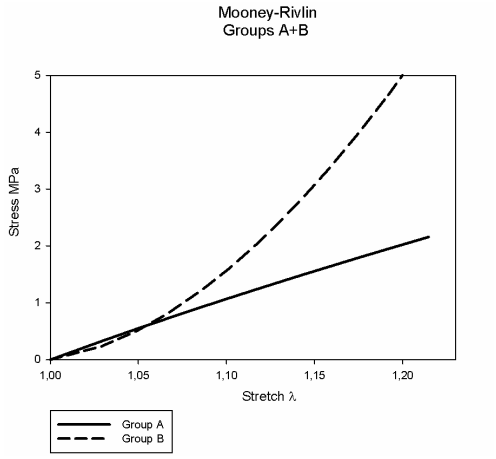

(a)Male groups

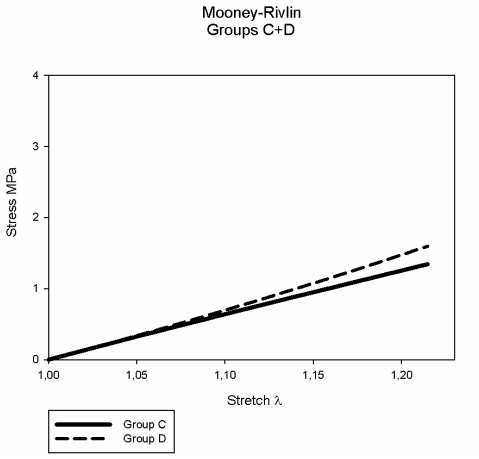

(b)Female groups

(c)Age separated groups

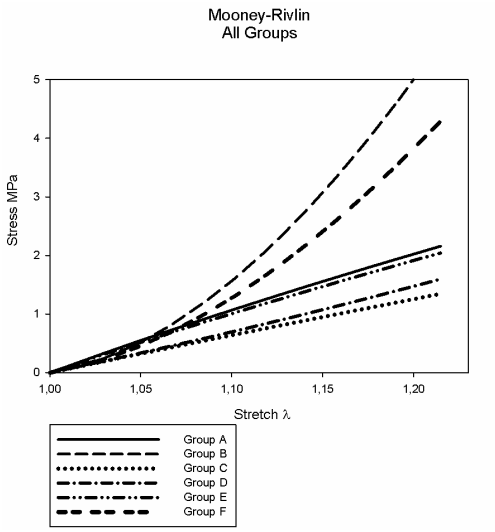

(d) all groups

Figure 48 The Money-Rivlin model for the selected groups.

A group is of concave shape whilst the other groups B, C and D are linear.

For the *Mooney-Rivlin* model applied to tendons, age is shown to be a factor as the older male group is shown to be stiffer then the younger male and both female groups, by observation (a) (B) and (d) plots;

- For male groups, on 1,2 stretch values, the matching stress values for the older group is 40% higher than the younger one;
- For female groups have similar slopes.

Gender wise, the results play a role on the stress value, for the older male group (A) the maximum stress value (to a stretch of 1,5) is consistently higher than the values of maximum stress for the female groups (to the same stretch value). The same doesn't happen however for the younger male group, which stress value wise is identical do the female groups for the same stretch; (d) plot shows that same fact.

6.3.2. The Neo-Hooke Model

The recommended constants to be used in case the *Neo-Hooke's* material model is used are as is shown on Table 67:

Table 67 Recommended constants.

	Male		Female	
	20-50	50-80	20-50	50-80
C_1	**1,3212**	**2,75806**	**1,387233**	**1,25175**

C_1's values are similar for the same age group of 20 to 50 years old, and twice the value for male 50 to 80 years when matching with the same age group on female.

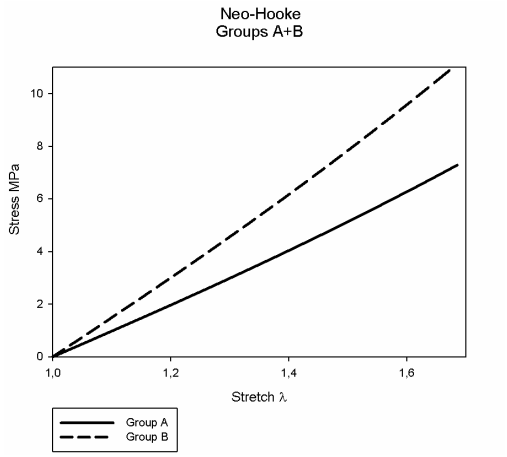

(a)Male groups

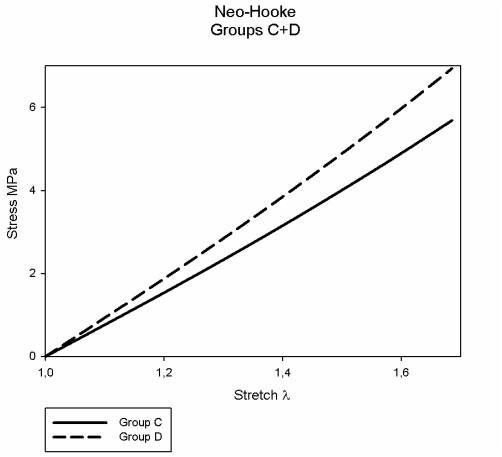

(b)Female groups

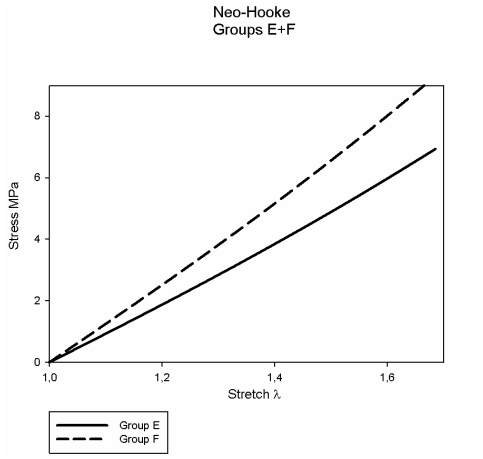

(c)Age separeted groups

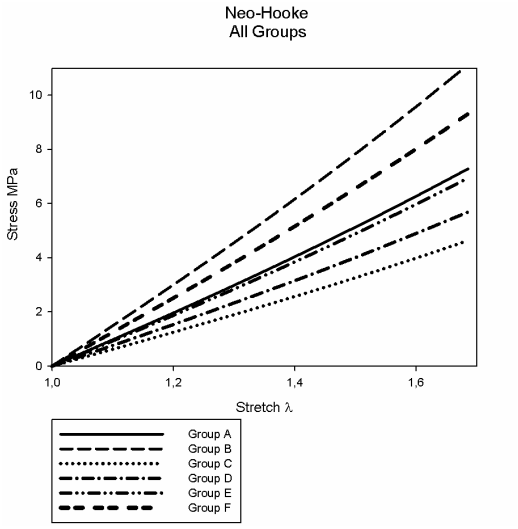

(d) All groups

Figure 49 The *Neo-Hooke* model for the selected groups.

All plots tend to be linear, although by simple (d) plot's observation, it can be noticed a sight tendency for a convex shape happening for all of them.

For the *Neo-Hooke* model applied to tendons, age is shown to be a factor as older male and older female groups are shown to be stiffer than younger male and female ones, reflection of (a) and (b);

- Considering older groups, the male has a stress value about 55% higher for the same stretch value than the female one;
- For younger groups, the male one has a stress value of almost 60% higher (for a same stretch value) than the female one.

- Generally older groups are stiffer than younger ones.

Gender wise, the results play a role on the stress value, for the older male group (A) the maximum stress value (to a stretch of 1,6) is consistently higher than the values of maximum stress for the female groups (to the same stretch value). The same doesn't happen however for the younger male group, which stress value wise is identical do the female groups for the same stretch; (d) plot shows that same fact.

6.3.3. The Yeoh model

The recommended constants to be used in case the *Yeoh's* material model is used are as is shown on Table 68:

Table 68 Recommended constants.

	Male		Female	
	20-50	50-80	20-50	50-80
C_1	**1,450886**	**0,973575**	**0,9115**	**0,898175**
C_2	**1,471143**	**80,48999**	**1,6934**	**1,593525**
C_3	**-4,73223**	**-1513,87**	**-5,67745**	**-2,01213**

The presented constants vary a great deal, which makes it rather difficult to extract a linear conclusion.

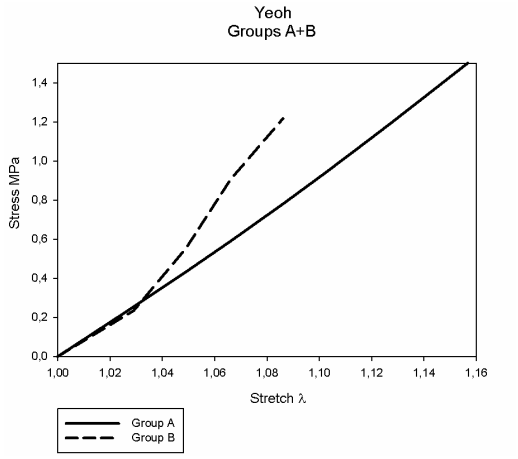

(a)Male groups

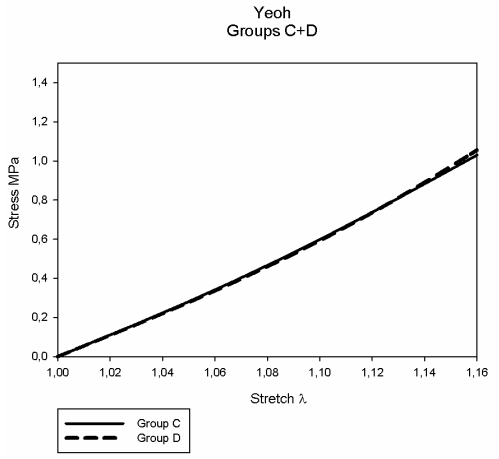

(b)Female groups

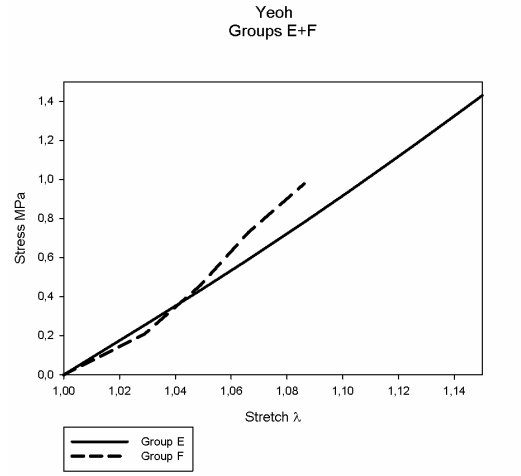

(c)Age separeted groups

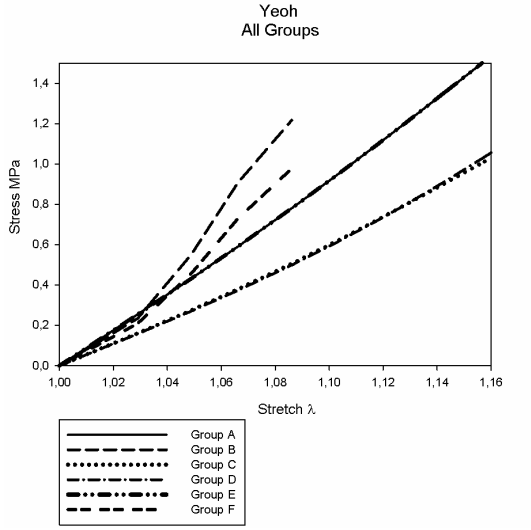

(d) All groups

Figure 50 The *Yeoh* model for the selected groups.

Examining (a) figure, A group (older one) shows itself to be of a concave tendency while B group is almost linear. Plots on (b) figure show a tendency towards concave shape again for the older group and again linearity for the younger one.

As for age differences whilst both female plots show approximately an 67% of inclination, the young male plot shows about 120% of inclination for the same stretch value; Although gender wise female groups show higher stress values then male's for the same stretch. Since this fact is isolated from the previous material model results, it would have to be tested on the lab, once more, in order to determine an answer and prove that it isn't a mistake.

6.3.4. Tendons' final discussion

Within tendons there will be presented some final conclusions regarding plot shape and stress values according to the stretch in accordance with and age and gender differences;

- Shape wise; Male groups, older ones, show a concave tendency while younger groups are linear independent of the material model. Female groups also show a tendency towards concave shape again for the older group and linearity for the younger ones.
- Age wise; age is shown to be a factor as the older male groups are stiffer then the younger male and both female groups. This fact is also true for all applied models.
- Gender wise; for *Mooney-Rivlin* and *Neo-Hooke* models gender plays a role on the stress value, for the older male groups (A) the maximum stress value is consistently higher than the values of maximum stress for the female groups. The same doesn't happen however for the younger male group, which stress value wise is identical do the female groups for the same stretch. For the *Yeoh*'s model groups show higher stress values then male's for the same stretch.

6.4. Final discussion notes

Recalling the obtained results parallel factors and major differences can be established between muscles, fasciae and tendons' and this is what will the main focus be.

- Regarding plots shape for muscles there is clear understanding that male groups mean plots have a are either linear or convex shapes and female plots are mainly concaved. This doesn't happen for fasciae and tendons, where the plots shape is apparently controlled by age and not gender because older ones plots, show a concave tendency while younger groups are linear or concave shaped;
- On the subject of age for muscles it's an important factor as younger groups are stiffer then older ones, and there is a noticed tendency for a bigger gap between stress values for younger and older male than there is in younger to older female groups (40 to 25% higher for younger plots), while for fascia and tendons it is the opposite and rather unanimous that age leads to the fact that older male groups are shown to be stiffer than younger ones and also stiffer than (old a young) female groups;
- Concerning gender there is an understanding for both fascia and tendons that applying *Mooney-Rivlin* and *Neo-Hooke* models for the older male groups the stress value is consistently higher than the values of for the female groups . The same doesn't happen however for the younger male groups, which stress value wise are identical do the female groups for the same stretch. For muscles this parameter behaves quite the opposite way has both the male group's maximum stress value are consistently higher than the values of maximum stress for the female groups.

7. Conclusions

This biomechanical study of the temporalis pretended to characterize the chosen muscle's behavior by means of the constitutive non-linear equations and their constants. The associated structures like the temporalis fasciae and the tendons were also intended to be studied, as well as their differences between each other considering age, gender and mouth constitution and lacking of teeth.
Another goal was to define the deformation mechanism for the microscopic structure, the endomysium, having a different approach in order to describe the muscle's behavior within the nonlinear regime and the large deformations' theory, as it has already been described by the linear sold mechanics theory.

All these objective were accomplished as muscles, fasciae and tendons were appointed constants. These recommended constants were divided in different groups according to age and gender but not according to the mouth constitution, this particular problem was not to able to be addressed.
An equation concerning the endomysium behavior within the nonlinear regime and the large deformations' theory has been drawn also.

Using the calculated constants some plotting work was done has done to help and determine what would the differences between muscles and the other studied tissues be.
Recalling the obtained plots shape for muscles there is clear understanding that male groups mean plots have a are either linear or convex shapes and female plots are mainly concaved. Whether for the fasciae and tendons, the plots shapes are apparently controlled by age and not gender because older ones plots, show a concave tendency while younger groups are linear or concave shaped;

Age in muscles becomes an important factor as younger groups are stiffer than older ones, while for fasciae and tendons it is the opposite; higher age generally is shown to lead to stiffer tissues than younger ones.

Concerning gender both fascia and tendons, for the older male groups stress values are consistently higher than the female groups. For muscles this parameter behaves quite the opposite way has both the male group's maximum stress value are consistently higher than the values of maximum stress for the female groups.

This conclusions are based from more than one hundred uniaxial testes, belonging to eleven donors; nevertheless further work is needed. Bigger sample size for instance, include the lack of teething problem, spread this study to all mastication muscles, revision the influence of nourishment and most importantly include a study the temporomandibular pathologies and its influence on the mastication muscles.

8. Bibliography and Future Works

[Bennett, M.B., et al. 1986] Bennett, M.B., Ker, R.F., Dimery N.J., Alexander, R.M., 1986. Mechanical properties of various mammalian tendons. *Journal of Zoology*, 209, 211-26.

[Bonet, J., et al. 1997] Bonet, J., Wood, R.D, 1997. *Non Linear Continuum Mechanics for Finite Element Analysis*. Cambridge University Press.

[D'Alessandro, M.P., 1995] D'Alessandro, M.P., 1995. Anatomy Atlases. Wiley-Liss.

[Fukunaga, T., et al. 1997] Fukunaga, T., Kawakami, Y., Kuno, S., Funato, K., Fukashiro, S., 1997. Muscle architecture and function in humans. Journal of Biomechanics 30, 457-63.

[Gray, H., et al. 1995] Gray, H., Williams, P.L., Warwick, R., Dyson, M., Bannister, L.H., 1995. *Gray's Anatomy of the Human Body.* Elsevier.

[Gregor, R. J., et al. 1988] Gregor, R. J., Roy, R.R., Whiting, W.C., Lovely, R.G., Hodgson, J.A., Edgerton, V.R., 1988. Mechanical output of the cat soleus during treadmill locomotion: in vivo vs in situ characteristics. *Journal of Biomechanics*, 21, 721-32.

[Gosling, J.A., et al., 2008] Gosling, J.A., Harris, P.F., Humpherson, J.R., Whitmore, I., Willan, P.L.T., 2008. *Human Anatomy: color Atlas and Textbook*. Mosby Elsevier, 5th Edition.

[Hinton, E., 1992] Hinton, E., (1992).*Introduction to Nonlinear Finite Element Analysis*. Nafems.

[Langevin, H.M., et al. 2009] Langevin, H.M., Huijing, P.A., 2009. Communicating About Fascia: History, Pitfalls, and Recommendations. *International Journal of Therapeutic Massage and Bodywork*, 2, 4.

[Holzappfel, G.A., 2004] Holzappfel, G.A., 2004. *Nonlinear Solid Mechanics*. John Wiley & Sons, Ltd.

[Jadidi, F., et al, 2007] Jadidi, F., Castrillon, E., Svensson, P., 2007. Effect of conditioning electrical stimuli on temporalis electromyographic activity during sleep. *Journal of Oral Rehabilitation*.

[James, H., et al., 2006] James, H., Wang, C., 2006. Review Mechanobiology of Tendon. *Journal of Biomechanics*, 39, 1563-1582.

[Junqueira, L.C., et al., 2005] Junqueira, L.C., Carneiro, J., 2005. *Histologia Básica*. Guanabara Koogan 10ª edição.

[Lai, M.W., et al. 1993] Lai, M.W., Rubin, D., Krempl, E., 1993. *Introduction to Continuum Mechanics*. Butterworth Heinmann, 3th Edition.

[Law, D.J., et al., 1993] Law, D.J., Lightner, V.A., 1993. Dystrophin deficiency is associated with myotendinous junction defects: ultra-structure and mechanics of failure. *Journal of Muscle Research and Cell Motility* 14, 173-185.

[Lin, T.W., et al., 2004] Lin, T.W., Cardenas, L., Soslowsky, L.J., 2004. Biomechanics of tendon injury and repair. *Journal of Biomechanics* 37, 865-877.

[Morgan, et al., 1978] Morgan, D.L., Proske, U., Warren, D., 1978. Measurements of muscle stiffness and the mechanism of elastic storage of energy in hopping kangaroos *Journal of Zoology*, 282, 253-261.

[Netter, F.H., 2001] Netter, F.H., 2001. *Atlas de Anatomia Humana*. Icon Learning Systems

[Martins, P., 2009] Martins, P., Peña, E., Calvo, B., Doblaré, M., Mascarenhas, T., Natal Jorge, R.M., Ferreira A.J.M., 2009. "Desenvolvimento de software interactivo para optimizar os parâmetros de modelos materiais hiperelásticos. *Congreso de Métodos Numéricos en Ingeniería 2009*, A. Huerta *et al.* (Eds), Livro de Resumos 379.

[Purslow, P.P., 2002] Purslow, P.P., 2002. Structure and function significance of variations in the connective tissue within muscle. *Comparative Biochemistry and Physiology*, Part A 133, 947-966.

[Purslow, P.P., 2010] Purslow, P.P., 2010. Muscle fascia and force transmission. *Journal of Bodywork & Movement* in press.

[Purslow, P.P., et al., 1994] Purslow, P.P., Trotter, J.A., 1994. The Morphology and mechanical properties of endomysium in series-fiber muscles; variations with muscle length. *Journal of Muscle Research and Cell Motility* 15, 299-308.

[McMinn, 2002] McMinn, 2002. *McMinn's Color Atlas of Human Anatomy*. Elsevier Science.

[Monti, R.J., et al., 1999] Monti, R.J., Roland, R.R., Hodgson, J.A., Edgerton, V.R., 1999. Transmission of forces within mammalian skeletal muscles. *Journal of Biomechanics* 32, 371-80

[Ogden, R.W., 1984] Ogden, R.W., 1984; *Non-linear Elastic Deformations*. Dover Publication, Inc.

[Seeley, et al., 2003] Seeley, R., Stephens, T., Tate, P., 2003. *Anatomy and Physiology*. McGraw-Hill.

[Street S.F., 1983] Street S.F., 1983. *Lateral transmission of tension in frog myofibrils: a myofibrilar network and transverse cytoskeletal connections ate possible transmitters*. *Journal of Cell Physiology* 114, 346-364.

[Swatland, H.J., 1975] Swatland, H.J., 1975. Morphology and development of connective tissue in porcine and bovine muscle. *Journal of Animal Science* 41, 78-86.

[Tindball, J.G., et al., 1991] Tindball, J.G., Law, D.J., 1991. Dystrophin is required for normal thin filament-membrane associations at myotendinous junctions. *American Journal of Pathology* 138, 17-21.

[Trotter J. A., 1990] Trotter J. A., 1990. Interfibber tension transmission in series fibered muscles of the cat hindlimb. *Journal of Morphology* 206, 351-361.

[Trotter, J.A., 1991] Trotter, J.A., 1991. Dynamic shape of tapered skeletal muscle fibers. *Journal of Morphology* 207, 211-23.

[Trotter, J.A., 1993] Trotter, J.A., 1993. Functional morphology of force transmission in skeletal muscle, a brief review. *Acta Anatomica* 146, 205-222.

[Trotter, J.A., et al., 1992] Trotter, J.A., Purslow, P.P., 1992. Functional morphology of the endomysium in series fibered muscles. *Journal of Morphology* 212, 109-22.

[Van Mameren, et al., 1984] Van Mameren, H., Drukker, J., 1984. A functional anatomical basis of injuries to the ligamentum and other soft tissues around the elbow joint: transmission of tensile and compressive loads. *Journal of Sports Medicine* 5, 88-92.

[Yeoh, O.H., 1993] Yeoh, O.H., 1993. Some forms of the strain energy function for rubber. *Rubber Chemistry and technology*, 66, 754-771.

Appendix A

Appendix B

Glossary of Terms

ADP – adenosine diphosphate, one of the end products of ATP hydrolysis; composed of adenine, ribose sugar and two phosphate groups.

Actin – It is a very common type of protein in the human body which when polymerized forms microfilaments that have multiple functions including regulation of muscle contraction, cytokinesis, phagocytosis, adhesion, morphology, cytology and providing structural support.

Action Potential – an electrical signal consisting of the depolarization and subsequent repolarisation of a nerve or muscle cell membrane; travels along the membrane and functions as a signal to initiate an activity (e.g., a muscle contraction)

ATP- Adenosine 5'-triphosphate (ATP) is a multifunctional nucleotide used by cells as a coenzyme. It is called the unity molecular energy transfer since intracellular ATP transports chemical energy within cells; it's the necessary energy for the metabolism to take place.

Calcium ions – calcium atoms with positive charges; concentrated in the extracellular fluid and terminal cisternae, but entre cytosol where they play an important role in many processes such as muscle contraction and the release of neurotransmitters.

Cytosol – the intracellular fluid in which the organelles are suspended and molecules and ions are dissolved.

Fibroblasts - are flat elongated fascial cells with cytoplasmic processes at each end, having a flat, oval, vesicular nucleus. Fibroblasts, which differentiate into chondroblasts, collagenoblasts, and osteoblasts, and myofibroblasts form the fibrous tissues in the body, including tendons, aponeuroses, supporting and binding tissues of all sorts.

Fibrocytes - mediate wound healing and fibrotic tissue repair.

Inorganic Phosphate – It's a phosphate group that is not bonded to an organic molecule such as ATP or creatin phosphate.

Mitochondrion – Te cytoplasm organelle that is the site of ATP synthesis; referred to as the "powerhouse" of the cell.

Myofibril – a cylindrical bundle of contractile filaments within the skeletal muscle cell.

Myosin – one of the proteins that composes the myofibril. Each myosin molecule includes two cross bridges (heads) and a tail region.

Nucleus - Is the cellular structure that contains the genetic material

Power Stroke – the flexing movement of the myosin cross bridge that pulls the actin filament inward toward the center of the sarcomere.

Sarcolemma - Is the specific name for the plasma membrane of the muscle cell

Sarcoplasmic Reticulum - Is the name for the endoplasmic reticulum of the muscle cell. Its interconnecting tubules surround each myofibril like the sleeve of a loosely knit sweater.

Terminal Cisternae - The sac-like regions of the sarcoplasmic reticulum lying adjacent to the tubules; serve as specialized reservoirs of calcium ions.

Tropomyosin – a protein molecule that entwines around actin and blocks the myosin binding sites. In this way tropomyosin prevents cross bridge cycling until it is moved aside by troponin.

Troponin – a three-polypetide complex that binds calcium ions and “drags” tropomyosin off te myosin binding sites on actin.

T Tubule – an invagination of the sarcolemma that projects deep into the muscle cell’s interior.

Triad – A three unit group consisting of one T tubule lying between two adjacent terminal cisternae.